Aus der
Medizinischen Klinik und Poliklinik II
Klinikum der Ludwig-Maximilians-Universität München

Understanding the effects of plasmacytoid dendritic cells on acinar cell damage in Autoimmune Pancreatitis

Dissertation
zum Erwerb des Doktorgrades der Medizin
an der Medizinischen Fakultät
der Ludwig-Maximilians-Universität München

vorgelegt von
Dr. med. univ. Elisabeth Maria Orgler-Gasche

aus
München

Jahr
2025

Mit Genehmigung der Medizinischen Fakultät der

Ludwig-Maximilians-Universität München

Erstes Gutachten:	Prof. Dr. Julia Mayerle
Zweites Gutachten:	Prof. Dr. Konstantin Stark
Drittes Gutachten:	Priv. Doz. Dr. Michael Haas

Dekan: Prof. Dr. med. Thomas Gudermann

Tag der mündlichen Prüfung: 28.07.2025

Zusammenfassung

Autoimmune Pankreatitis (AIP) ist eine seltene Form der chronischen Pankreatitis. Bis zum heutigen Zeitpunkt konnte der genaue Pathomechanismus noch nicht vollständig nachvollzogen werden. Jedoch ist bekannt, dass plasmazytoide dendritische Zellen (pDC) und deren Zytokine, Interleukin (IL)-33 und Interferon (IFN)-α, eine zentrale Rolle in der Pathophysiologie der AIP spielen. Durch die Aktivierung der IFN-regulierenden Faktoren 3 und 7 (IRF3 / IRF7) in pDC wird IFN-α produziert, welches als wahrscheinlicher Auslöser der inflammatorischen Kaskade gilt. AIP führt oft zur Atrophie und Insuffizienz des exokrinen Pankreasgewebes. Jedoch ist es aktuell unklar, ob und wie pDC zu einer Zellschädigung von pankreatischen Azinuszellen beitragen und deren Regenerationsfähigkeit beeinflussen.

Die vorliegende Studie beabsichtigt den Effekt der pDC-initiierten IFN-Kaskade auf die Zellschädigung und die Regerationskapazität von Azinuszellen in der AIP zu verstehen. Um zunächst das Immunzellinfiltrat und die Azinuszellschädigung in der AIP zu charakterisieren, wurde das MRL/MpJ Mausmodel verwendet und mit einem Mausmodell für akute Pankreatitis verglichen. Für die Untersuchung des Effekts von pDC auf Azinuszellen, wurden pDC aus dem Knochenmark von Wildtyp (WT) und Irf3/7-Knockout (Irf3/7-KO) Mäusen, welche keine IFN-Kaskade auslösen können, generiert. Azinuszellen von Mäusen wurden dann mit dem Überstand von WT pDC, Irf3/7-KO pDC oder den pDC-assoziierten Zytokinen IL-33 oder IFN-α behandelt. Um den Effekt auf Azinuszellstress und -regeneration zu messen, wurden Genexpression-Analysen via qRT-PCR und Zellstress-Analysen via LDH Assay durchgeführt. In weiteren Experimenten wurden 3D-Kulturen von Azinuszellen aus WT Mäusen hergestellt und mit IL-33 und IFN-α inkubiert, um den Effekt auf Azinuszellproliferation, als Marker für die Regenerationsfähigkeit, zu messen.

Das Immunzellinfiltrat in AIP bei MRL/MpJ Mäusen bestand vorrangig aus CD8+ T Zellen, dendritischen Zellen und regulatorischen T Zellen. Zusätzlich fiel ein schwerer zellulärer Schaden der Azinuszellen auf. Das geschädigte exokrine Gewebe wurde durch Fettgewebe ersetzt. Die Azinuszellen in den MRL/MpJ Mäusen zeigten, gegenüber den WT Kontrollen, eine signifikant geringere Proliferation (sichtbar durch reduzierte PHH3 Färbung). Ebenfalls konnte in den Azinuszell 3D-Kulturen nach Behandlung mit den pDC-assoziierten Zytokine IL-33 und IFN-α eine Größenreduktion der azinär-duktalen-Metaplasien festgestellt werden, die als Indikator für eine reduzierte Proliferation und Regenerationsfähigkeit der Azinuszellen gewertet werden kann. Zusätzlich zeigten die Co-Kultur-Experimente eine veränderte Genexpressionen der Azinuszellen, die mit Irf3/7-KO pDC behandelt worden waren:

Azinuszellen exprimierten vermehrt *Irf7, Tumornekrosefaktor-α, Il-6* und den Apoptoseinhibitor *Flip*, was darauf schließen lässt, dass pDCs Zellstress verursachen und Signale zum Zelltod beeinflussen könnten.

Zusammenfassend zeigen die Ergebnisse der vorliegenden Arbeit, dass pDC die Proliferation von Azinuszellen via IL-33 und IFN-α beeinflussen und inflammatorische Signale in den Zellen induzieren. Weitere Studien sind nötig, um den komplexen Einfluss von pDC auf Azinuszellen und deren Zelltod tiefergehend zu verstehen.

Summary

Autoimmune pancreatitis (AIP) is a rare form of chronic pancreatitis with relapsing acute phases. Although the exact pathomechanism remains incompletely understood, plasmacytoid dendritic cells (pDC) and their cytokines, IL-33 and interferon (IFN)-α, are recognized as central players in the pathophysiology of AIP. The activation of IFN-regulatory factors 3 and 7 (IRF3 / IRF7) in pDC initiates IFN transcription, which likely triggers an inflammatory cascade. Often AIP may lead to atrophy and insufficiency of the pancreatic exocrine tissue, however it is currently unknown how and if pDCs affect acinar cell damage and regeneration.

This study seeks to investigate the impact of the IFN-cascade, triggered by pDCs, on acinar regeneration capacity and cell damage in AIP. The MRL/MpJ mouse model for AIP was utilized to initially characterize the immune cell infiltrate and acinar cell damage in murine AIP. To examine the effects of pDCs on pancreatic acinar cells, pDCs were generated from bone marrow of wild type (WT) or Irf3/7-knock out (Irf3/7-KO) mice, who are incapable of triggering an IFN-cascade. Murine acinar cells were then incubated with WT pDC supernatant, Irf3/7-KO pDC supernatant or the pDC cytokines IL-33 and IFN-α. Gene expression and cell stress analysis were performed via qRT-PCR and LDH assay, respectively, to measure effects on acinar cell stress and regeneration. In a separate set of experiments, acinar 3D cultures were generated from WT mice and incubated with IL-33 and IFN-α to measure the effect on acinar proliferation.

The AIP immune cell infiltrate in MRL/MpJ mice was characterized by a predominance of CD8+ T cells, dendritic cells and regulatory T cells. Furthermore, severe acinar damage was seen and accompanied by fatty replacement and significantly reduced proliferation of acinar cells (shown in PHH3 staining), indicating pancreatic atrophy. This was reflected in the results from acinar 3D cultures, in which the pDC-associated cytokines IL-33 and IFN-α negatively influenced ADM size, indicating reduced proliferation and regeneration capacity of acinar cells. Furthermore, co-culture experiments of acinar cells showed altered gene expression in acinar cells treated with Irf3/7-KO pDC: acinar cells increasingly expressed *Irf7, Tumor necrosis factor-α, Il-6* and the apoptosis inhibitor *Flip*, indicating that pDC might cause cellular stress and influence cell death signaling.

Taken together, these findings suggest that pDC affect acinar proliferation via IL-33 and IFN-α and induce inflammatory signaling within the cell. Further studies are needed to completely understand the complex effect of pDC on acinar cell death.

Table of content

List of Figures

List of Tables

Abbreviations

%	Percentage
°C	Degrees in Celsius
ADM	Acinar-to-ductal metaplasia
AIP	Autoimmune pancreatitis
AP	Acute pancreatitis
BAFF	B cell activating factor
BF	Brightfield microscopy
cDC	Classical dendritic cell
cDNA	Complementary DNA
CFTR	Cystic fibrosis transmembrane conductance regulator
Ck19	Cytokeratin-19
CTLA4	Cytotoxic T-lymphocyte–associated protein 4
DAMP	Damage-associated molecular pattern
DNA	Deoxyribonucleic acid
ddH_2O	Deionized water
EDTA	Ethylenediaminetetra acetate
FBS	Fetal bovine serum
FLT3	Fms-like tyrosine kinase 3
g	Gram
Gpr84	G-protein-coupled-receptor-84
h	Hour
H&E	Hematoxylin and Eosin
HSP	Heat shock protein
IDCP	Idiopathic duct-centric pancreatitis
IL	Interleukin
IF	Immunofluorescence
IFN	Interferon
IHC	Immunohistochemistry
IgG	Immunoglobin G
IRF	Interferon-regulating factor
Irf3/7-KO	Irf3/Irf7-Knock out
LDH	Lactate dehydrogenase
MAMP	Microbe associated molecular pattern
min	Minutes
ml	Milliliter

mM	Millimolar
ms	Millisecond
MyD88	Myeloid differentiation primary response protein 88
NET	Neutrophil extracellular traps
NF-κB	Nuclear factor kappa-light-chain-enhancer
ng	Nano gram
PBP	Plasminogen-binding protein
PBS	Phosphate buffered saline
PBS-T	Phosphate buffered saline with Tween20
PCR	Polymerase chain reaction
pDC	Plasmacytoid dendritic cell
PFA	Paraformaldehyde
PI	Propidium iodide
pH	Pondus Hydrogenii
PHH3	Phosphohistone-3
PRSS1	Cationic trypsinogen
P/S	Penicillin / Streptomycin
PSC	Pancreatic stellate cell
qRT-PCR	Quantitative real-time polymerase chain reaction
RNA	Ribonucleic acid
rpm	Rounds per minute
s	Second
SD	Standard deviation
SOX9	SYR Box transcription factor 9
SPINK1	Secretory trypsin inhibitor
TBS-T	Tris buffer saline Tween 20
TGF	Transforming growth factor
TLR	Toll-like-receptor
TNF-α	Tumor necrosis factor α
Tregs	Regulatory T cells
µg	Microgram
µl	Microliter
µM	Micromolar
Unc93b1	Unc-93 homolog B1
WT	Wild type

1. Introduction

Autoimmune pancreatitis (AIP) is a rare, chronic, relapsing form of pancreatitis that often affects multiple organs (1, 2). Unlike "classical" chronic pancreatitis, which is usually due to alcohol abuse, smoking or underlying genetic mutations, AIP features an autoimmune inflammation with different clinical, morphologic and histologic traits (1). The disease is characterized by an infiltration of lymphocytes into the pancreas, causing obstructive jaundice, which is usually the main presenting symptom (1). Histologically, there are two main subtypes of AIP (type I and type II AIP) with probably different underlying pathomechanisms (2). Despite biological differences, the subtypes share similar clinical presentations and respond to corticosteroid therapy (1, 3). Essentially, both forms of AIP manifest as an autoimmune disease wherein the immune system fails to recognize self-antigens, leading to an immune-mediated attack on pancreatic cells (1, 3). The etiology of both subtypes remains incompletely understood; however, both subtypes are thought to have a multifactorial pathogenesis, influenced by genetic predispositions and environmental factors that may trigger specific immunologic responses (1).

1.1. Type I AIP

Type I AIP or lymphoplasmacytic sclerosing pancreatitis is a manifestation of Immunoglobin G (IgG) 4-related disease, and histologically defined by lymphoplasmacytic infiltrates in pancreatic lobules associated with obliterative phlebitis and storiform fibrosis (1, 2). Furthermore, IgG4-related disease often affects other organs such as biliary ducts, results in retroperitoneal fibrosis and causes typical renal lesions and submandibular enlargements (1). The prevalence of type I AIP is low, with an estimated <1 per 100,000 in the general population, and patients are predominantly male (75 %) and in later decades of their lives (60 years and older) (4). Clinically, patients frequently present with painless obstructive jaundice due to a focal pancreatic mass, that often is mistaken for a tumor in the pancreas. Moreover, patients show signs of pancreatic endocrine and / or exocrine insufficiency and sometimes acute pancreatitis (1, 5). Therefore, pancreatic cancer is frequently suspected and distinction can be clinically challenging. Laboratory findings include increased levels of IgG4 in about 66 % of patients (6). Diagnostic imaging commonly shows diffuse enlargement of the pancreas (sausage-like) and / or a focal pancreatic mass, as well as pancreatic duct strictures without upstream dilatation, the latter usually occurring in malignant tumors (1, 7).

An international consensus guideline of the International Association of Pancreatology has been established for both AIP type I and II, for which five criteria (imaging, histology, serology, other organ involvement and response to steroids as only an optional criterium) have been selected (8). According to the diagnostic reliability, levels of diagnostic certainty have been suggested. This consensus guideline aims not only to diagnose AIP, but also to simplify the distinction between type I and II (8). For the diagnosis of type I AIP the HISORt criteria have been suggested, combining typical histology, typical imaging, serology (elevated IgG4 levels), other organ involvement and response to steroids as characteristics (Table 1) (7). The diagnosis of AIP can be made if a) histology criteria are fulfilled completely – this would be the gold standard, or if b) imaging criteria are met and serology for IgG4 is elevated or if c) patients with a strong clinical suspicion respond to steroids (7). However, the effect of corticosteroids as a diagnostic criterion has been criticized (1).

Recognizing and diagnosing AIP is not only crucial to differentiate it from pancreatic cancer, but also because it is the only form of chronic pancreatitis with causative treatment options (6). Since it is an autoimmune disorder, patients usually respond well to immunosuppressive agents (1). Initial treatment of type I AIP is a high-dose corticosteroid therapy, which is slowly tapered and withdrawn in responding patients (9). However, relapses of AIP are quite common and re-induction with steroids may not be sufficient for long-term remission (5, 9, 10). In that case, Rituximab a CD20 antibody may be used (9).

Table 1. HISORt criteria for diagnosing AIP. Taken and adapted from *Chari et al*. (7).

Category	Criteria
Histology	At least one of the following criteria: - lymphoplasmacytic infiltrate around ducts with storiform fibrosis and obliterative phlebitis - lymphoplasmacytic infiltrate with abundant IgG4-positive cells (> 10 IgG4-positive cells/ high power field in microscopy) and storiform fibrosis
Pancreatic Imaging	- Diffusely enlarged (sausage-like) pancreas with delayed enhancement; irregular, diffuse main pancreatic duct (typical) - Or focal mass/ enlargement of the pancreas; focal pancreatic duct stenosis; pancreatic calcification; pancreatic atrophy (less typical)
Serology	Elevation of serum IgG4 levels
Other organ involvement	Biliary strictures, involvement of the parotid/ lacrimal gland, retroperitoneal fibrosis, mediastinal lymphadenopathy

Response to steroid therapy	Resolution or improvement of the described manifestation after steroid treatment

1.2. Type II AIP

Type II AIP, or idiopathic duct-centric pancreatitis (IDCP), shares some similarities with type I AIP, but is characterized by a specific histology. This might be due to a different pathomechanism, which is still incompletely understood, and is reflected in different patient characteristics (1). Type II AIP is defined by specific histologic findings, which includes inflammatory infiltrates centering around pancreatic ducts and neutrophils are prominent with granulocytic epithelial lesions, the latter being highly specific for type II AIP (1, 11). This entity of AIP is even less prevalent than type I AIP and exact prevalence numbers are lacking (1). Typically, affected patients are younger than type I patients (around the age of 40) and women and men are at the same risk for developing type II AIP (1, 11). Other organ involvement does not occur, however around 15 % of patients have inflammatory bowel disease, usually ulcerative colitis (12). Diagnostic imaging shows similar features to type I AIP including diffuse enlargement of the pancreas, duct strictures, and also possibly a focal mass, however serum IgG4 levels are usually not elevated (2, 12). Response to corticosteroids is typically rapid and relapses, in contrast to type I, are significantly less common (11).

1.3. MRL/MpJ, a mouse model for AIP

The MRL/MpJ mouse line is used as a model for AIP, and mostly represents type I AIP (13). The mouse model is actually a parental and control strain for the more commonly used MRL/MpJ-Fas^{lpr} mouse model, which is a lupus erythematosus model that displays a more aggressive autoimmune phenomena (14). The MRL/MpJ mouse line features a mutation of interleukin (Il)-2, a T cell growth factor, making it hypoactive (15). Il-2 plays a key function in immune tolerance, and its mutation is associated with reduced cell activation and reduced apoptosis of T cells (15). Furthermore, the MRL/MpJ mouse line has a G-protein-coupled-receptor-84 (*Gpr84*) frameshift deletion resulting in a Stop codon (16). The receptor functions as a mediator of fibrosis and is a regulator of myeloid cells (16). Interestingly, the mouse model shows faster healing and decreased scaring and fibrosis in wound healing studies (17). However, it is likely that the hypoactivation of Il-2 leads to weaker immune regulatory function, enabling autoimmune processes to arise (15).

MRL/MpJ mice develop mild to medium AIP spontaneously at a rather old age (approximately 30 weeks), and without further treatment only female mice are affected (18). For research purposes, a more severe form of AIP-like pancreatitis can be induced in these mice via Poly(I:C)

treatment at an earlier stage in life (18). Poly(I:C) is a a synthetic double-stranded polyribonucleotide and has a structural resemblance to viral RNA (13). Through the binding at Toll-like-receptor 3 (Tlr3), Poly(I:C) triggers the activation of dendritic cells, B cells, macrophages and natural killer cells, thereby setting of an inflammatory cascade in the pancreas similar to human type I AIP (13, 18).

1.4. Plasmacytoid dendritic cells

Plasmacytoid dendritic cells (pDC) are a subclass of dendritic cells, which are unique in their function and role in immunologic contexts (19). The majority of dendritic cells are classical dendritic cells (cDC), which are specialized in antigen presentation to T cells (19). pDC on the other hand are specialized in endosomal TLR-induced activation of type I interferons (IFN) (meaning IFN-α and -β), which are usually released in response to viruses (19). The classification and development of pDC is still not completely understood and heavily debated. However, most likely the cells have a predominantly lymphoid origin and only a small percentage comes from myeloid progenitors, which explains why pDC share a developmental path with B cells (20). For differentiation of progenitor cells into pDC, Fms-like tyrosine kinase 3 (FLT3) is the key growth factor and therefore also used for *in vitro* pDC generation (21).

The high abundance of endosomal TLR7 and TLR9, which recognize single-stranded RNAs and mediate type I IFN expression is an important feature in pDCs (22). Interestingly, the type I IFN production is stronger when pDCs are in physical contact with virus-infected host cells compared to a direct virus interaction (23). Most likely viral RNA or DNA fragments are transferred through exosomes from infected host cell into pDCs (24, 25). Upon ligand stimulation of TLR7 or TLR9, signal transduction occurs through the myeloid differentiation primary response protein 88 (MyD88) (26). This is followed by phosphorylation and nuclear translocation of the transcription factor Interferon-regulating factor (IRF) 7, resulting in production of IFN-α (27). Alongside, activation of TLR7 and TLR9 also results in activation of nuclear factor kappa-light-chain-enhancer (NF-κB) and tumor necrosis factor (TNF)-α expression (19, 22, 28). Depending on the context and the TLR ligand, pDC can either initiate an inflammatory cascade via IFN-α, but also promote immunotolerance, for instance by inducing regulatory T cells (Tregs) (29). On a side note, IRF3 is continuously expressed in many immune cells but is generally not activated in pDCs, which primarily rely on the IRF7 signaling cascade (30, 31). Along IFN-α and -β, pDC are also capable of producing other cytokines, such as IL-6, IL-12, TNF-α and IFN-γ, and present antigens to CD4+ T helper cells (19, 22).

Besides their function in viral infections, pDC are also known to play an important role in autoimmunity, including Lupus erythematosus, psoriasis, arthritis and type I diabetes (19, 22, 32). Especially in Lupus erythematosus, pDC seem to have a central role, in which IFN-α production is triggered via TLR9 by recognizing neutrophil extracellular traps (NETs) (33). These NETs are characteristic features in lupus, composed of granular peptides, anti-neutrophil cytoplasmic antibodies, and self-DNA (33). They are released by neutrophils and serve as antigen source that stimulate autoantibody production (33).

NETs are not an exclusive phenomenon of Lupus erythematosus, but can occur in other contexts, too (34). NET production can for instance be triggered by TLR4-mediated recognition of lipopolysaccharides (LPS), which are components of bacterial membranes (22, 33, 34). Additionally, other bacterial components can activate TLR7 and TLR9 receptors on pDCs, leading to an immune response with IFN (22). For example, in autoimmunity, microbe associated molecular patterns (MAMPs), which are derived from the intestinal microbiome, could mistakenly be recognized by pDC via TLR receptors, resulting in an IFN cascade even in the absence of pathogen invasion (35).

1.5. Pathophysiology of AIP

This section aims to give an overview on the current state of knowledge about the pathomechanisms in development of AIP, focusing on IgG4-related type I AIP, since research on type II AIP is scarce. Furthermore, the similarities between the human disease and the MRL/MpJ mouse model representing type I AIP will be introduced.

As already mentioned, AIP is a multifactorial disease. Genetic susceptibility seems to play a role in AIP type I. A high prevalence of AIP is found in association with certain HLA-alleles (*DRB1*0405-DQB1*0401*) in Japan (36). A recent German study found that *HLA-DRB1*16* and -*DQB1*05* alleles are both strongly associated with AIP type I and II, suggesting similar underlying pathomechanisms (37). Besides that, some studies have found an association between AIP type I with nucleotide polymorphisms, coding for cytotoxic T-lymphocyte–associated protein 4 (*CTLA4*), cationic trypsinogen (*PRSS1*), secretory trypsin inhibitor (*SPINK1*) and TNF-α and Fc receptor-like 3 (1, 38, 39).

Some autoantibodies have been identified in AIP, as potential triggers of the disorder: antinuclear antibodies are found in 40 % of patients, carbonic anhydrase II antibodies in 55 %, lactoferrin antibodies in 75 %, and SPINK1 antibodies are detected in 33 % of AIP patients (40-43). Even though these antibodies are neither specific nor sensitive for AIP, they might still

play a central role and also demonstrate that many of the autoimmune targets are actually pancreatic enzymes and surface proteins of acinar cells (41-43). Known autoantigens include laminin 511, a protein of the extracellular matrix, and heat shock protein (HSP) 10, which is a mitochondrial component, which is released by necrotic or damage tissue and recruits immune cells (44, 45). Molecular mimicry might also play a significant role in triggering AIP. An example of this is the plasminogen-binding protein (PBP) of *Helicobacter pylori*, which shares a strikingly similar structure with ubiquitin-protein ligase E3 component n-recognin 2 (UBR2), which is a highly expressed enzyme in acinar cells (40). Antibodies against PBP are a unique and prevalent (90 %) finding in AIP, suggesting that molecular mimicry is a critical factor in the disease's development (40, 46).

Moreover, it could be shown that AIP predominantly affects blue-collar workers (61-88 %), who are often exposed to industrial substances serving as potential antigens, thereby highlighting the possible impact of environmental factors (47). Taken together, molecular mimicry and environmental factors might be able to induce AIP in genetically susceptible individuals, however, the exact pathogenesis and order of vents is still unknown.

More is known about the inflammatory infiltrate and the involved cytokines in AIP type I. In human AIP the inflammation is known to rely heavily on CD4+ T helper cells 1 and 2 as well as IgG4 positive plasma cells (1, 48). Beside CD4+ T cells, their cytokines IFN-γ, IL-4, IL-5 and IL-13 are typically increased in AIP and eosinophilia can be an additional finding (49, 50). B cells also play an important role in AIP and are the origin of IgG4 plasma cells, which infiltrate the pancreas and produce high amounts of IgG4 antibodies, both characteristic histologic and serologic features of AIP (51). Furthermore, B-cell activating factor (BAFF) is increased in serum of AIP patients, indicating constant recruitment of B cells (52). In addition, an increase of regulatory B cells has been observed in AIP, indicating both pro-inflammatory and immunosuppressive functions of B cell subtypes in the disease (53). The fact that therapy with Rituximab, a B cell depleting agent, is highly effective in AIP, emphasizes their importance (9).

Interestingly, Tregs and the associated cytokine IL-10 are actually upregulated in AIP, which is untypical for autoimmune diseases, as Tregs have immunosuppressive functions and are usually downregulated in autoimmunity (50). This seemingly contradicting presence of pro-inflammatory IL-4 and immunosuppressive IL-10 might in fact be responsible for the often rather mild clinical course (7, 11, 50, 54). Additionally, the combination of these cytokines might induce the antibody class switch to IgG4 (55). Even though, IgG4 is a unique feature of

the disease, it is unlikely that the production of IgG4 is the central driver of the pathomechanism, but might be important for modulating the inflammatory cascade (55, 56). While IgG4 itself has some damaging effects on pancreatic tissue, it these are less severe than those caused by IgG1 (55) . This is because IgG4 lacks the ability to bind complement factors effectively and has limited capacity to engage Fc receptors, rendering it incapable of inducing typical antibody-mediated cytotoxic effects, such as phagocytosis activation and complement system engagement (55, 56). Moreover, IgG4 can mitigate the harmful effects of IgG1 when both are present (55, 56). These findings highlight a complex immunosuppressive component in the disease.

Emerging studies are showing that pDC and their associated cytokines IL-33 and IFN-α, might play a central role in AIP in upholding the inflammatory reaction together with T cells or plasma cells (35, 57-59). This has been mostly studied using the MRL/MpJ mouse model, which has demonstrated that after Poly(I:C) stimulation of Tlr3, pDC accumulate in the pancreas (57). Active Tlr3 signaling induces production of high amounts of Inf-α, which is associated with severe inflammation (58). As mentioned above, Ifn production is regulated via transcription factor Irf7, which expression is also increased in pDC of the murine AIP model and human AIP patients (35). Notably, when pDC are depleted in MRL/MpJ mice, AIP is prevented, revealing a central role of pDC in AIP development (58). Additionally, an inhibition of Inf-α or Irf7 ameliorates AIP disease (35, 58). Furthermore, Ifn signaling induces Il-33 production in murine pDC that further activates profibrotic signaling via transforming growth factor (Tgf)-β and Il-13, which leads to fibrosis (Figure 1) (57). Upon depletion of pDC, Il-33 production is inhibited and fibrosis reduced in the mouse model (57). In human disease, pDC also significantly accumulate in pancreatic tissue samples from AIP patients and pDCs strongly express IFN-α and BAFF (58). Furthermore, IFN-α and IL-33 are markedly increased in serum of AIP patients and have been suggested as potential biomarkers for disease activity (60). These data show that pDCs are central for the inflammatory cascade in AIP using IL-33 and IFN-α, and might therefore also be responsible for acinar damage.

As previously described, NETs are known to trigger pDC activation via TLR9 and induce IFN-α production in systemic lupus erythematosus (33), therefore making them likely to play a role in recruiting and triggering pDC in AIP as well. In fact, in murine AIP, NETs were found to be accumulated in AIP and spatially associated with pDC localization (58). Furthermore, co-cultures from AIP patients containing isolated pDC and neutrophils revealed that upon exposure

to NETs IRF7 translocated from the cytosol / membrane to the nucleus, indicating their potential to trigger pDC activation and IFN production (35).

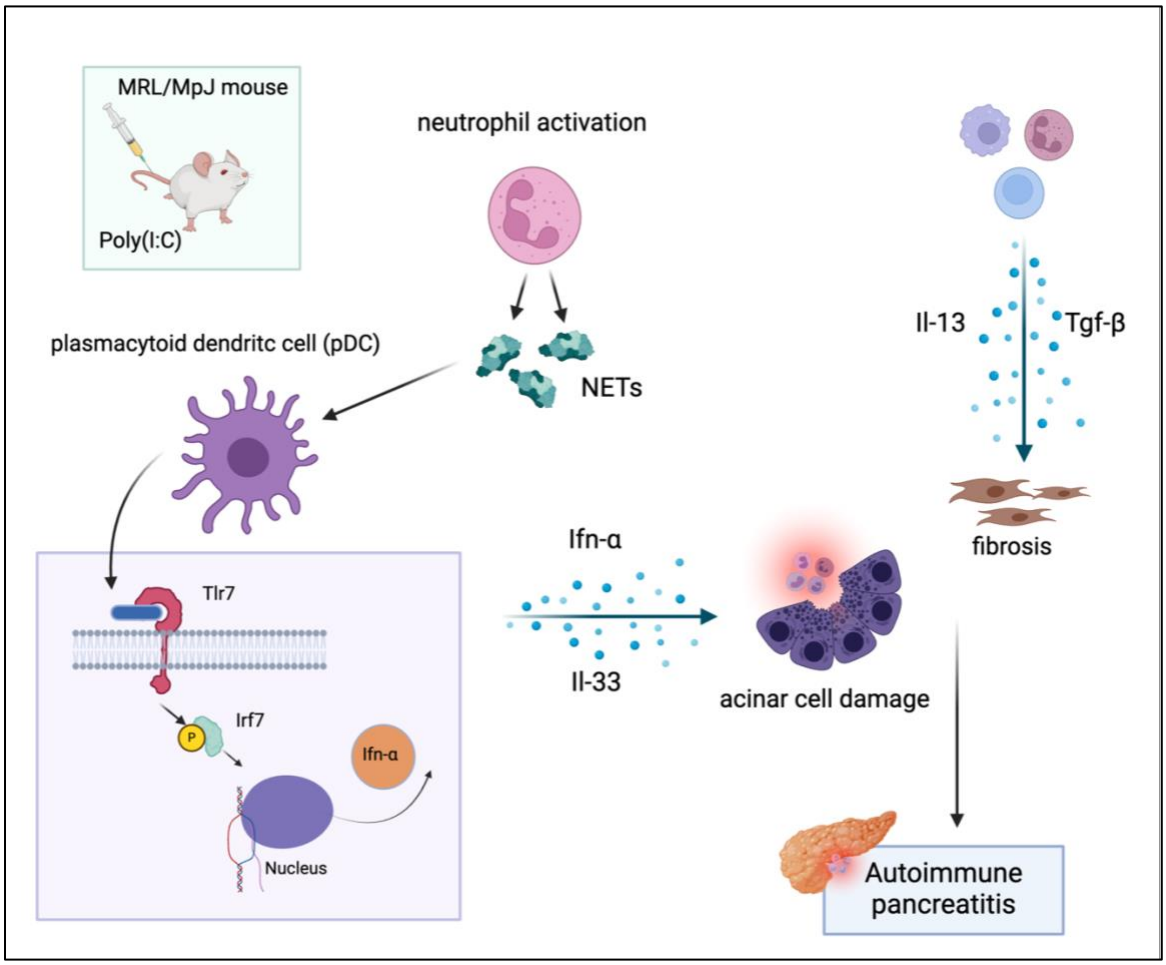

Figure 1. AIP pathomechanism in MRL/MpJ mouse model. Activation of pDC via NETs leads to translocation of Irf7 into the nucleus, followed by type I *Ifn* transcription. Ifn-α and Il-33 are key cytokines in the AIP inflammatory process, which might trigger acinar cell damage. Il-13 and Tgf-β are drivers of fibrosis in AIP.

In the AIP mouse model, the pancreatic acinar cells are severely damaged after treating MRL/MpJ mice with the Tlr3 ligand Poly(I:C) (13, 18). Similarly, human AIP patients showed decreased digestive enzyme secretion from acinar cells as a sign of severe acinar cell injury, and reduced bicarbonate secretion from the ductal cells, because of a low abundance of the cystic fibrosis transmembrane conductance regulator (CFTR) at the apical membrane (61). Interestingly, upon treatment with corticosteroids the expression of CFTR at the apical membrane of ductal cells was restored and acinar cells were regenerated, as shown in increased bicarbonate and digestive enzyme secretion, respectively (61). However, only a partial regeneration of acini was detected that was accompanied by persistent tissue fibrosis (61). Also other studies have shown that during an acute episode of AIP the secretion of digestive enzymes

by acinar cells is significantly reduced in human AIP patients analyzed by secretin test, which measures the excretion of pancreatic juices upon hormonal stimulation of the pancreas (10). After a three-month corticosteroid therapy, the exocrine insufficiency was only partially restored, indicating an incomplete regeneration of acinar cell function (10). Additionally, pancreatic atrophy was observed in morphological imaging such as CT or MRI scans in 28 % of AIP type I and 14 % of AIP type II patients (10). Another Japanese study found that AIP patients with signs of chronic pancreatitis in imaging also have a high prevalence of exocrine (39-56 %) and endocrine insufficiency (26-31 %) (62). This demonstrates that AIP is clinically associated with impaired acinar regeneration after an acute flare.

The exact mechanism of how acinar cell damage occurs in AIP is poorly understood. Current understanding suggests that immune cells fail to recognize self-antigens such as acinar enzymes or acinar cytoskeleton components, leading to an immune-mediated attack on pancreatic cells (1, 2). More studies exist on acute pancreatitis (AP), which is triggered by an intracellular activation of exocrine enzymes, leading to acinar cell self-digestion and pancreatitis (63). During acinar damage, small cell components, including damage-associated molecular patterns (DAMPs) are released, attracting immune cells and causing a severe inflammatory reaction (64). During AP, expression of Tlr3 on acinar cells is increased, which is associated with an amelioration of acinar cell damage (65). Depletion of Tlr3 in a mouse model led to an increase in NF-κB signaling and necrosis, emphasizing, that Tlr3 is a regulator of apoptosis, that prevents unrestricted cell necrosis and severe organ damage during a flare of pancreatitis (65).

Although these findings are based on AP studies, a similar mechanism may apply to acinar injury in AIP. This is particularly plausible given that AIP typically follows a clinically mild course without evidence of necrosis (1, 9-11). In AIP, acinar cell injury caused by an attack from T cells or plasma cells could result in the release of DAMPs. These DAMPs may interact with TLR7 receptors on pDCs, potentially sustaining inflammation in AIP via the release of IFN and IL-33. This could lead to further recruitment of additional immune cells in a vicious inflammatory cycle, eventually leading to pancreatic atrophy and replacement of exocrine tissue by fibrosis.

A phenomenon often observed in the pancreas after injury is acinar-to-ductal metaplasia (ADM). ADM is a form of transdifferentiation of acinar cells into ductal-like cells, which have a high plasticity, similar to progenitor cells (66, 67). ADM often occurs during acute and chronic pancreatitis, where it plays a role in facilitating tissue regeneration (68). During AP, acinar cells are severely damaged leading to cell death via both apoptosis and necrosis of some

cells, while others undergo ADM to allow regeneration (68). During this process, acinar cells lose typical features such as zymogene granules and cell polarity, but become proliferative, allowing tissue replacement (68). However, ADM can also serve as a precursor to pancreatic neoplastic lesions with further progression to cancer in the presence of oncogenes (69). The regulation of ADM formation involves numerous signaling pathways, and its dual function in tissue repair and cancer initiation highlights the critical need for precise molecular control (68). Despite AIP having features of both acute and chronic pancreatitis, such as inflammation, exocrine atrophy, and ADM formation, the role of acinar cell damage and their regeneration capacities in AIP has not been studied yet.

To summarize, even though the exact pathomechanism is incompletely understood, pDC and their cytokines IL-33 and IFN-α are central to the AIP inflammatory process and induction of fibrosis. Through activation of IRF-7, *IFN-α* transcription is initiated in pDC, triggering the inflammatory cascade. The effect of pDC and its cytokines on acinar cell damage and regeneration, which seems to be impaired in AIP, has not been studied yet.

2. Aim of the study

In addition to inflammation and fibrosis, AIP often leads clinically to pancreatic atrophy and endocrine as well as exocrine insufficiency. Specifically, exocrine insufficiency is characterized by a significant decrease in digestive enzyme secretion, caused by a severe damage to the acinar cells and potentially by an inhibition of acinar cell regeneration in AIP. The accumulation of pDCs in AIP tissue and increased levels of IFN-α and IL-33 in the serum of AIP patients indicate that the pDC-IFN-IL-33 axis not only plays a major role in driving the inflammatory reaction, but might also contribute to acinar cell damage and the inhibition of acinar cell regeneration.

Therefore, this study aims to understand the effect of the pDC-IFN-IL-33 cascade on acinar cell damage and regeneration capacity in AIP. The study hypothesizes that pDCs and their release of cytokines induce acinar cell stress and cell damage and impair acinar cell regeneration. In addition, it was investigated if persistent acinar cell damage might trigger pDC differentiation, which potentially maintain the autoimmune process.

As a first step, the immune cell infiltrate, acinar cell damage and ADM formation, as a marker for regeneration capacity, were investigated in an AIP mouse model using MRL/MpJ mice and compared with a model of AP. Next, pancreatic acinar cell explants were co-cultured with *in vitro* generated pDCs, either from wild type (WT) mice, or Irf3/Irf7 knockout (Irf3/7-KO) mice, which are unable to release IFN type I cytokines. Although the Irf3/7-KO pDCs are incapable of producing Ifn-α, other effectors such as Nf-κb and Tnf-α remain functional. The effect of WT and Irf3/7-KO pDCs on acinar cells was assessed by measuring the released cell stress marker LDH and on gene expression levels. Regeneration capacity of acinar cells was investigated under IL-33 and IFN-α treatment by embedding acinar cells in 3D cultures. Here, ADM formation and cell proliferation rates were measured to determine if the typical pDC cytokines impair acinar cell regeneration. To test if persistent acinar cell damage trigger pDC differentiation, bone marrow of wild type mice was treated with supernatant from isolated acinar cell cultures and flow cytometry was performed to detect differentiated pDC.

3. Materials and Methods

3.1. Materials

3.1.1. Chemicals and reagents

Table 2. Chemicals and reagents

Reagent	Manufacturer
5-Bromo-2-deoxyuridine (BrdU) #B5002	Sigma-Aldrich, St. Louis, Missouri, USA
Agarose SERVA for DNA Electrophoresis #11404.07	SERVA, Heidelberg, Germany
Ambion™ Nuclease-Free Water, 10x50ml, #AM9937	Invitrogen, Waltham, Massachusetts, USA
Aqueous mounting medium #06522-100ML	Sigma-Aldrich, St. Louis, Missouri, USA
β-mercaptoethanol # M3148-100ML	Thermo Fisher Scientific, Waltham, USA
Bovine serum albumin #900.022	Aurion Biotech, Seattle, Washington, USA
Cerulein #C9026-1MG	Sigma-Aldrich, St. Louis, Missouri, USA
Collagen I rat tail #354236	Corning, Corning, New York, USA
Collagenase P #11213865001	Sigma-Aldrich, St. Louis, Missouri, USA
DAPI (4-6-Diamino-2-phylindol) #6335.1	Carl Roth, Karlsruhe Germany
Dexamethasone #D4902	Sigma-Aldrich, St. Louis, Missouri, USA
Donkey serum #S30-100ML	Sigma-Aldrich, St. Louis, Missouri, USA
Dulbecco´s Phosphate Buffered Saline (1X) (PBS) #D8537	Sigma-Aldrich, St. Louis, Missouri, USA
eBioscience red blood cell lysis buffer #00-4333	Invitrogen, Waltham, Massachusetts, USA
Ethanol # ETO-5000-99-7	SAV Liquid Production GmbH, Germany
Eosin # HT110216	Sigma-Aldrich, St. Louis, Missouri, USA
FastStart Essential DNA Green Master #6924204001	Roche, Basel, Switzerland
Fetal Bovine Serum (FBS) #F-9665	Sigma-Aldrich, St. Louis, Missouri, USA
FLT3L #550702	BiolegendSan Diego, California, USA
Formamide # S4117	EMD Milipore Corp, MA, USA
GeneRuler 100 bp Plus SM0324 DNA Ladder # SM0322	Thermo Fisher Scientific, Waltham, USA
Glycerol #3783.1	Carl Roth, Karlsruhe, Deutschland
Goat serum #S26-100ML	Sigma-Aldrich, St. Louis, Missouri, USA
Go Taq® G2 Hot Start Green Master Mix #M7423	Promega, Madison, Wisconsin, USA

Hematoxylin # T865.2	Sigma-Aldrich, St. Louis, Missouri, USA
Hank's balanced salt solution (HBSS) GIBCO #14025092	Thermo Fisher, Waltham, Massachusetts, USA
HEPES #15630	Invitrogen, Waltham, Massachusetts, USA
Hydrogen peroxide #CP26.1	Carl Roth, Karlsruhe, Deutschland
IFN-a recombinant protein #122105-1	PBL assay science, Piscataway, NJ, USA
IL-33 recombinant protein #3626-ML-010	R&D systems, Minneapolis, Minnesota, USA
TriTrack DNA loading dye (6x) #R1161	Thermo Fisher, Waltham, Massachusetts, USA
MEM 1X Non-Essential Amino Acids Solution GIBCO #1140035	Thermo Fisher, Waltham, Massachusetts, USA
Methanol #1.06009.2511	Merck, Darmstadt, Germany
$NaHCO_3$ #6885.3	Carl Roth GmbH, Karlsruhe, Germany
Paraformaldehyde 16 % solution # RT15710	Electron Microscopy Sciences, Hatfield, PA
Penicillin/ streptomycin GIBCO #15140122	Thermo Fisher, Waltham, Massachusetts, USA
Permanent Mounting Medium, VectaMount #H5000	Sigma-Aldrich, St. Louis, Missouri, USA
Poly(I:C) #31852-29-6	Invitrogen, Waltham, Massachusetts, USA
Propidium Iodide solution #421301	BioLegend, San Diego, California, USA
RPMI medium1640 GIBO #11875093	Thermo Fisher, Waltham, Massachusetts, USA
Sodium acetate # X891.1	Carl Roth GmbH, Karlsruhe, Germany
Sodium dodecyl sulfate (SDS) Pellets #2326.1	Carl Roth GmbH, Karlsruhe, Germany
Sodium pyruvate GIBCO #1136003	Thermo Fisher, Waltham, Massachusetts, USA
SYBR™ Safe DNA Gel Stain #S33102	Invitrogen, Waltham, Massachusetts, USA
Transforming growth factor-α #PHG0051	Thermo Scientific, Waltham, Massachusetts, USA
TRIS base #9140.8	Carl Roth GmbH, Karlsruhe, Germany
TRIS HCl #9090.3	Carl Roth GmbH, Karlsruhe, Germany
Triton X-100 #X100-100ml	Sigma-Aldrich, St. Louis, Missouri, USA
Trypan Blue solution 0.4 % # T8154	Sigma-Aldrich, St. Louis, Missouri, USA
Trypsin-EDTA Solution (10X) #59418C	Sigma-Aldrich, St. Louis, Missouri, USA
Trypsin Inhibitor (17075-029) #17075-029	Thermo Fisher, Waltham, Massachusetts, USA

Tween® 20 #9127.1	Carl Roth GmbH, Karlsruhe, Germany
Waymouth's MB 752/1 #31220023	Invitrogen, Waltham, Massachusetts, USA
Xylol Histo Grade #A2476.5000	AppliChem, Darmstadt, Germany

3.1.2. Mice

Table 3. Mouse models

Official Name	Background	Internal Name (Usage)
MRL/MpJ	C57BL6/J	MRL/MpJ (AIP model)
Description and Origin: Hypoactive mutation of Il-2, G-protein-coupled-receptor-84 deletion, Charles River Laboratory (Boston, USA). 20-week-old female mice underwent a three-day cycle of Poly(I:C) injections from Sigma-Aldrich (Deisenhofen, Germany) (5 mg/kg bodyweight) intraperitoneally for eight weeks in order to induce severe AIP (Animal proposal no: LALLF M-V/TSD/7221.3-2.4-008/10). Mice were sacrificed and pancreases were fixed in 4 % formaldehyde buffered PBS overnight and embedded in paraffin for histologic analysis. Paraffin-embedded tissue blocks provided by the Medical University of Greifswald.		
Official Name	**Background**	**Internal Name (Usage)**
Ptf1aCre$^{ERT/+}$;LSL-tdTomato$^{flox/flox}$	C57BL6/J	PT (AP model)
Description and Origin: This mouse line was generated through crossbreeding of Ptf1aCreERT/+ (B6.129S6(Cg)-*Ptf1atm2(cre/ESR1)Cvw/J,* #019378, Jackson Laboratory, Bar Harbor, USA) and LSL-tdTomatoflox/flox mice (B6.Cg *Gt(ROSA) 26Sortm14 (CAGtdTomato) Hze*/J, #007914, Jackson Laboratory, Bar Harbor, USA). Own breeding stock, University Hospital, LMU Munich, Germany. The mouse line has an inducible fluorescence reporter in Ptf1a-positive acinar cells. Eight-week-old mice received Cerulein-induced pancreatitis (two days with eight hourly intraperitoneal injections of 100µg/kg bodyweight Cerulein from Sigma-Aldrich (St. Louis, Missouri, USA) in 0.9 % NaCl) and served as AP controls (Animal proposal no: ROB-55.2-2532.Vet-02-17-10, ROB-55.2-2532.Vet-02-19-169). Mice were sacrificed and pancreases were fixed in 4 % formaldehyde buffered PBS overnight and embedded in paraffin for histologic analysis. Paraffin-embedded tissue blocks were used in this study.		
Official Name	**Background**	**Internal Name (Usage)**
WT **(Wildtype)**	C57BL6/J	WT (acinar cell explants and pDC generation)
Description and Origin: Own breeding stock, University Hospital, LMU Munich, Germany. Mice were used for generation of pDC.		
Official Name	**Background**	**Internal Name (Usage)**
Irf3/Irf7-KO **(B6.126-*Irf3*^{tm1Ttg}; *Irf7*^{tm1Ttg} (*Irf3*$^{-/-}$;*Irf7*$^{-/-}$)**	Mixed B6;129	Irf3/7-KO (pDC generation)
Description and Origin: Knockout of *Irf3* and *Irf7*, own breeding stock, University Hospital, LMU Munich, Germany. Mice were used for generation of pDC.		

3.1.3. Kits

Table 4. Kits

Kit	Manufacturer
ImmPACT® DAB Substrate Kit Peroxidase (HRP) #SK-4105	Vector Laboratories, Newark, California, USA
ImmPACT® AMEC Red Substrate Kit, Peroxidase (HRP) #SK-4285	Vector Laboratories, Newark, California, USA
LDH-Glo cytotoxicity Assay #J2380	Promega, Madison, Wisconsin, USA
RevertAid First Strand cDNA Synthesis Kit #K1621	Thermo Scientific, Waltham, Massachusetts, USA
RNeasy Plus Mini Kit #74134	Qiagen, Hilden, Germany
VECTASTAIN Elite ABC Kit #PK-6100	Vector Laboratories, Newark, California, USA

3.2. Antibodies

3.2.1. Primary Antibodies for IHC

Table 5. Primary antibodies for IHC

Antibody	Host	Dilution	Company	Catalogue number
CD45	rat	1:10	BD Pharmingen, Franklin Lakes, New Jersey, USA	#550539
CD4	rabbit	1:100	cell signaling, Danvers, Massachusetts, USA	#D7D2Z
CD8	rabbit	1:100	cell signaling, Danvers, Massachusetts, USA	#D4W2Z
F 4/80	rat	1:100	BioRad, Hercules, California, USA	#MCA497R
FoxP3	rabbit	1:10	cell signaling, Danvers, Massachusetts, USA	#D2W8E
CD11c	rabbit	1:100	cell signaling, Danvers, Massachusetts, USA	#97585
IRF3	rabbit	1:200	cell signaling, Danvers, Massachusetts, USA	#D83B9
IRF7	rabbit	1:500	Novus Biologicals, Englewood, Colorado, USA	#NBP1-77263
Cytokeratin (Ck19)	rabbit	1:750	Abcam, Cambridge, UK	#ab133496
Phosphohistone-H3 (PHH3)	rabbit	1:200	cell signaling, Danvers, Massachusetts, USA	#cs:53348

3.2.2. Secondary antibodies for IHC

Table 6. Secondary antibodies for IHC

Antibody	Company	Catalogue number
Dako Envision+ System-HRP labelled polymer Anti-mouse	Agilent Technologies, Santa Clara, California, USA	#K4001
Dako Envision+ System-HRP labelled polymer Anti-rabbit	Agilent Technologies, Santa Clara, California, USA	#K4003
Donkey Anti-rat HRP secondary antibody	Jackson Immuno Research, West Grove, Pennsylvania, USA	#712-035-150

3.2.3. Antibodies for flow cytometry

Table 7. Antibodies for flow cytometry

Antibody	Company	Catalogue number
B220-APC	BioLegend, San Diego, California, USA	#103211
SiglecH-FITC	BioLegend, San Diego, California, USA	#129603
PE Annexin V	BioLegend, San Diego, California, USA	#422201

3.3. Primer for gene expression analysis

Table 8. Primers for gene expression

Gene	Forward Primer (5‘-3‘)	Reverse Primer (3‘-5‘)
Irf3	CAGAAGCCAGTGGTGCCTA	CGCAACACTTCTTTCCGGTT
Irf7	AGAGCGAAGAGGCTGGAAGAC	CACCTTATGCGGATCAACTGGA
Tnfa	TTCTCATTCCTGCTTGTGGCA	AGGGTCTGGGCCATAGAACT
IL-6	TCCTCTCTGCAAGAGACTTCCATCC	CCTCTGTGAAGTCTCCTCTCCGG
Flip	TCCAGAATGGGCGAAGTAAAGA	AAGTCTCTTCACGGATGTGCG
Xiap	GTGGTACCCAGGGTGCAAATA	TCTTGCACCATAGGATTCTGGA
Ccnb1	GCTCTCCATGCTGGACTACG	AGTTGGTGTCCATTCACCGT
Ppib	GGAGCGCAATATGAAGGTGC	CTTATCGTTGGCCACGGAGG

3.4. Buffers

Table 9. Buffers

Buffer	Composition	Final concentration
Antibody stripping buffer (IHC)	SDS	1 %
	glycine	25mM
	in ddH2O	
Citrate buffer	Citric acid, pH 6.0	10 mM
	in ddH2O	
FACS buffer	EDTA	0.1 %
	Fetal bovine serum	1 %
	in PBS	
IHC blocking buffer	Bovine serum albumin	1 %
	in PBS	
LDH assay storage buffer	TRIS-HCl, pH 7.3	200 mM
	Glycerol	10 %
	BSA	1 %
	in ddH2O	
PBS-T	PBS	
	Tween-20	0.1 %
TBS-T	TRIS-HCl, pH 7.4	20 mM
	NaCl	150 ml
	Tween-20	0.1 %
TAE buffer	TRIS-Base	40 mM
	Acetic acid	20 mM
	EDTA	1 mM

3.5. Cell culture mediums

3.5.1. Acinar cell culture medium

Table 10. Acinar cell medium

Reagent	Company	Catalogue number	Final concentration
RPMI 1640 medium GIBCO	Thermo Fisher, Waltham, Massachusetts, USA	#11875093	

Penicillin/ streptomycin GIBCO	Thermo Fisher, Waltham, Massachusetts, USA	#15140122	1 %
Trypsin Inhibitor	Thermo Fisher, Waltham, Massachusetts, USA	#17075-029	0.1 mg/ml
Dexamethasone	Sigma-Aldrich, St. Louis, Missouri, USA	#D4902	1 mg/ml
FBS	Sigma-Aldrich, St. Louis, Missouri, USA	#F-9665	10 %

3.5.2. pDC medium

Table 11. pDC medium

Reagent	Company	Catalogue number	Final concentration
RPMI 1640 medium GIBCO	Thermo Fisher, Waltham, Massachusetts, USA	#11875093	
Fetal bovine serum (FBS)	Sigma-Aldrich, St. Louis, Missouri, USA	#F-9665	10 %
Sodium pyruvate GIBCO	Thermo Fisher, Waltham, Massachusetts, USA	#1136003	1 mM
Penicillin/ streptomycin GIBCO	Thermo Fisher, Waltham, Massachusetts, USA	#15140122	1 %
MEM 1X Non-Essential Amino Acids Solution GIBCO 1	Thermo Fisher, Waltham, Massachusetts, USA	#1140035	1 %
β-mercaptoethanol GIBCO	Thermo Fisher, Waltham, Massachusetts, USA	#11528926	0.05 mM

3.5.3. Waymouth 2D medium

Table 12. Waymouth 2D medium

Reagent	Company	Catalogue number	Final concentration
Waymouth's MB 752/1	Invitrogen, Waltham, Massachusetts, USA	#31220023	
FBS	Sigma-Aldrich, St. Louis, Missouri, USA	#F-9665	10 %
Penicillin/ streptomycin GIBCO	Thermo Fisher, Waltham, Massachusetts, USA	#15140122	1 %
Trypsin Inhibitor	Thermo Fisher, Waltham, Massachusetts, USA	#17075-029	0,1 mg/ml
Dexamethasone	Sigma-Aldrich, St. Louis, Missouri, USA	#D4902	0.005 mM
HEPES	Invitrogen, Waltham, Massachusetts, USA	#15630	5 mM
$NaHCO_3$	Carl Roth GmbH, Karlsruhe, Germany	#6885.3	0.13 %

3.5.4. Waymouth 3D medium

Table 13. Waymouth 3D medium

Reagent	Company	Catalogue number	Final concentration
Waymouth's MB 752/1	Invitrogen, Waltham, Massachusetts, USA	#31220023	
FBS	Sigma-Aldrich, St. Louis, Missouri, USA	#F-9665	20 %
Penicillin/ streptomycin GIBCO	Thermo Fisher, Waltham, Massachusetts, USA	#15140122	2 %
T Trypsin Inhibitor	Thermo Fisher, Waltham, Massachusetts, USA	#17075-029	0.2 mg/ml
Dexamethasone	Sigma-Aldrich, St. Louis, Missouri, USA	#D4902	0.01 mM
HEPES	Invitrogen, Waltham, Massachusetts, USA	#15630	10 mM
$NaHCO_3$	Carl Roth GmbH, Karlsruhe, Germany	#6885.3	0.26 %

3.6. Consumables

Table 14. Consumables

Consumable	Manufacturer
6-well plate (qRT-PCR), white #I1402-9909	STARLAB, Hamburg, Germany
BD Microlance 26 gauge needle #4657683	BD, New Jersey, USA
BD Syringe Filcons 30 µm # 340600	BD Biosciences, San José, USA
Cell culture flasks (25 cm #83.3910.002, 75 cm #83.3911.002)	Sarstedt, Nürnbrecht, Germany
Cell culture plates (6 well #657160, 24-well #662160)	Greiner Bio-One, Kremsmünster, Austria
Cell culture plates (12-well #833.921.500, 96-well #833.924)	Sarstedt, Nürnbrecht, Germany
Cell counting slides #1450015	Bio-Rad, Hercules, USA
Cryogenic tube #E3110-6122	STARLAB, Hamburg, Germany
EZ Cytofunnels #11972345	Thermo Scientific, Waltham, MA, USA
Falcon, 5 ml Polystyrene Round bottom tube 55.1579.002	Sarstedt, Nürnbrecht, Germany
Falcon cell culture dish (10 cm), untreated #821.473.001	Sarstedt, Nürnbrecht, Germany
Falcon® Cell strainer (100 µm, nylon) #352360	Corning, Bedford, USA
Falcon tubes (15 ml #62.554.502, 50 ml #62.547.254)	Sarstedt, Nürnbrecht, Germany
Filtropur S syringe filter 0.2 µm #83.1826.001	Sarstedt, Nümbrecht Germany
Parafilm® #701606	Brand GmbH, Wertheim, Germany
PCR reaction tube (0.2 ml) #710970	Biozym, Oldendorf, Germany
Pipette filter tips (10 µl #70.3020.255, 200 µl #70.3031.255, 1000 µl #70.3050.255)	Sarstedt, Nürnbrecht, Germany
Pipette tips (10 µl, 200 µl, 1000 µl)	Sarstedt, Nürnbrecht, Germany
qRT-PCR 96-Well plate	STARLAB, Hamburg, Germany

Reaction tubes (1.5 ml #72.706.200, 2 ml #72.695.200)	Sarstedt, Nürnbrecht, Germany
Scalpel, Feather disposable scalpel #NC9999403	Feather, Osaka, Japan
Serological pipettes, sterile, single packed (5 ml #86.1253.001, 10 ml #86.1254.001, 25 ml #86.1254.025)	Sarstedt, Nürnbrecht, Germany
Xtra-Clear Advanced Polyolefin Starseal #E2796-9795	STARLAB, Hamburg, Germany

3.7. Laboratory Equipment

Table 15. Equipment

Equipment	Manufacturer
Brightfield microscope	Zeiss, Jena, Germany
Centrifuge 5417R	Eppendorf, Hamburg, Germany
Centrifuge 5418R	Eppendorf, Hamburg, Germany
Centrifuge 5702R	Eppendorf, Hamburg, Germany
Cytospin Cytocentrifuge	Thermo Scientific, Waltham, MA, USA
Eppendorf Mastercycler® PCR cycle	Eppendorf, Hamburg, Germany
Flow cyotmeter FACS Canto II	BD Bioscience, NJ, USA
Fluorescence microscope	Zeiss, Jena, Germany
Freezer -20 ° C	Liebherr, Biberach an der Riss, Germany
Freezer -80 ° C	Sanyo, Tokio, Japan
Fusion FX	Vilber Lourmat GmbH, Eberhardzell, Germany
IX50 Phase contrast inverted microscope	Olympus, Shinjuku, Japan
LightCycler® 96	Roche, Penzberg, Germany
Mini Plate Spinner Centrifuge-230EU	Corning, New York, USA
NanoDrop 200 spectrophotometer	Thermo Scientific, Dreieich, Germany
Pannoramic MIDI II RX	Sysmex Corporation, Kobe, Japan
pH meter	Knick, Berlin, Germany
Pipetboy acu 2	Integra, Biebertal, Germany
PIPETMAN® classic	Gilson, Middleton, USA

SpectraMax® Plus 384 Microplate Reader	Molecular Devices, San José, USA
TC20 Automated cell counter	Bio-Rad, Hercules, USA
TS1 ThermoShaker	Biometra GmbH, Göttingen, Germany
Vortexer	IKA, Staufen, Germany

3.8. Software and applications

Table 16. Software

Software	Manufacturer
GraphPad Prism 9	GraphPad Software, Inc., La Jolla, USA
Lightcycler®96 software	Roche, Basel, Switzerland
Leica MM AF	Leica, Wetzlar, Deutschland
Microsoft Office	Microsoft, Redmond, USA
R version 4.2.1 GUI 1.79 Big Sur ARM build	R Core Team, Auckland, New Zealand
Softmax Pro 7.0	Molecular Devices, San José, USA
SlideViewer Software	Sysmex Corporation, Kobe, Japan

3.9. Histology

3.9.1. Hematoxylin and Eosin (H&E) staining and scoring

H&E staining was performed of paraffin slides of pancreatic tissue from MRL/MpJ and PT mice following a standard protocol. Slides were first deparaffinized in xylol 3x10 minutes, followed by gradual rehydration in descending ethanol series (100 %, 95 %, 70 % and 50 % ethanol, each 3 minutes) and a rinse in distilled water. Sections were then stained with hematoxylin for 40 seconds and rinsed in running tap water for 2 minutes. Eosin staining was performed by adding the slides in eosin solution for 30 seconds, with a brief rinse in tap water to remove excess stain. After staining, slides were dehydrated through a graded ethanol series (50 %, 70 %, 95 %, and 100 % ethanol, each 30 seconds), fixed in xylol, and mounted with coverslips using permanent mounting medium. A scoring system for inflammatory infiltrate, acinar cell damage, ADM formation and fatty replacement of pancreatic tissue was established, with scores ranging from 0-3 (0=none, 1=mild, 2=moderate, 3=severe).

3.9.2. Immunohistochemistry

For immunohistochemistry (IHC) staining, paraffin slides were first deparaffinized in xylol (3x10 minutes) and rehydrated in a descending ethanol series (100 %, 95 %, 70 %, 50 % each 3 minutes), finishing with water. Antigen demasking was performed with boiling slides in 10 mM citrate buffer for 10 minutes with a minimum cool down phase of 30 minutes. Slides were washed in PBS buffer 3x5 minutes, followed by blocking of endogenous peroxidase activity with 3 % hydrogen peroxide for 10 minutes. Next, washing with PBS buffer was done 3x5 minutes, followed by blocking with 1 % bovine serum albumin and 5 % serum of the host of the secondary antibody in PBS for one hour. Then primary antibodies were diluted in respective concentrations in the blocking buffer and applied to the slides and incubated overnight at 4°C.

After incubation, slides were washed with PBS buffer 3x5 minutes and then incubated with the respective secondary antibody for one hour (**Error! Reference source not found.**), followed by another washing phase with 3x5 minutes in PBS buffer. Finally, slides were treated with ImmPACT® DAB Substrate Kit. Staining reaction was observed under a brightfield (BF) light microscope and stopped in water. Counterstaining was performed with hematoxylin for 40 seconds and slides were dehydrated in an ascending ethanol series (30 seconds each) and fixed in xylol.

For Irf3 and Irf7 staining the VECTASTAIN Elite ABC Kit was used according to the provided manual. TBS-T was used for washing steps.

IHC staining were scored based on the intensity and number of positive cells for the respective marker on a scale from 0-3 (0=none, 1=mild, 2=moderate, 3=severe). Cell markers expressed in epithelial cells and immune cells, such as PHH3, Irf3 and Irf7, were scored for immune and acinar cells, separately.

3.9.3. Multiplexing

The immune cell markers CD45, CD8 and FoxP3 were stained consecutively by multiplex-IHC staining. Slides were prepared and incubated with the primary and secondary antibody as in normal IHC staining. Washing steps were performed with PBS-T. After secondary antibody was washed off with PBS-T, substrate development was done with ImmPACT® AMEC Red Substrate Kit, and observed with a BF microscope. Slides were counterstained with hematoxylin, washed in tap water for 2 minutes, directly mounted with aqueous mounting medium and scanned with Pannoramic MIDI II RX for documentation of staining results. After scanning, slides were dipped into PBS for 20 minutes to remove the cover slip. AMEC Red was destained with washing slides in deionized water (2 minutes), 70 % ethanol (1 minute), 95 % ethanol (3 minutes), 70 % ethanol (1 minute) and deionized water (2 minutes). Next antibody stripping was performed with incubating slides in antibody stripping buffer for 30 minutes in a 55°C warm, shaking water bath. Afterwards, slides were washed in PBS (2x 5 minutes) and another staining cycle was started beginning again with blocking buffer for one hour.

3.10. Plasmacytoid dendritic cells

3.10.1. In vitro generation of pDCs

pDCs were generated from murine bone marrow using an established protocol (55). WT and Irf3/7-KO mice (**Error! Reference source not found.**) were sacrificed at the age of eight weeks and bone marrow was immediately processed according to an established protocol (56).

In short, femur and tibia were dissected and skin and muscle scraped off with a scalpel. Under sterile conditions, femur and tibia were cut open on both ends and bones were flushed from both sides with 10 ml of PBS with 10 % FBS using a 26 gauge needle and collected in a 15 ml tube. Bone marrow was pipetted up and down with a syringe and then flushed through a 100 µm cell strainer with a nylon net. The net was washed with 10 ml PBS/ 10 % FBS. Cells were transferred into a 50 ml tube and centrifuged at 300 xg at 4°C for seven minutes. Supernatant was aspirated and cell pellet was dissolved in 2 ml of eBioscience red blood cell lysis buffer for three minutes at room temperature. In order to neutralize, 8 ml of PBS/10 % FBS were added. Cells were centrifuged again and supernatant was discarded. Cells were resuspended in 5 ml of PBS/ 10 % FBS. After centrifugation and discarding the supernatant, cells were

resuspended in pDC medium and counted. 1.5 x 10^6 cells/ml were seeded in a 10 cm petri dish with low-binding conditions. Cells were cultured in suspension for seven days with 200 ng/ml recombinant mouse FLT3L. Medium was changed after 3 days in culture.

3.10.2. Flow cytometry

To evaluate efficacy of in vitro pDC generation, flow cytometry was performed. To identify pDCs from progenitor immune cells and cDC, the antibodies SiglecH and B220 were used since only pDCs carry both surface markers. Cells from the in vitro generated pDC approach were harvested and centrifuged at 500 xg at 4°C for 8 minutes. pDC supernatant was filtered sterile through a Filtropur S syringe filter (0.2 µm) and saved for acinar cell experiments (stored at -20°C). Cells were washed in 1 ml FACS buffer and centrifuged at 400 xg at 4°C for five minutes. 10 µl of cells were mixed with an equal volume of 0.4 % Trypan Blue solution. 10 µl of the mixture were spread on a cell counting slide and placed on a TC20 Automated cell counter. The cell pellet was resuspended in 160 µl FACS buffer. From the resuspended cells, 30 µl were used as negative control and 30 µl for live/dead staining (see below). These samples were treated as described below, but without antibody staining. From this point on, all following incubation steps were performed under light protection. To the remaining 100 µl of resuspended cells 1 µl of each antibody, SiglecH-FITC and B220-APC was added. Cells were incubated for one hour on ice. Afterwards, cells were dispensed through 30 µm syringe filcons to dissociate into single cells. Filcons were flushed with 1 ml of FACS buffer. Cells were centrifuged at 400 xg at 4°C for five minutes. Cells were washed twice in 1 ml FACS buffer. Cells were finally resuspended in 300 µl FACS buffer and gently pipetted up and down. The sample for live/dead staining was incubated with 5 µl of PE Annexin V and 10 µl of Propidium Iodide for 15 minutes before flow cytometry analysis. Flow cytometry analysis was performed externally at the Flow Cytometry Core Facility at the Biomedical Center, LMU Munich.

3.11. Pancreatic acinar cell culture experiments

3.11.1. Isolation of pancreatic acinar cells

WT mice were sacrificed at the age of eight weeks. The pancreas was dissected quickly, put on a 10 cm culture dish, infiltrated with 10 ml collagen-solution (0.5 mg/ml Collagenase P in RPMI medium) using a syringe and cut into small pieces. Tissue was incubated at 37°C for 15 to 20 minutes in an incubator. Afterwards, tissue pieces were pipetted up and down gently to completely dissolve. The cell solution was transferred into a 50 ml tube and the dish was rinsed with 10 ml of RPMI medium with 5 % FBS, which was also added to the tube. Cells were centrifuged at 300 xg for 5 minutes and the cell pellet was resuspended in 10 ml RPMI medium with 5 % FBS and gently pipetted up and down. Next, the pancreatic cell suspension was filtered

through a 100 µm nylon mesh that was put on top of a 50 ml tube and centrifuged as before. Three washing steps with HBSS were performed. Afterwards, the cell pellet was resuspended in acinar cell culture medium, seeded on uncoated petri-dishes and incubated at 37°C in suspension.

3.11.2. Treatment of acinar cell suspension cultures

After acinar cell isolation, cells were rested for two hours to reduce cell stress due to the isolation process. The 0h time point was set at two hours after isolation. Afterwards, acinar cell suspension cultures were treated with 0.05 ng/ml recombinant IL-33 and 500 U/ml recombinant IFN-α for 6 hours, or isolated acinar cells were centrifuged at 300 xg at RT for 5 minutes and resuspended in pDC supernatant from WT mice (WT pDC) and Irf3/7-KO mice (Irf3/7-KO pDC) and incubated for 6 hours.

3.12. Acinar 3D collagen culture

3.12.1. Establishment of acinar 3D cultures

Acinar cells were isolated from WT mice as described above. After the third washing step with HBSS, acinar cells were resuspended in 10 ml Waymouth 2D medium and transferred onto a 10 cm dish for incubation at 37°C overnight.

On the next day, a 12-well plate was first coated with a 1 mg/ml collagen layer prepared to the manufacturer's protocol with Waymouth 3D medium on ice. $NaHCO_3$ was added to the collagen mix in 10 µl steps until a pink color occurs to adjust pH value. 200 µl of the collagen mix were carefully pipetted onto each well of 12-well plate and left to polymerize for 30 minutes at 37°C.

After overnight culture, acinar cells were washed with 10 ml HBSS and centrifuged at 300 xg for five minutes, supernatant was discarded and cells were resuspended in Waymouth 3D medium. In order to distribute the cells on top of the collagen layer in the 12-well plate, the cellular layer mix was prepared as described above , however instead of Waymouth 3D media, the cell suspension was used. Then 1000 µl of the cell suspension were carefully transferred onto the collagen-coated 12-well plate and left to polymerize for one hour at 37°C.

3.12.2. Treatment of acinar 3D collagen cultures

After embedding acinar cells in the 3D cultures and polymerization of the collagen, 1000 µl of 2D medium and 50 ng/ml of Transforming growth factor-α (TGF-α) from Thermo Scientific (Waltham, Massachusetts, USA) were added. Additionally, acinar 3D cultures were treated with 0.05 ng/ml recombinant IL-33 and 500 U/ml recombinant IFN-α for the total amount of

cell culturing, which was added to the 2D medium (concentration was calculated for the combined volume of the cellular layer and medium above). Cells were incubated at 37°C for seven days, with a change of Waymouth 2D medium twice.

24 hours before harvesting the 3D cultures, cells were treated with 5-Bromo-2-deoxyuridine (BrdU) from Sigma-Aldrich (St. Louis, Missouri, USA) in a concentration of 10 µM to enable BrdU staining later. On the seventh day, 3D cultures were harvested, fixed with 4 % paraformaldehyde in PBS overnight at RT and embedded in paraffin.

3.12.3. Cytospin

Cells in suspension can be attached to slides in a Cytospin by centrifugation at 750 xg for five minutes. Therefore, 160 µl of the acinar suspension or 100 µl of pDCs was applied to each slide using the EZ Cytofunnels. Slides were left to dry overnight, fixed in methanol for 10 minutes, and stored at -20° C.

3.12.4. LDH-Glo cytotoxicity Assay

To analyze cell stress, lactate dehydrogenase (LDH) was measured using the LDH-Glo cytotoxicity Assay according the manufacturer's instructions. 1 µl of fresh supernatant from the cell culture was mixed with 99 µl of LDH storage buffer. Samples were stored at -20°C if needed. For LDH assay, 50 µl of a stored sample was pipetted into a well of an opaque 96-well plate and mixed with 50 µl of LDH detection mix (50 µl LDH enzyme buffer with 0.25 µl reductase substrate). The samples were incubated for one hour at room temperature under light protection. Luminescence was measured via spectrophotometer SpectraMax® Plus 384 Microplate Reader. Acinar medium was used as a negative control.

3.12.5. RNA isolation, quantity and quality control

RNA isolation was done using the RNeasy Plus Mini Kit according to the manufacturer's protocol. 600 µl of RLT Plus buffer including β-mercaptoethanol were used per sample. RNA samples were stored at -80°C.

After RNA isolation, RNA concentration was measured using the SpectraMax Plus 384 Microplate Reader according to manufacturer's instructions. The RNA quality was assessed via gel electrophoresis. For gel preparation, 0.8 % agarose was boiled in TAE buffer until dissolved completely. After cooling down and before casting the gel, paraformaldehyde was added to a final concentration of 0.4 % as well as SYBR Safe DNA gel stain (10 µl / 100 ml). Meanwhile, RNA samples were prepared for electrophoresis. For each sample 4 µl formamide, 2 µl 6x loading dye, 5 µl RNase-free water and 1 µl RNA was mixed, heated at 60°C for ten minutes and then loaded onto the gel. Gels were run at 70 Volts for about 30 minutes. Gene ruler 100bp

Plus was used as a ladder. Gels were scanned under UV light in a Fusion FX device after running.

3.12.6. cDNA synthesis and quantitative real-time PCR (qRT-PCR)

For cDNA synthesis the RevertAid First Strand cDNA Synthesis Kit was used. Procedures were followed from the provided protocol, using 2 µg template RNA and the Random Hexamer primer. cDNA was diluted in 80 µl water and stored at -20°C.

In quantitative real-time polymerase chain reaction (qRT-PCR), cDNA is amplified while the fluorescent dye (SYBR Green) binds to double-strand DNA during the process, allowing real-time monitoring of PCR product generation. Quantification is expressed as the cycle threshold (CT) value - the point when fluorescent intensity of a sample exceeds that of the background. The amplification of the housekeeping gene Ppib (Peptidyl-prolyl cis-trans isomerase B) was included as an endogenous control.

For qRT-PCR, samples were run in duplicates. Primers were designed to target genes of interest and with a melting temperature of 60°C. For each sample, a reaction mix was prepared containing 7.5 µl Go Taq® G2 Hot Start Green Master Mix, 4.5 µl water, 1 µl forward and 1 µl reverse primer and 1 µl of cDNA sample for on well of a qRT-PCR 96-Well plate. The qRT-PCR was run on a LightCycler® 96 using the PCR program depicted in

Table ***17***.

Table 17. qRT-PCR program

Step	**Temperature (°C)**	**Time (sec)**	**Cycle**
Pre incubation	95	300	
Amplification	95 55 68	15 15 15	40
Melting curve	95 65 98	1 20 Continuous 0.11°C/sec	 5 Acquisitions/sec
Cooling	37	∞	1

The ΔΔCt-value was used to calculate the normalized gene expression levels of each sample to controls (57). Therefore, the difference between the CT values of the housekeeper and the

sample marker were calculated (ΔCt) and experimental groups were additionally normalized to controls.

3.13. Statistical analysis

All experiments were performed at least three times. Shapiro test was performed to test for normality, which was not reached in all samples. Statistical analysis of H&E and IHC scores was done in R. Mann Whitney U test was performed with continuity correction to test for differences between the cohorts.

Analysis of flow cytometry of generated pDC and isolated bone marrow treated with acinar cell supernatant was done using GraphPad Prism Software, unpaired t-test was applied for testing for differences between the groups.

Analysis of LDH levels was done using GraphPad Prism Software, and unpaired t-test was performed with continuity correction to test for differences between the groups.

Calculations of ΔCt and ΔΔCt of qRT-PCR data was done in Excel. Statistical testing of gene expression was done in GraphPad with unpaired t-test.

For quantification of H&E-stained 3D culture slides, ADM structures were counted manually on scanned pictures. For each treatment group two samples were counted. Size of the ADM structures were determined by measuring the major and minor axes of each elliptical formation using Slideviewer Software. The elliptical circumference was calculated based on Ramanujan approximation:

$$u \approx (a+b)\,\pi\left(1+\frac{3\,\lambda^2}{10+\sqrt{4-3\,\lambda^2}}\right) \qquad \text{with} \qquad \lambda=\frac{a-b}{a+b}$$

Statistical testing for ADM numbers and size was done in GraphPad Prism Software, using unpaired t-test.

In all experiments p-values < 0.05 were considered significant (* P < 0.05; ** P < 0.01; *** P < 0.001; **** P < 0.0001).

4. Results

4.1. Histologic characterization of murine autoimmune pancreatitis

To characterize the immune cell infiltrate and pathophysiological changes in the pancreas of autoimmune pancreatitis (AIP), the MRL/MpJ mouse model was used and compared to acute pancreatitis (AP). MRL/MpJ mice treated with Poly(I:C) developed a strong phenotype of AIP and histologic features in the pancreas were compared to PT mice, which were treated with cerulein and developed AP. Histologic alterations of the inflammatory infiltrate, acinar cell damage, fatty replacement and acinar-to-ductal metaplasia (ADM) were assessed in the pancreas based on H&E staining (Figure 2A).

The inflammatory infiltrate was significantly more severe in AIP with intra- and interlobular immune cell infiltration into the exocrine compartment, compared to AP controls, in which immune cells infiltrated the pancreas less densely (mean score 2.7± 0.5 vs. 1.3 ± 0.5, p = 0.0021) (Figure 2B). Consistent with this observation, prominent lymph nodes were found interspersed within the pancreatic tissue in AIP. Acinar cell damage, determined by necrotic and apoptotic acinar cells, was significantly more severe in AIP compared to AP (mean score 2.4 ± 0.8 vs 1.2 ± 0.4, p = 0.0119) (Figure 2B). Most prominent was the significantly higher amount of fatty replacement in AIP, which was hardly seen in AP (mean score 2.3 ± 0.7 vs. 0.2 ± 0.4, p = 0.0011) (Figure 2B) and accompanied by atrophy of the pancreatic tissue. In AIP, the exocrine tissue was reduced in size, and pancreatic lobules were more distinctly separated by fibrotic septa compared to AP, which is a sign for edema. Furthermore, ADMs were a significantly more frequent finding in AIP than in AP (mean score 2.0 ± 0.8 vs. 0.5 ± 0.8, p = 0.0099) and were often located in the areas of the pancreas with the highest immune cell infiltration (Figure 2B).

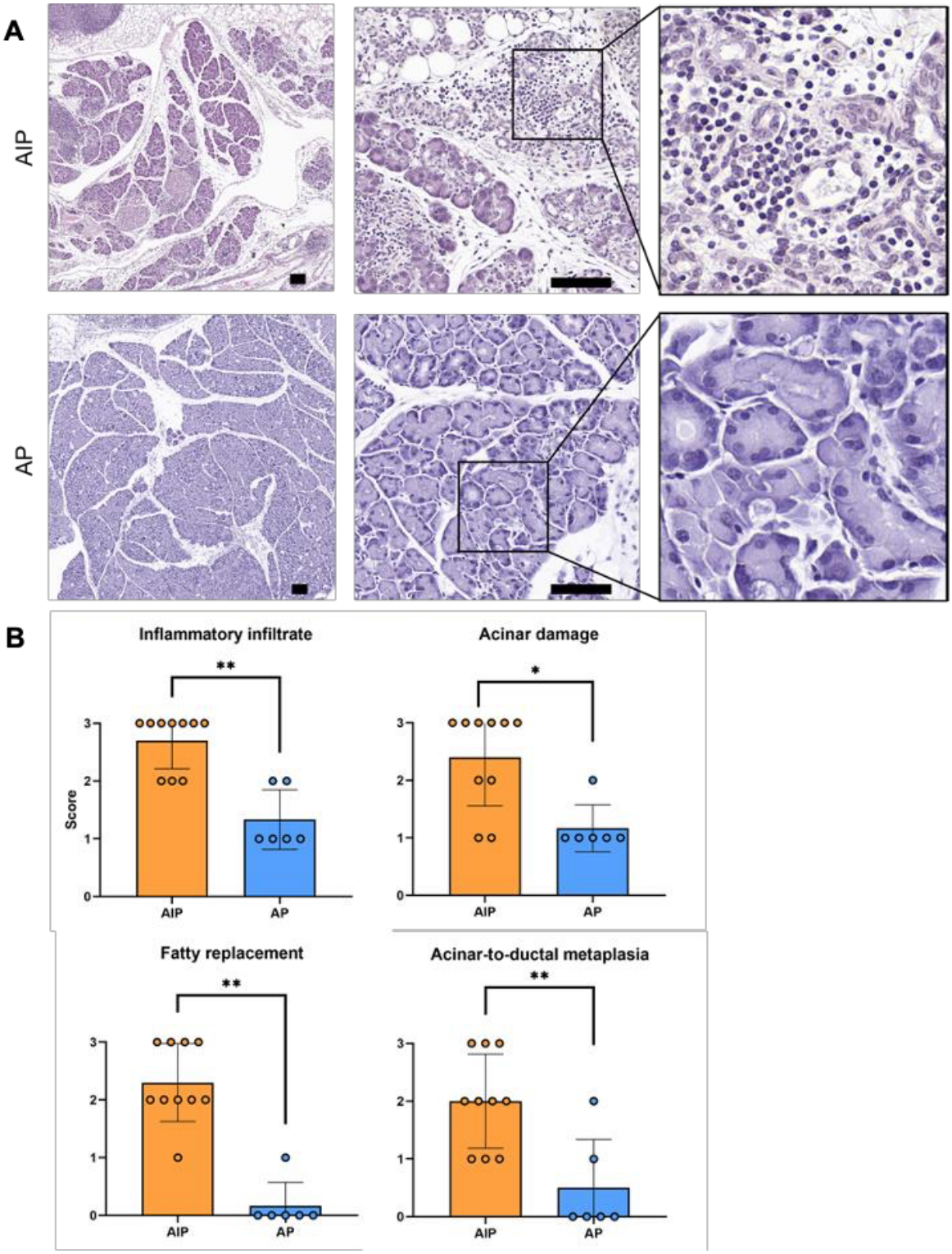

Figure 2. Histological comparison of AIP and AP. (A) H&E staining of pancreatic tissue of MRL/MpJ mice with autoimmune pancreatitis (AIP) and PT mice with acute pancreatitis (AP). Representative images show immune cell infiltrate, acinar damage, fatty replacement and ADM formation. Scale bar 100 µm. **(B)** Quantification of histological features with the following scores: 0=none, 1=mild, 2=moderate, 3=severe. Data are represented as mean ± SD, each dot represents a sample (n= 10 for AIP, n = 6 for AP). Mann Whitney U test was performed with continuity correction to test for differences between the groups. A two-tailed p-value was used, p-values < 0.05 were considered significant (* $P < 0.05$; ** $P < 0.01$).

To determine the immune infiltrate in detail for specific immune cell populations, IHC staining was performed using the following markers: CD45 for general immune cells, CD4 for T helper cells, CD8 for cytotoxic T cells, FoxP3 for Tregs, CD11c for dendritic cells and F4/80 for macrophages. Comparison of AIP and AP immune cell infiltrates was done using regular IHC, except for CD45, CD8 and FoxP3, which was done using IHC multiplex staining.

The overall amount of the general immune cell population was visualized by CD45 staining (Figure 3A). Here, AIP revealed significantly more infiltrating immune cells in the pancreatic tissue, compared to AP, which showed only mild infiltration of CD45 positive cells (mean score 2.4 ± 0.7 vs. 0.7 ± 0.8, $p = 0.0041$) (Figure 3B). In AIP, CD45 positive cells were predominantly concentrated around the outer regions of the pancreatic lobules, appearing to infiltrate from the septa toward the center of exocrine tissue. This is in line with the histological assessment in H&E staining, which showed a highly inflammatory process during AIP accompanied by severe acinar damage. In comparison, the immune cell infiltrate appeared to be more evenly spread and less dense in AP.

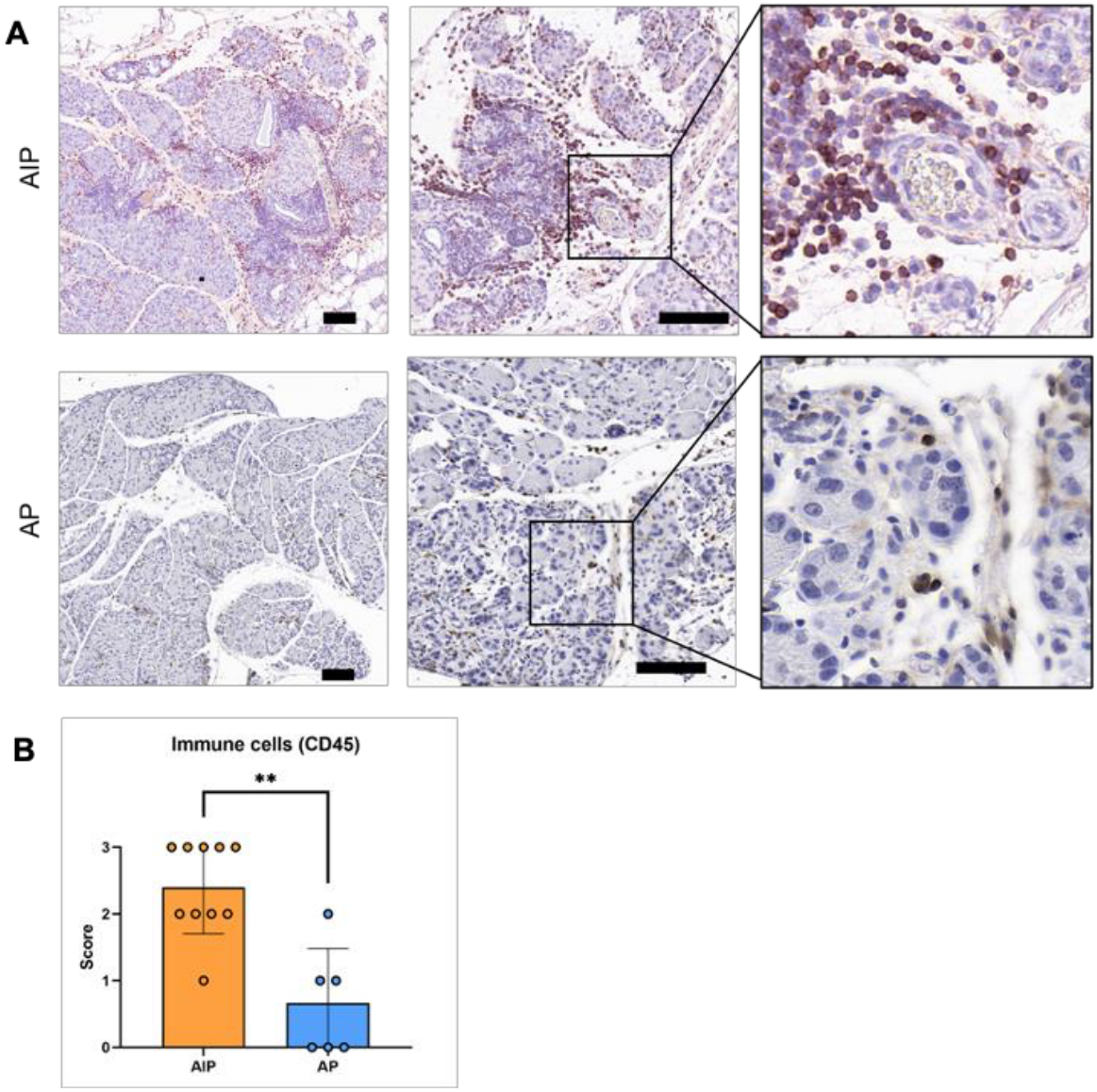

Figure 3. Immunohistochemical analysis of CD45 on AIP and AP pancreatic tissue. (**A)** Representative images of CD45 IHC staining of pancreatic tissue of MRL/MpJ mice with autoimmune pancreatitis (AIP) and PT mice with acute pancreatitis (AP). Scale bar 100 µm. (**B)** Presence of CD45 positive cells was scored as following: 0=none, 1=mild, 2=moderate, 3=severe. Data are represented as mean ± SD, each dot represents a sample (n= 10 for AIP, n = 6 for AP). Mann Whitney U test was performed with continuity correction to test for differences between the cohorts. A two-tailed p-value was used, p-values < 0.05 were considered significant (* $P < 0.05$; ** $P < 0.01$).

To determine immune cell subtypes, further IHC staining was performed. Since AIP is known to be a T cell driven disease (1, 48), CD4 staining was done (Figure 4A), which revealed a complete absence of T helper cells in AIP and hardly any CD4 positive cells in AP (mean score 0.0 ± 0 vs. 0.2 ± 0.4, p = 0.2453) (Figure 4B). This observation is distinctive and prompts the question of which other immune cell subpopulations may serve as the principal mediators of inflammation in AIP, given the pronounced CD45 infiltration. In the picture of AP in Figure 4A, the adjacent spleen showed a high abundance of T helper cells, serving as a positive control and further highlighting that T helper cells do not play a central role in AP.

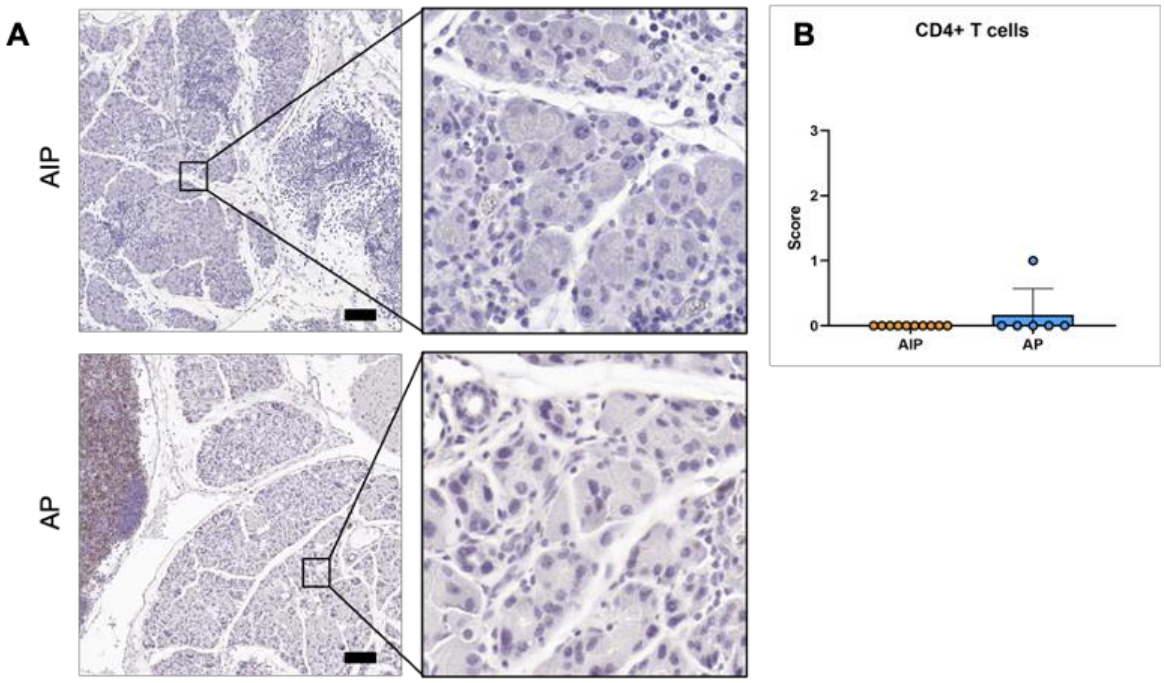

Figure 4. Immunohistochemical analysis of CD4 on AIP and AP pancreatic tissue. **(A)** Representative images of CD4 IHC staining of pancreatic tissue of MRL/MpJ mice with autoimmune pancreatitis (AIP) and PT mice with acute pancreatitis (AP). Scale bar 100 µm. **(B)** Presence of CD4 positive cells was scored as following: 0=none, 1=mild, 2=moderate, 3=severe. Data are represented as mean ± SD, each dot represents a sample (n= 10 for AIP, n = 6 for AP). Mann Whitney U test was performed with continuity correction to test for differences between the cohorts. A two-tailed p-value was used, p-values < 0.05 were considered significant (* P < 0.05).

Since AIP is a T-cell driven disease, cytotoxic T cells were evaluated by CD8 IHC staining (Figure 5A). In AIP, an intense infiltrate of cytotoxic T cells was found, whereas hardly any CD8 positive cells were found in AP, reaching significance (mean score 2.3 ± 0.7 vs. 0.2 ± 0.4, p = 0.0015) (Figure 5B). Similar to the CD45 staining pattern, CD8 T cells in AIP were primarily concentrated around the outer regions of the pancreatic lobules, appearing to infiltrate from the outer membranes toward the center of the lobules. In these densely infiltrated tissue sections, acinar damage also appeared most severe, aligning with the findings of H&E. In AP, cytotoxic T cells were rarely detected within the tissue, further emphasizing the distinct differences in immune cell recruitment pathways between the two diseases.

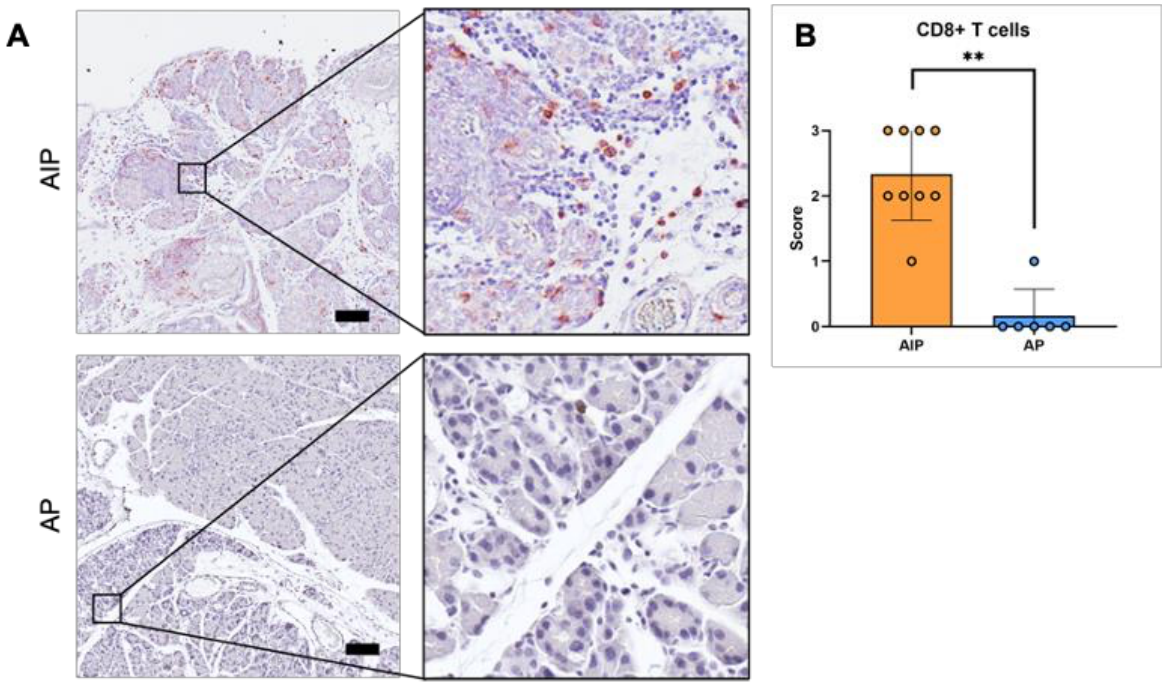

Figure 5. Immunohistochemical analysis of CD8 on AIP and AP pancreatic tissue. **(A)** Representative images of CD8 IHC staining of pancreatic tissue of MRL/MpJ mice with autoimmune pancreatitis (AIP) and PT mice with acute pancreatitis (AP). Scale bar 100 µm. **(B)** Presence of CD8 positive cells was scored as following: 0=none, 1=mild, 2=moderate, 3=severe. Data are represented as mean ± SD, each dot represents a sample (n= 10 for AIP, n = 6 for AP). Mann Whitney U test was performed with continuity correction to test for differences between the cohorts. A two-tailed p-value was used, p-values < 0.05 were considered significant (* P < 0.05; ** P < 0.01).

Another critical T cell subtype are Tregs, which are essential for modulating immune activation and immune suppression (50). Treg cells were quantified by FoxP3 staining. In AIP, particularly within pancreas-associated lymph nodes, Tregs were notably abundant (Figure 6A). This observation aligns with the H&E findings, in which a prominent presence of lymph nodes was observed in AIP tissue samples. However, within the pancreatic tissue itself, Tregs were scarce in AIP. When present, Tregs appeared mostly as single cells closely associated with other immune cells. In contrast, Tregs were entirely absent in acute pancreatitis (AP), also in pancreas-associated lymph nodes, highlighting the cells as a distinguishing feature of AIP (mean score 0.8 ± 0.4 vs. 0.0 ± 0, p = 0.003) (Figure 6B).

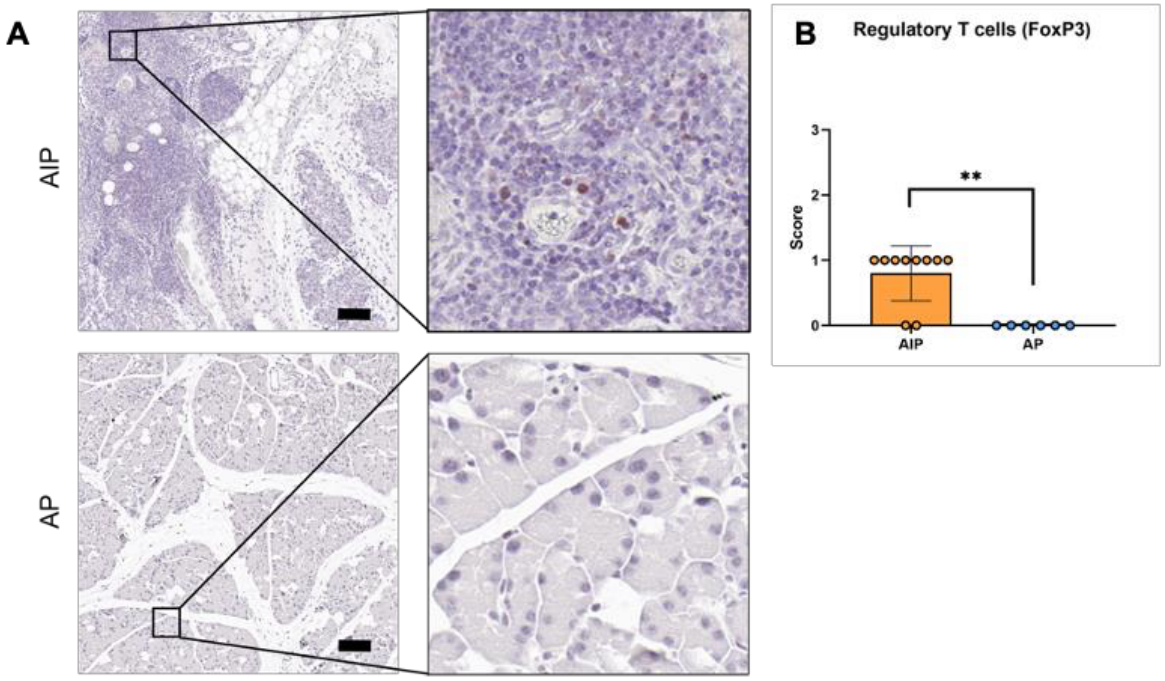

Figure 6. Immunohistochemical analysis of FoxP3 on AIP and AP pancreatic tissue. **(A)** Representative images of FoxP3 IHC staining of pancreatic tissue of MRL/MpJ mice with autoimmune pancreatitis (AIP) and PT mice with acute pancreatitis (AP). Scale bar 100 µm. **(B)** Presence of FoxP3 positive cells was scored as following: 0=none, 1=mild, 2=moderate, 3=severe. Data are represented as mean ± SD, each dot represents a sample (n= 10 for AIP, n = 6 for AP). Mann Whitney U test was performed with continuity correction to test for differences between the cohorts. A two-tailed p-value was used, p-values < 0.05 were considered significant (* P < 0.05; ** P < 0.01).

To investigate pDCs within the inflammatory infiltrate, which are known key mediators in AIP, CD11c staining was performed (Figure 7A). CD11c is a marker for both plasmacytoid and classical dendritic cells. This staining revealed a high abundance of dendritic cells in AIP, whereas they were scarcely observed in AP (mean score 1.7 ± 0.7 vs. 0.3 ± 0.5, p = 0.0036) (Figure 7B). This finding underscores the unique role of dendritic cells in the inflammatory environment of AIP, as they appear to play little to no role in AP. Although CD11c marks both plasmacytoid and classical dendritic cells, the staining confirms that overall dendritic cell presence is significantly higher in AIP compared to AP.

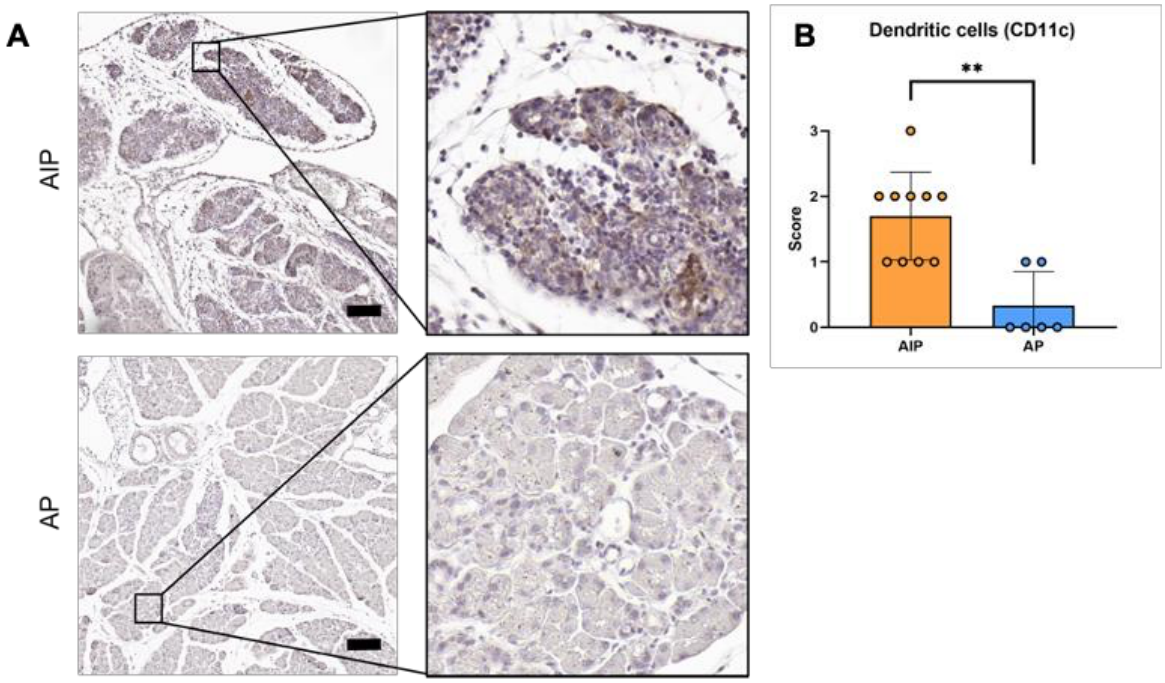

Figure 7. Immunohistochemical analysis of CD11c on AIP and AP pancreatic tissue. **(A)** Representative images of CD11c IHC staining of pancreatic tissue of MRL/MpJ mice with autoimmune pancreatitis (AIP) and PT mice with acute pancreatitis (AP). Scale bar 100 µm. **(B)** Presence of CD11c positive cells was scored as following: 0=none, 1=mild, 2=moderate, 3=severe. Data are represented as mean ± SD, each dot represents a sample (n= 10 for AIP, n = 6 for AP). Mann Whitney U test was performed with continuity correction to test for differences between the cohorts. A two-tailed p-value was used, p-values < 0.05 were considered significant (* P < 0.05; ** P < 0.01).

Macrophages are usually the predominant cells within the immune infiltrate of AP (70). To examine their role in AIP, F4/80 staining was used. As anticipated, macrophages were highly abundant in AP, forming an even distribution around damaged acinar cells and ADMs (Figure 8A). In contrast, no macrophages were observed in AIP, marking this as a distinguishing feature to AP (mean score AIP 2.0 ± 0.9 vs. AP 0.0 ± 0, p = 0.0002) (Figure 8B). This observation aligns with the current understanding of AIP, which is not triggered by external stressors leading to acinar cell damage and subsequent recruitment of cells of the innate immune system, as seen in AP, but is instead likely initiated by cells of the adaptive immune system.

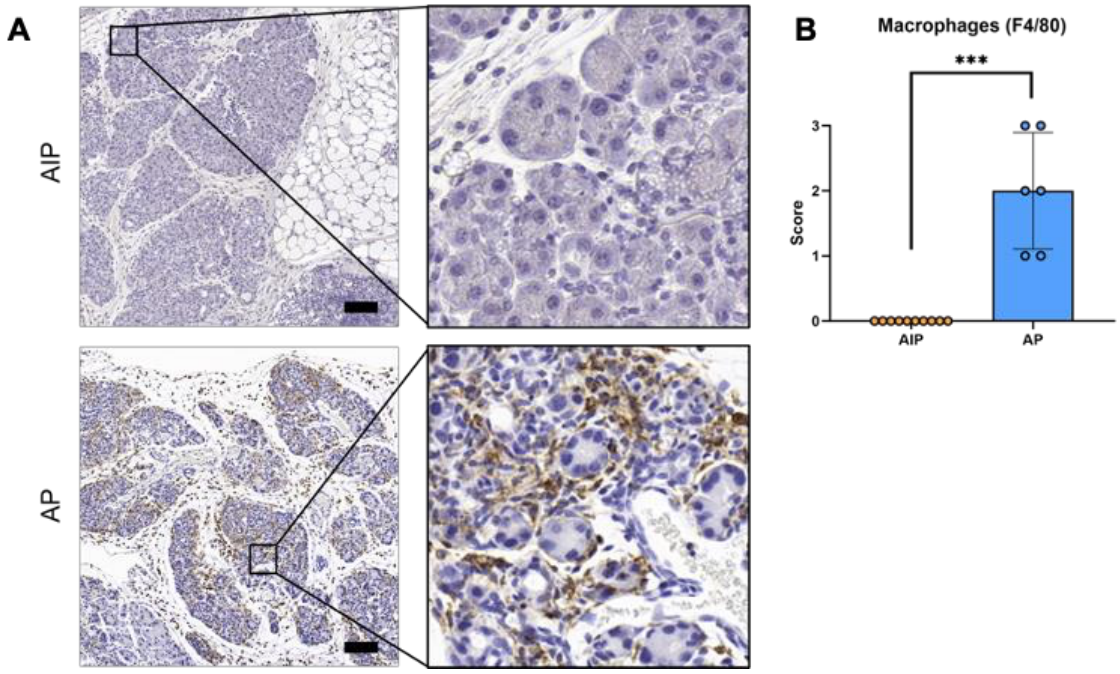

Figure 8. Immunohistochemical analysis of F4/80 on AIP and AP pancreatic tissue. **(A)** Representative images of F4/80 IHC staining of pancreatic tissue of MRL/MpJ mice with autoimmune pancreatitis (AIP) and PT mice with acute pancreatitis (AP). Scale bar 100 µm. **(B)** Presence of F4/80 positive cells was scored as following: 0=none, 1=mild, 2=moderate, 3=severe. Data are represented as mean ± SD, each dot represents a sample (n= 10 for AIP, n = 6 for AP). Mann Whitney U test was performed with continuity correction to test for differences between the cohorts. A two-tailed p-value was used, p-values < 0.05 were considered significant (* P < 0.05; ** P < 0.01; *** P < 0.001).

Besides the immune cell infiltrate, additional cell markers were examined with IHC to study markers of acinar cell regeneration, such as ADM formation and acinar cell proliferation, Additionally, the expression of Ifn-activating transcription factors Irf3 and Irf7 were assessed in acinar and immune cells. The scoring was evaluated separately between acinar and immune cells. Cytokeratin (Ck)19 was used as a marker for ADM, and phospho-histone H3 (PHH3) for cell proliferation.

To further investigate the increased prevalence of ADM, observed in AIP with H&E staining, Ck19 staining was used to quantify ADM formations within the exocrine compartment. Ck19, a cytoskeletal marker exclusively expressed in ductal cells and not in acinar cells, provides a reliable marker for detecting ADM (71). In AIP, Ck19 signal consistently appeared in ADM formations, whereas minimal expression was noted in AP (Figure 9A). This staining confirmed the H&E findings, with ADM significantly more prevalent in AIP (mean score 1.7 ± 0.5 vs. 0.3 ± 0.5, p = 0.0021) (Figure 9B). Ck19 is not expressed in immune cells, therefore it was only scored for the exocrine pancreatic tissue.

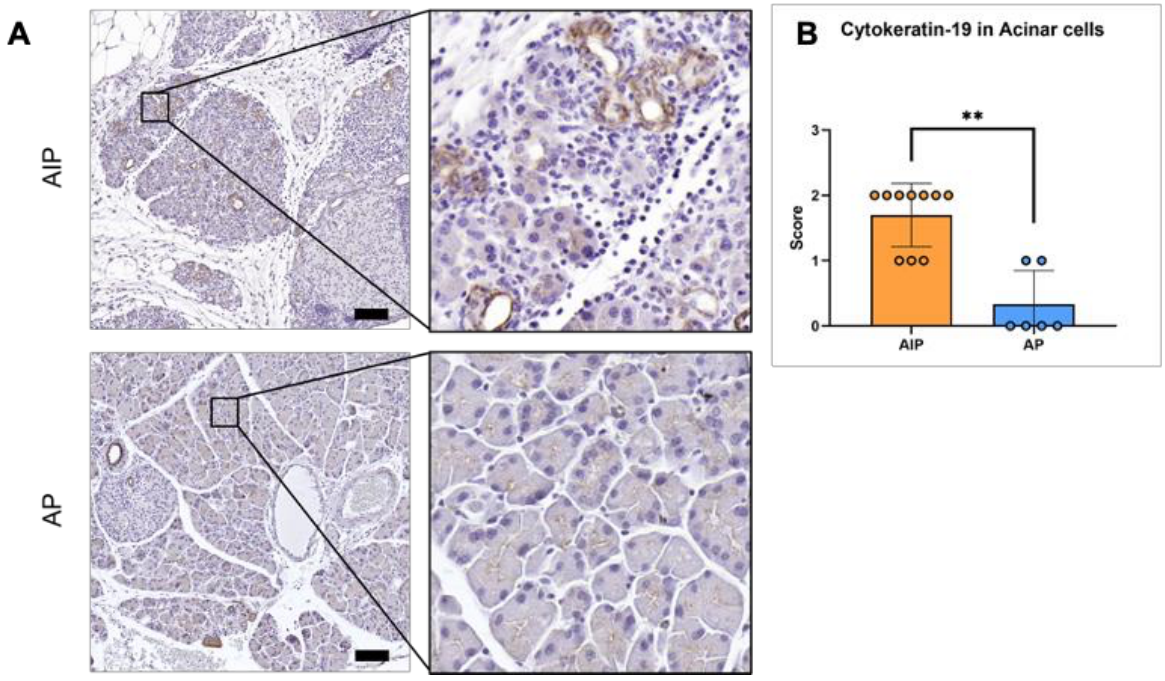

Figure 9. Immunohistochemical analysis of Ck19 on AIP and AP pancreatic tissue. **(A)** Representative images of Ck19 IHC staining of pancreatic tissue of MRL/MpJ mice with autoimmune pancreatitis (AIP) and PT mice with acute pancreatitis (AP). Scale bar 100 μm. **(B)** Presence of Ck19 positive cells was scored as following: 0=none, 1=mild, 2=moderate, 3=severe. Data are represented as mean ± SD, each dot represents a sample (n= 10 for AIP, n = 6 for AP). Mann Whitney U test was performed with continuity correction to test for differences between the cohorts. A two-tailed p-value was used, p-values < 0.05 were considered significant (* P < 0.05; ** P < 0.01).

To further assess pancreatic regenerative capacity, PHH3 staining was conducted to examine the proliferation of acinar and immune cells (Figure 10A). In acinar cells, PHH3 staining revealed a significantly weaker signal in AIP compared to AP (mean score 0.0 ± 0 vs. 0.7 ± 0.5, p = 0.0049), indicating a reduced proliferative capacity (Figure 10B). This aligns with H&E staining findings, which showed increased acinar cell damage and fatty replacement of exocrine tissue, indicative of pancreatic atrophy. In immune cells, PHH3 staining demonstrated mild levels in both AIP and AP, suggesting some degree of immune cell proliferation in both forms of pancreatitis (mean score 1.0 ± 0 vs. 1.2 ± 0.4, p = 0.2453) (Figure 10B).

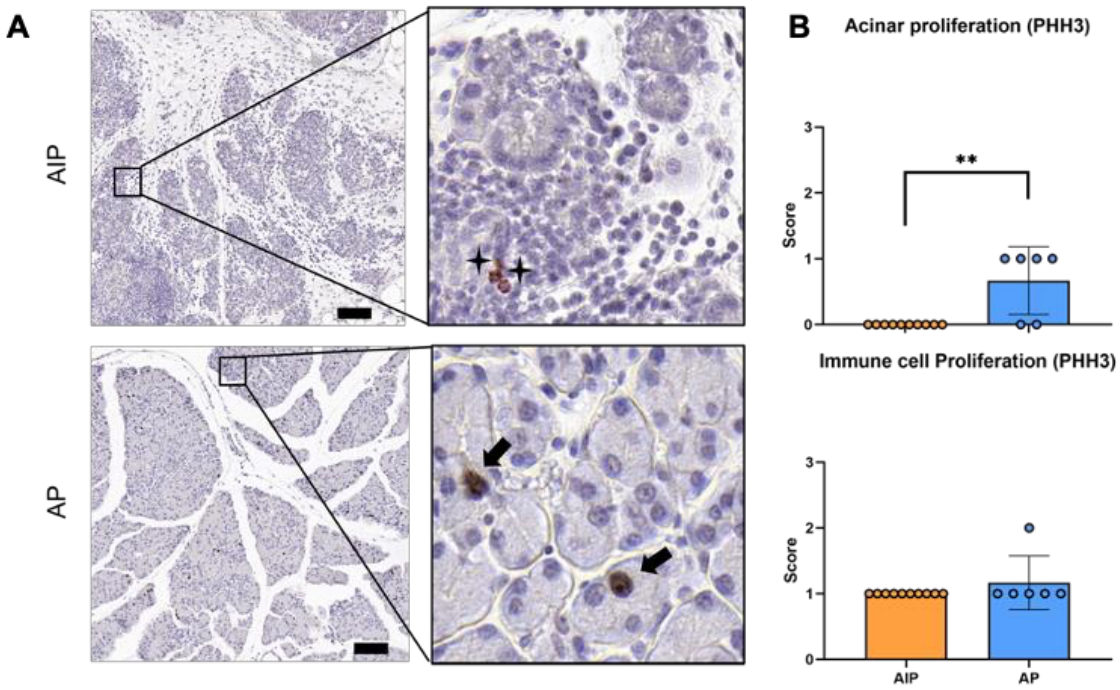

Figure 10. Immunohistochemical analysis of PHH3 on AIP and AP pancreatic tissue. **(A)** Representative images of PHH3 IHC staining of pancreatic tissue of MRL/MpJ mice with autoimmune pancreatitis (AIP) and PT mice with acute pancreatitis (AP). Examples of immune cells marked with stars; examples of acinar cells marked with arrows. Scale bar 100 µm. **(B)** Presence of PHH3 positive cells was scored as following: 0=none, 1=mild, 2=moderate, 3=severe. Data are represented as mean ± SD, each dot represents a sample (n= 10 for AIP, n = 6 for AP). Mann Whitney U test was performed with continuity correction to test for differences between the cohorts. A two-tailed p-value was used, p-values < 0.05 were considered significant (* P < 0.05; ** P < 0.01).

Given that Irf3 is expressed in many immune cells and important for IFN-α and IFN-β production (27), we performed IHC staining of Irf3. Since its role in acinar cells remains unclear, it was analyzed it separately in acinar and immune cells. Irf3 positive immune cells, were detected only in AIP (Figure 11A), and not in AP (mean score 2.0 ± 0.8 vs. 0.0 ± 0, p = 0.0011) (Figure 11B). Notably, the previous IHC profiling revealed that AIP was characterized by an immune cell infiltrate dominated by T cells (CD4 and CD8) and pDCs, whereas macrophages were the primary immune cell population in AP. These different cell types produce a variety of cytokines with pDCs as the main producers of IFN-α in AIP. The absence of Irf3-positive immune cells in AP suggest that Irf3 positive immune cells are a specific feature of AIP. Interestingly, Irf3 was additionally detectable in acinar cells. There was a trend toward stronger Irf3 signals in AIP than in AP; however, this difference was not statistically significant (mean score 1.6 ± 0.9 vs. 0.7 ± 0.8, p = 0.0838) (Figure 11B). The data suggest that Irf3 expression is moderately activated in acinar cells during inflammation, regardless of the type of pancreatitis.

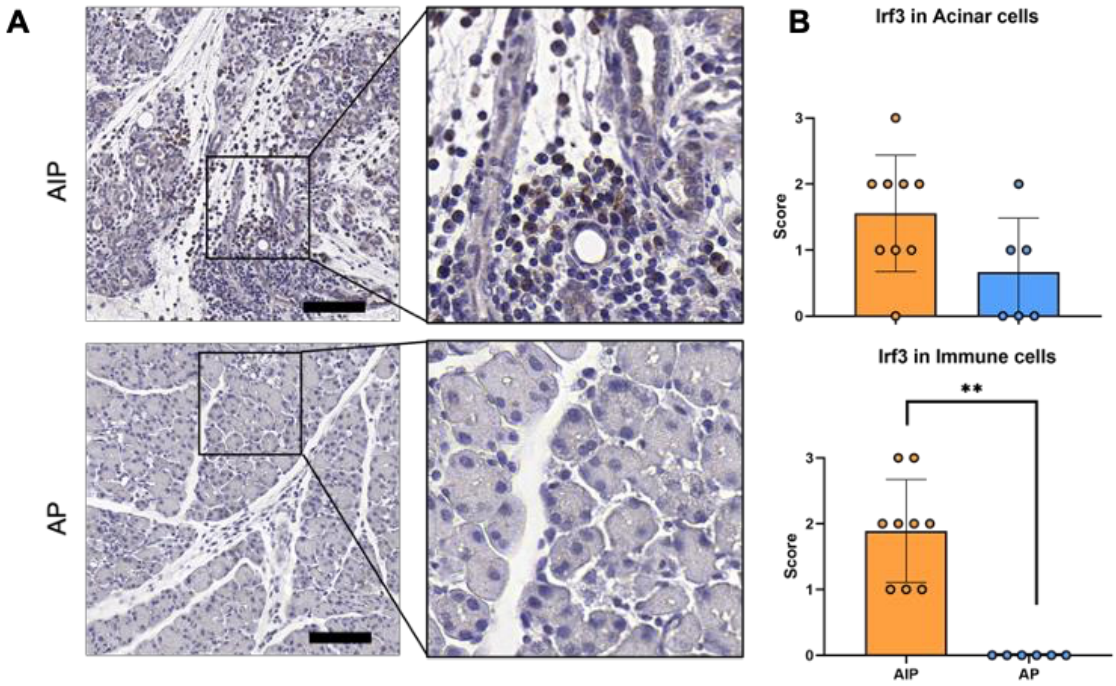

Figure 11. Immunohistochemical analysis of Irf3 on AIP and AP pancreatic tissue. **(A)** Representative images of Irf3 IHC staining of pancreatic tissue of MRL/MpJ mice with autoimmune pancreatitis (AIP) and PT mice with acute pancreatitis (AP). Scale bar 100 µm. **(B)** Presence of Irf3 positive cells was scored as following: 0=none, 1=mild, 2=moderate, 3=severe. Data are represented as mean ± SD, each dot represents a sample (n= 10 for AIP, n = 6 for AP). Mann Whitney U test was performed with continuity correction to test for differences between the cohorts. A two-tailed p-value was used, p-values < 0.05 were considered significant (* $P < 0.05$; ** $P < 0.01$).

In addition to Irf3, Irf7 regulates IFN-α production in pDCs (35) and was therefore analyzed in both acinar and immune cells. Irf7 positive immune cells were exclusively detected in AIP (Figure 12A), but not in AP (mean score: 0.8 ± 0.6 vs. 0.0 ± 0; p = 0.0114) (Figure 12B). Similarly to Irf3, Irf7 is expressed by T cells (CD4 and CD8) and pDCs, the main producers of IFN-α, while macrophages dominate in AP. The absence of Irf3-positive cells in AP highlights their specificity to AIP. Similarly, Irf7 staining was significantly elevated in acinar cells in AIP compared to AP (Figure 12A), where only mild activation was observed (mean score: 1.8 ± 0.6 vs. 0.3 ± 0.5; p = 0.0025) (Figure 12B). This indicates that Irf7 activation in acinar cells is a characteristic feature of AIP.

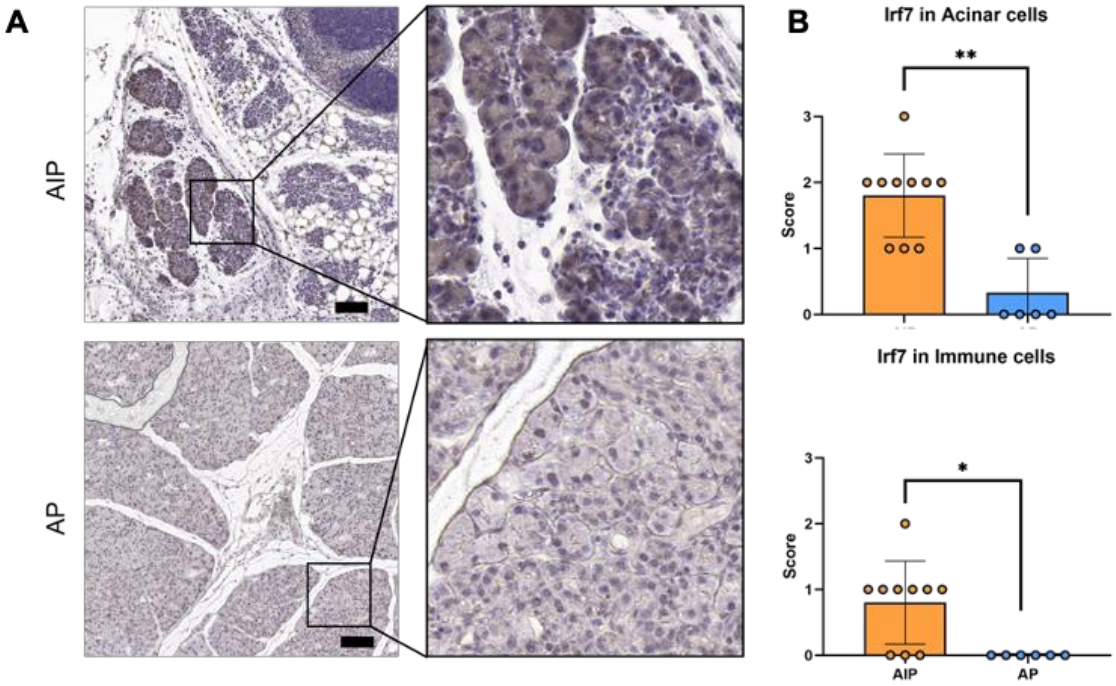

Figure 12. Immunohistochemical analysis of Irf7 on AIP and AP pancreatic tissue. **(A)** Representative images of Irf7 IHC staining of pancreatic tissue of MRL/MpJ mice with autoimmune pancreatitis (AIP) and PT mice with acute pancreatitis (AP). Scale bar 100 µm. **(B)** Presence of Irf7 positive cells was scored as following: 0=none, 1=mild, 2=moderate, 3=severe. Data are represented as mean ± SD, each dot represents a sample (n= 10 for AIP, n = 6 for AP). Mann Whitney U test was performed with continuity correction to test for differences between the cohorts. A two-tailed p-value was used, p-values < 0.05 were considered significant (* $P < 0.05$; ** $P < 0.01$).

4.2. Generation and characterization of plasmacytoid dendritic cells

The direct effects of pDCs on acinar cell stress, damage and regenerative capacities were studied in the following experiments, for which pDCs were generated *in vitro*. Generation of pDC was performed from bone marrow of WT and Irf3/7-KO mice as described in the Methods (Plasmacytoid dendritic cells) section. Before harvesting the cells on day seven after FLT3L treatment, cell suspension was photographed under light microscopy and showed single cells with some cells presenting a star-like shape, perhaps forming dendritic extensions (Figure 13A). To further confirm efficient *in vitro* generation of pDCs, flow cytometry of the suspension cell culture was performed (Figure 13B). Flow cytometry analysis revealed that out of all measured events (including dead cells and debris), the Irf3/7-KO group (n=3) exhibited a significantly higher percentage of live cells compared to the WT group (n=3) (49.6 % ± 3.6 % vs. 19.2 % ± 7.4 % alive cells, $p = 0.0031$) (Figure 13C). This suggests that WT bone marrow cells were significantly less viable during cell culturing, perhaps due to immune cells in the WT group being able to activate the IFN cascade, which may have resulted in a more aggressive response to the culture conditions. Out of all living cells, 35.4 % ± 6.0 % in the WT group were positive for the SiglecH/ B220 double staining, identifying them as pDCs. In comparison, in Irf3/7-KO cell suspension 31.8 % ± 8.2 % were identified as pDCs via SiglecH/ B220 double staining (no significant difference, $p = 0.5743$) (Figure 13D). Thus, although WT bone marrow produced fewer viable cells after culturing, pDC generation was successful regardless of Irf3/7 status, resulting in comparable percentages of pDCs among alive cells.

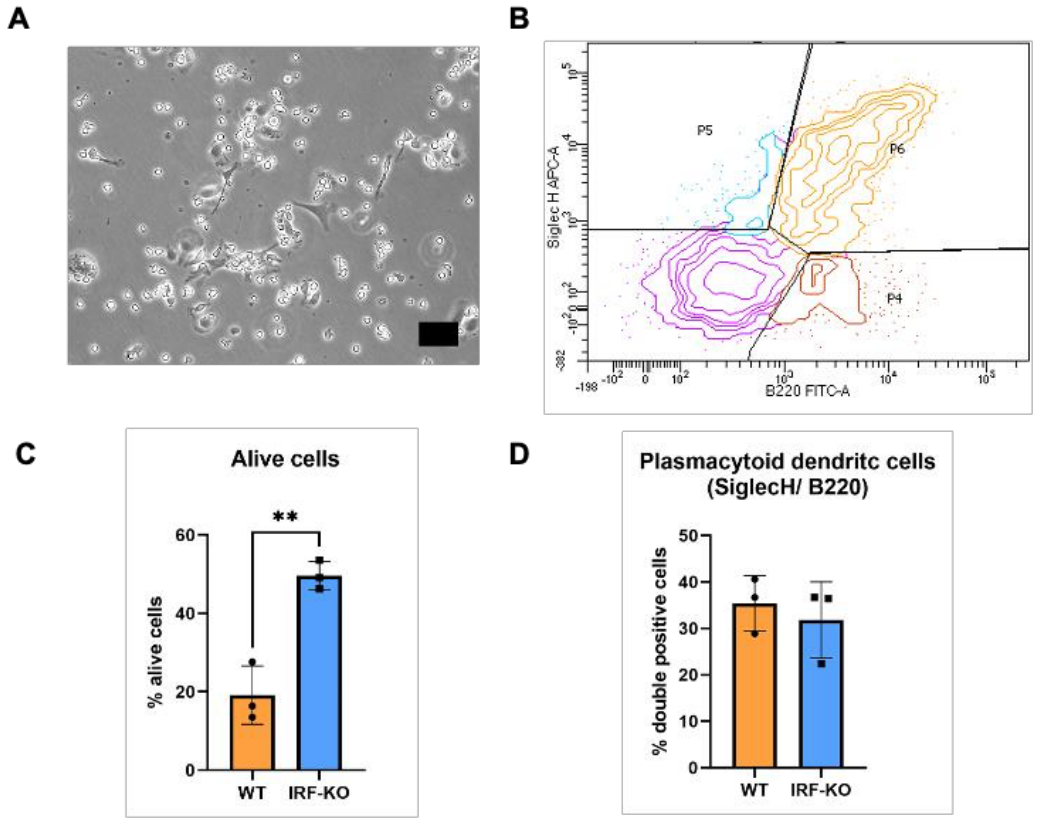

Figure 13. pDC generation from bone marrow. (A) Representative image of an *in vitro* WT cell suspension for pDC generation, under BF microscopy, showing isolated bone marrow cells on day seven after FLT3L (200 ng/ml) treatment. Scale bar 50 µm. **(B)** Representative image of flow cytometry of a WT pDC culture. Cells were first gated for single and alive cells using Annexin and Propidium Iodide solution, then gating was done using SiglecH and B220 to detect pDCs. **(C)** Quantification of living cells using Annexin and Propidium Iodide staining from WT and Irf3/7-KO pDC. **(D)** Quantification of pDCs defined as SiglecH and B220 double-positive cells from WT and Irf3/7-KO bone marrow. Data are represented as mean ± SD, each dot represents an independent experiment (n=3). Unpaired t-test was performed to test for differences between the cohorts. A two-tailed p-value was used, p-values < 0.05 were considered significant (* $P < 0.05$; ** $P < 0.01$).

4.3. Acinar cells do not trigger pDC differentiation

To test the hypothesis if acinar cell damage might trigger pDC differentiation in a reciprocal way, bone marrow of WT mice was isolated and put into cell suspension as before, however this time without the pDC stimulant FLT3L. Instead, different variations of supernatant from overnight acinar suspension cultures, in which the cells are under strong stress conditions and also exhibit acinar cell damage, were used to cultivate the bone marrow cells. After 7 days the bone marrow cells were analyzed with flow cytometry for pDC differentiation.

As a positive control, bone marrow cells were cultivated in regular pDCs generation media, whereas the negative control lacked FTL3 supplement. To account for potential effects of the acinar culture medium, bone marrow cells were cultured with supernatants from acinar cell

cultures using various medium combinations, either with and without dexamethasone (dexa) or trypsin inhibitor (TI). Dexamethasone is a corticosteroid and suppresses immune function, while trypsin inhibitors prevent trypsin activation in acinar cells. Typically, trypsin inhibitors are added to minimize acinar cell damage. However, in this experiment, the trypsin inhibitor was omitted from the medium to promote increased acinar cell damage.

The positive control (regular pDC generation) resulted in a mean of 19.2 % ± 7.4 % alive cells; and out of all alive cells, 35.4 % ± 6.0 % were SiglecH/ B220 positive, identifying them as pDC (Figure 14). The negative control showed an average amount of 12.8 % ± 4.4 % alive cells, and only 1.8 % ± 1.7 % of Siglec H/B220 double positive cells, signifying that as expected only very few pDC develop spontaneously (Figure 14).

The survival of bone marrow cells treated with acinar supernatant depended on the composition of the acinar culture medium. Acinar supernatant derived from the harshest conditions (containing dexa and no TI) resulted in only 1.9 % ± 1.0 % cell survival, significantly lower than the positive ($p = 0.0051$) and negative control ($p = 0.0042$) (Figure 14A). This outcome aligns with the immunosuppressive effects of dexamethasone combined with the enhanced release of acinar enzymes due to the absence of trypsin inhibitor. In contrast, acinar supernatant containing medium with TI was associated with cell survival, likely due to decreased acinar cell damage.

Treatment of bone marrow cells with acinar supernatants, did not result in pDC differentiation, regardless of the acinar media conditions. Across all treatment groups, ≤1 % of live cells were SiglecH/ B220 positive. This was comparable to the negative control and significantly lower compared to the positive control (acinar supernatant vs. positive control: $p < 0.0001$, $p = 0.0043$, $p < 0.0001$) (Figure 14B).

These experiments showed that supernatant from various acinar cell cultures, from more or less damaged acinar cells, do not trigger pDC differentiation of bone marrow cells.

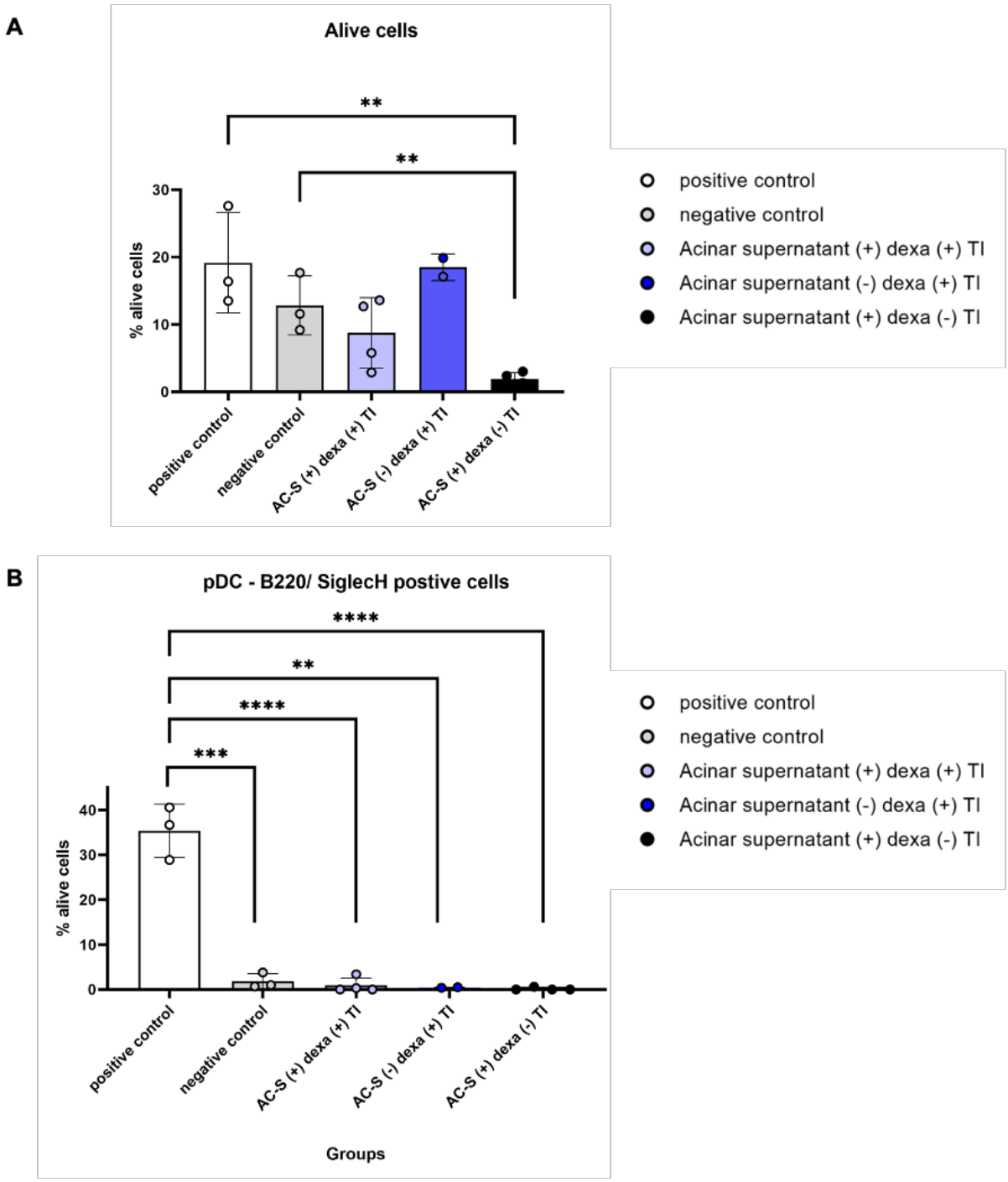

Figure 14. Treatment of bone marrow with acinar supernatant. Quantification of alive bone marrow cells depending on treatment status: After isolation of bone marrow, cells were treated with different variations of acinar cell supernatants and incubated for seven days. (**A)** Flow cytometry using Annexin and Propidium Iodide solution was used to gate single and alive cells. (**B)** Further gating was done using SiglecH and B220 to detect pDC in flow cytometry. Data are represented as mean ± SD, each dot represents an independent experiment sample (n=3-4). Unpaired t-test was performed with continuity correction to test for differences between the cohorts. A two-tailed p-value was used, p-values < 0.05 were considered significant (* $P < 0.05$; ** $P < 0.01$; *** $P < 0.001$; **** $P < 0.0001$).

4.4. Effect of pDC supernatant and related cytokines on acinar cells

To test if pDCs affect cell stress and damage in acinar cells through their associated cytokines, IFN-α and IL-33, acinar cell culture experiments were conducted: Isolated acinar cells from WT mice were cultured in suspension and treated with IL-33 and IFN-α. To further test the hypothesis of cell stress and damage being mediated through a pDC-IFN-α cascade, acinar cell suspensions were treated with supernatants from generated pDCs of WT mice (WT pDC) and Irf3/7-KO mice (Irf3/7-KO pDC), the latter being unable to produce IFN-α. All described cell suspensions were treated for 6 hours as described in the Methods section "Treatment of acinar cell suspension cultures". A control at 0 and 6 hours for regular acinar cell culture was included, in addition.

The effects on acinar cells were assessed through LDH measurements to evaluate cell stress and qRT-PCR to analyze RNA expression of selected target genes involved in proinflammatory signaling and cell death, providing insights into cell stress, damage, and regenerative capacities.

4.4.1. LDH measurement for cell stress

Cell stress of acinar cells under the different treatment conditions was measured with an LDH-Glo cytotoxicity Assay. A negative control was used to detect background noise and all measurements were normalized to the negative control.

No differences in LDH levels were observed in IFN-α and IL-33 treated acinar cells compared to untreated cells after 6 hours, suggesting no significant changes in cell stress in these conditions. In contrast, acinar cells treated with supernatant from Irf3/7-KO pDCs showed a significant increase in LDH levels compared to both the 6-hour control and acinar cells treated with WT pDC supernatant ($p = 0.0010$ and $p = 0.0187$, respectively) (Figure 15A). This suggests that supernatant from Irf3/7-KO pDCs induces increased cell stress in acinar cells, whereas WT pDC supernatant does not.

To investigate potential biases within the pDC supernatant itself, LDH levels were measured directly in the original supernatant samples. Correlating with the findings in acinar cells, supernatant from Irf3/7-KO pDCs exhibited significantly higher LDH levels compared to WT pDC supernatant ($p = 0.0187$), indicating increased cell stress in the Irf3/7-KO pDCs. Furthermore, no differences in LDH levels were observed between the supernatant of a given pDC-type and the acinar cells treated with it (Figure 15B). This reveals that the elevated LDH levels in acinar cells treated with Irf3/7-KO pDC supernatant originate from the pDCs themselves, rather than being a downstream effect in the acinar cells. This experiment therefore does not provide further insight into the effects of pDCs on acinar cell stress.

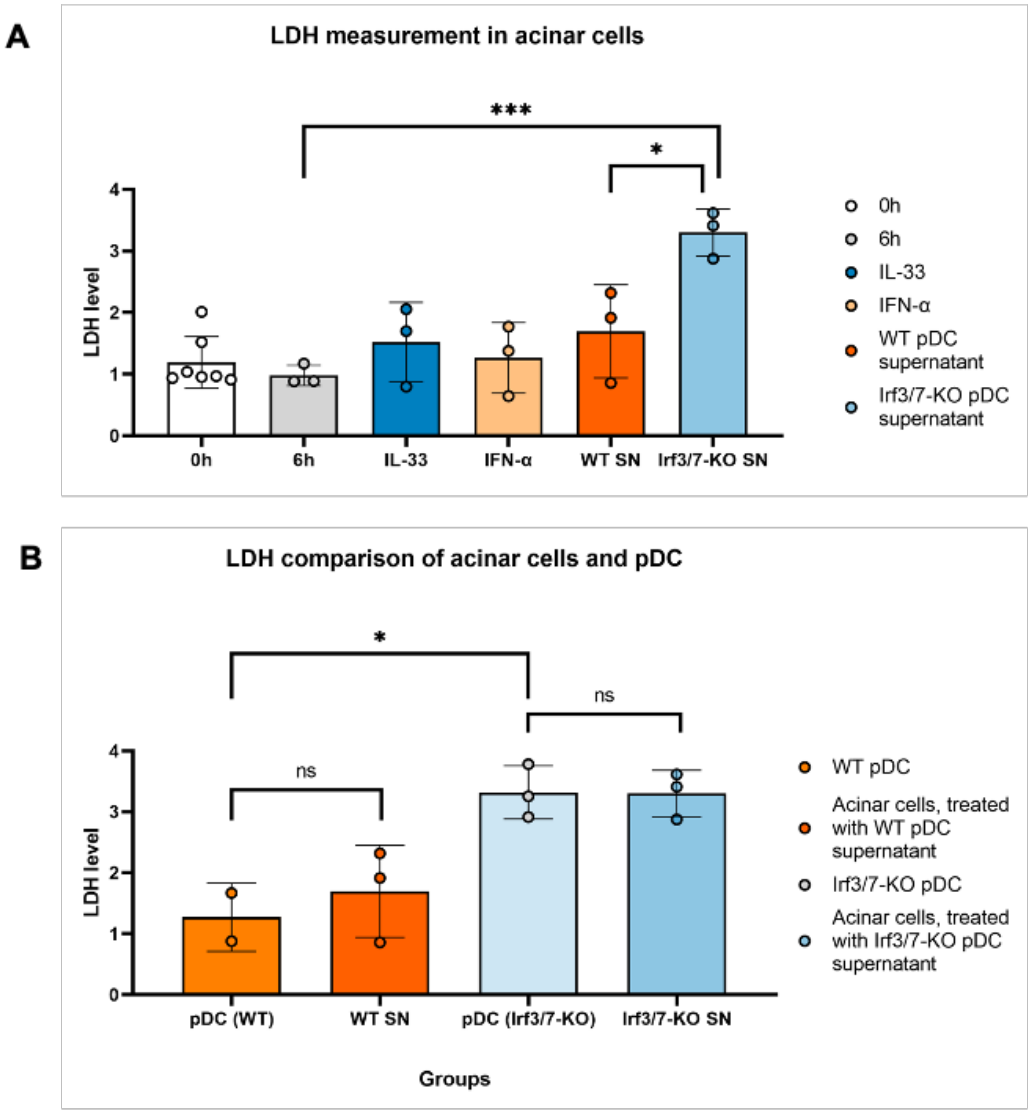

Figure 15. Quantification of LDH levels in acinar cells and pDCs. (A) Acinar cell suspensions were treated with IL-33, IFN-α, WT and Irf3/7-KO pDC supernatant for six hours. Untreated acinar cells at a 0h and 6h timepoint served as controls. LDH-Glo cytotoxicity Assay was performed to measure LDH levels. **(B)** LDH-Glo cytotoxicity Assay was performed with supernatants of WT and Irf3/7-KO pDC and compared with treated acinar cell suspensions. Data are represented as mean ± SD, each dot represents an independent experimental sample (n=3-7). Unpaired t-test was performed with continuity correction to test for differences between the cohorts. A two-tailed p-value was used, p-values < 0.05 were considered significant (* $P < 0.05$; ** $P < 0.01$; *** $P < 0.001$).

4.4.2. qRT-PCR for gene expression in acinar cells

To analyze the effects of pDCs and their associated cytokines on acinar cell signaling pathways for cell stress, damage and regeneration, RT-qPCR was performed for selected target genes: *Irf3* and *Irf7* to examine the pDC-IFN-acinar axis and evaluate *Irf* signaling within acinar cells; *Tnf-α* and *Il-6* to assess cellular stress and activation of pro-inflammatory pathways; *Flip* and *Xiap* to evaluate cell death signaling; and *Ccnb1* to analyze the effect on proliferation. These target genes were chosen due to the preliminary results from H&E and IHC staining, which had suggested decreased acinar proliferation (PHH3 staining), severe inflammation and acinar damage.

Relative gene expression of each gene was normalized to the housekeeper gene, and all samples were normalized to the 6-hours time point. This approach was chosen to identify differences between treatments, as cells may still experience residual stress at the 0-hour time point, potentially due to their recent isolation.

There were no significant differences in *Irf3* expression among the groups of acinar cells (Figure 16A, B). These findings align with IHC results, which showed no significant alterations in *Irf3* expression in acinar cells of AIP.

However, for *Irf7* signaling acinar cells showed altered expression levels: A significant upregulation of *Irf7* was detected in the INF-α-treated ($p = 0.0089$) acinar cells compared to the 6-hours control (Figure 16C). Furthermore, acinar cells treated with supernatant from Irf3/7-KO pDC also showed significantly increased *Irf7* expression compared to the 6-hours control ($p = 0.0014$) (Figure 16D). Interestingly, this was not observed in acinar cells treated with supernatant of WT pDC. However, no significant difference was detected between acinar cells treated with supernatant from WT and Irf3/7-KO pDC. Additionally, *Irf7* was upregulated at the 0-hour time point compared to the 6-hours time point ($p = 0.0087$) (Figure 16C), indicating increased inflammatory signaling directly after isolation of acinar cells, supporting the decision to use the 6-hours time point as a control.

These results are consistent with the findings of *Irf7* staining in IHC, which revealed a marked increase in acinar cells in AIP compared to AP, highlighting it as a distinctive feature of AIP. Combined with the acinar cell suspension experiments, the IHC findings support the hypothesis that pDCs might induce *Irf7* expression in acinar cells. Moreover, the increased *Irf7* expression in acinar cells treated with supernatant from Irf3/7-KO pDCs suggests that pDCs may drive this pathway independently of IFN-α, as Irf3/7-KO pDCs lack the ability to produce IFN-α.

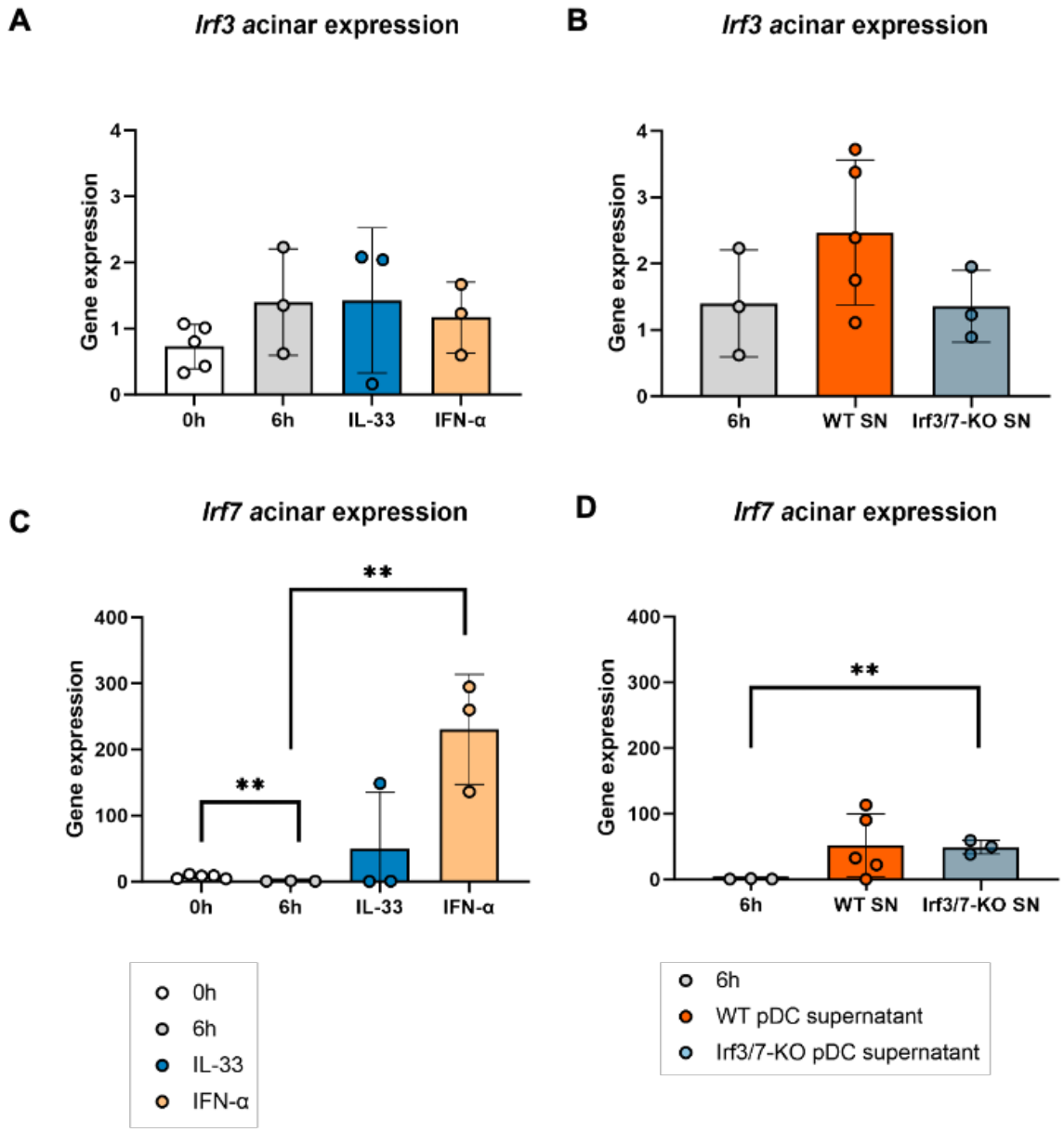

Figure 16. qRT-PCR of *Irf3* and *Irf7* expression in acinar cells. Acinar cell suspensions were treated with IL-33, IFN-α, WT and Irf3/7-KO pDC supernatant for six hours. Untreated acinar cells at a 0h and 6h time point served as controls. RNA expression levels of acinar cells were measured by qRT-PCR. **(A)** *Irf3* expression of acinar cells treated with IL-33 and IFN-α. **(B)** *Irf3* expression of acinar cells treated with WT and Irf3/7-KO pDC supernatant. **(C)** *Irf7* expression of acinar cells treated with IL-33 and IFN-α. **(D)** *Irf7* expression of acinar cells treated with WT and Irf3/7-KO pDC supernatant. (**A-D)** Data are represented as mean ± SD, each dot represents a sample (n=3 in each group, except n=7 of 0h timepoint control and n=5 of WT pDC). Unpaired T test was performed with to test for differences between the cohorts. A two-tailed p-value was used, p-values < 0.05 were considered significant (* $P < 0.05$; ** $P < 0.01$).

To evaluate pro-inflammatory and cellular stress markers, *Tnf-α* and *Il-6* expression were analyzed.

For *Tnf-α,* a significant upregulation was overserved in acinar cells treated with supernatant of Irf3/7-KO pDC compared to the 6 hours control ($p = 0.0112$), indicating increased pro-inflammatory signaling. Again, a similar trend was observed in acinar cells treated with supernatant of WT pDC, but did not reach significance. No significant difference was detected between WT and Irf3/7-KO pDC treated cells (Figure 17B).

For *Il-6* expression, a significant upregulation was found in both acinar cells treated with supernatant of WT pDC and Irf3/7-KO pDC compared to the 6 hours control ($p = 0.0300$ and 0.0030 respectively), suggesting activation of inflammatory signaling. No significant difference was detected between WT and Irf3/7-KO pDC treated cells (Figure 17D).

Upregulation of *Il-6* and *Tnf-α* proves inflammatory signaling upon treatment with pDC supernatant and aligns well with the findings of H&E, which showed severe acinar damage in AIP. Since supernatant of Irf3/7-KO pDC is also capable of inducing *Tnf-α* expression in acinar cells, this activation of proinflammatory signaling and cellular stress seems to be at least partially IFN-α-independent.

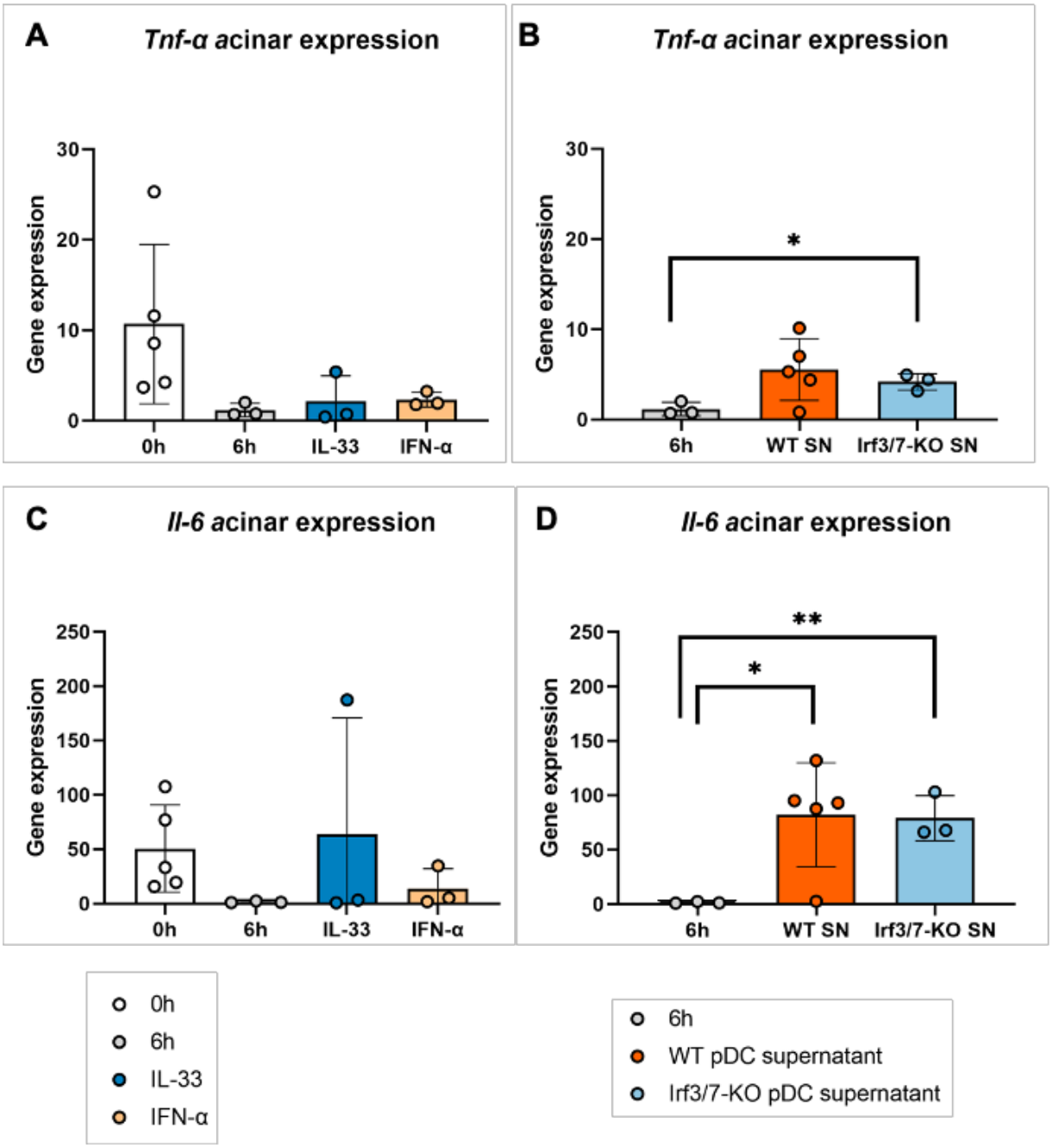

Figure 17. qRT-PCR of *Tnf-α* and *Il-6* expression in acinar cells. Acinar cell suspensions were treated with IL-33, IFN-α, WT and Irf3/7-KO pDC supernatant for six hours. Untreated acinar cells at a 0h and 6h time point served as controls. RNA expression levels of acinar cells were measured by qRT-PCR. **(A)** *Tnf-α* expression of acinar cells treated with IL-33 and IFN-α. **(B)** *Tnf-α* expression of acinar cells treated with WT and Irf3/7-KO pDC supernatant. **(C)** *Il-6* expression of acinar cells treated with IL-33 and IFN-α. **(D)** *Il-6* expression of acinar cells treated with WT and Irf3/7-KO pDC supernatant. **(A-D)** Data are represented as mean ± SD, each dot represents an independent experimental sample (n=3-7). Unpaired T test was performed with to test for differences between the cohorts. A two-tailed p-value was used, p-values < 0.05 were considered significant (* $P < 0.05$; ** $P < 0.01$).

Given that pancreatic atrophy is a prominent feature of human AIP (10, 61) and was similarly observed in MRL/MpJ mice with severe fatty replacement in H&E staining, apoptosis signaling was analyzed to investigate the effects of pDCs on acinar cell death.

Flip expression, an apoptosis inhibitor, was significantly upregulated in acinar cells treated with supernatant of Irf3/7-KO pDC compared to the 6 hours control ($p = 0.0007$), indicating an inhibition of apoptosis. A similar trend was observed in acinar cells treated with supernatant of WT pDC without reaching significance. No significant difference was detected between acinar cell treated with supernatants of WT and Irf3/7KO pDC (Figure 18B).

In contrast to these findings, *Xiap* expression, another apoptosis inhibitor, showed no significant alterations between all groups (Figure 18D).

These results suggest an inhibition of apoptosis in acinar cells through Irf3/7-KO pDC, therefore IFN-α-independent; however, this signal was only observed in *Flip*, and not in *Xiap* expression.

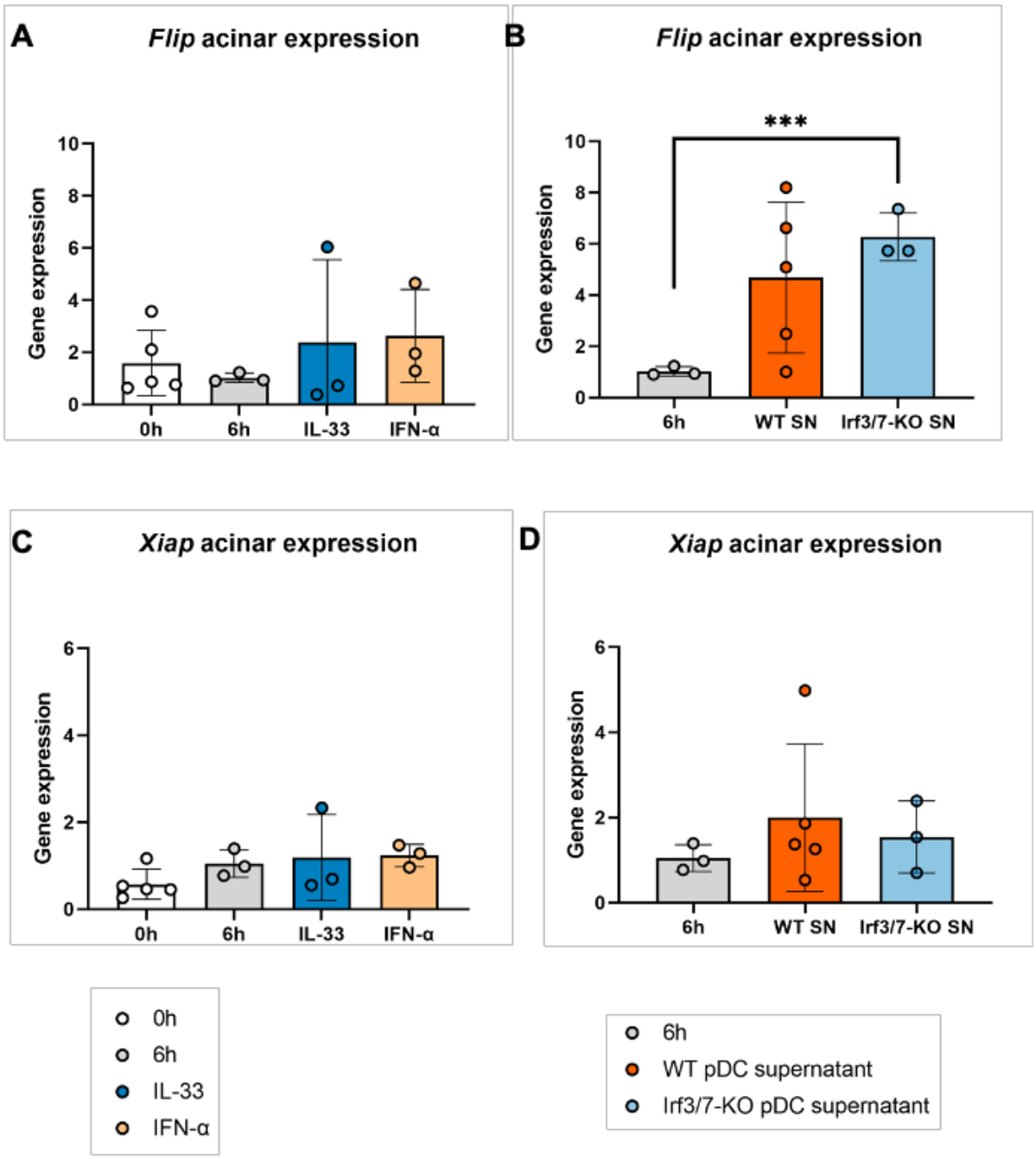

Figure 18. qRT-PCR of *Flip* and *Xiap* expression in acinar cells. Acinar cell suspensions were treated with IL-33, IFN-α, WT and Irf3/7-KO pDC supernatant for six hours. Untreated acinar cells at a 0h and 6h time point served as controls. RNA expression levels of acinar cells were measured by qRT-PCR. **(A)** *Flip* expression of acinar cells treated with IL-33 and IFN-α. **(B)** *Flip* expression of acinar cells treated with WT and Irf3/7-KO pDC supernatant. **(C)** *Xiap* expression of acinar cells treated with IL-33 and IFN-α. **(D)** *Xiap* expression of acinar cells treated with WT and Irf3/7-KO pDC supernatant. **(A-D)** Data are represented as mean ± SD, each dot represents an independent experimental sample (n=3-7). Unpaired T test was performed with to test for differences between the cohorts. A two-tailed p-value was used, p-values < 0.05 were considered significant (* $P < 0.05$; ** $P < 0.01$; *** $P < 0.001$).

To evaluate the effects of pDCs and their associated cytokines on proliferation of acinar cells, expression of *Ccnb1*, a mitosis-promoting gene, was measured.

There were no significant alterations between all groups for *Ccnb1* expression of acinar cells, indicating no notable induction or suppression of acinar proliferation (Figure 19). These results vary from the findings of PHH3 staining in IHC, which showed reduced acinar proliferation in AIP compared to AP. Additionally, the severe fatty replacement of acinar cells observed in H&E staining of AIP, indicative of pancreatic atrophy, supports the notion of diminished regenerative capacity in acinar cells.

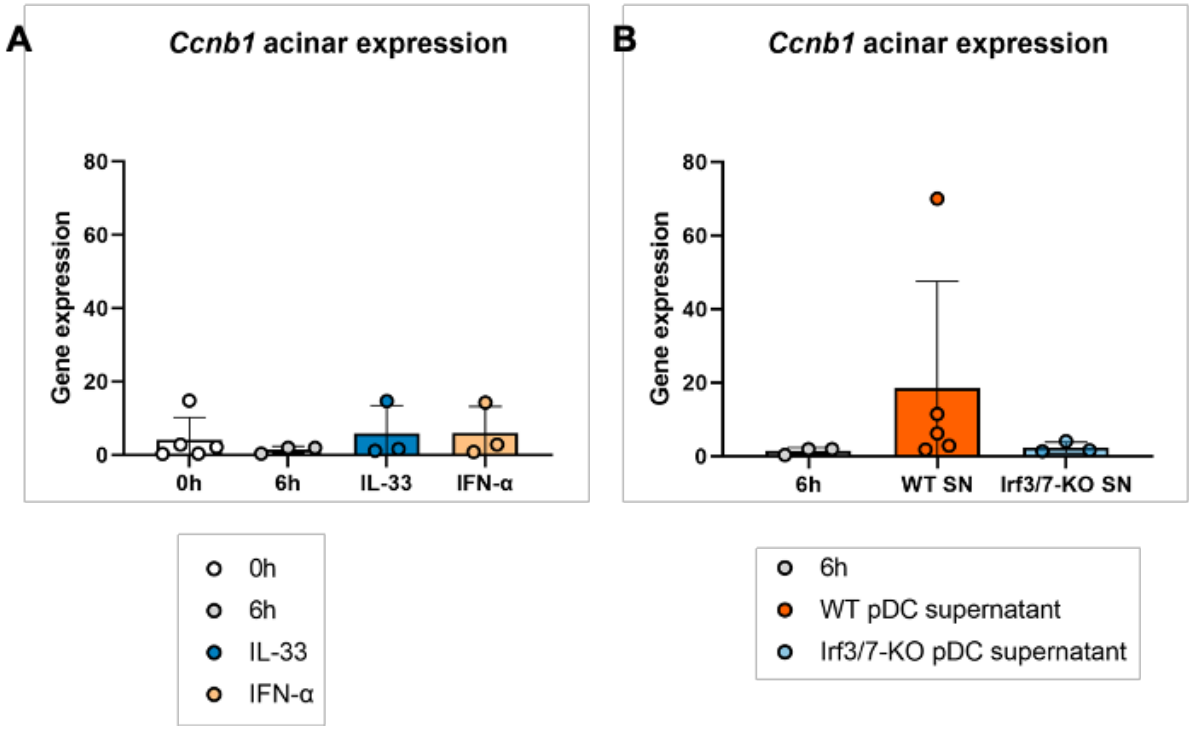

Figure 19. qRT-PCR of *Ccnb1* expression in acinar cells. Acinar cell suspensions were treated with IL-33, IFN-α, WT and Irf3/7-KO pDC supernatant for six hours. Untreated acinar cells at a 0h and 6h time point served as controls. RNA expression levels of acinar cells were measured by qRT-PCR. **(A)** *Ccnb1* expression of acinar cells treated with IL-33 and IFN-α. **(B)** *Ccnb1* expression of acinar cells treated with WT and Irf3/7-KO pDC supernatant. **(A) and (B)** Data are represented as mean ± SD, each dot represents a sample (n=3 in each group, except n=7 of 0h timepoint control and n=5 of WT pDC). Unpaired T test was performed with to test for differences between the cohorts. A two-tailed p-value was used, p-values < 0.05 were considered significant (* $P < 0.05$).

To summarize, significant upregulations in gene expressions were found in acinar cells treated with supernatant of Irf3/7-KO pDC for *Irf7, Tnf-α, Il-6* and *Flip*. In acinar cells treated with supernatant of WT pDC, only *Il-6* was significantly upregulated. No significant differences were detected between acinar cells treated with supernatant of WT pDC vs. of Irf3/7-KO pDC.

4.5. Acinar 3D cell culture experiments

To investigate the hypothesis that pDCs impair acinar regeneration capacities through the release of their associated cytokines, IFN-α and IL-33, acinar 3D cultures were generated from WT mice as described in the "Acinar 3D collagen culture" section. To assess the direct effects of IFN-α and IL-33 on acinar-to-ductal metaplasia, the 3D cultures were treated with these cytokines for seven days before being harvested. Given that acinar cells in 3D cultures consistently form ADM structures during culturing, the impact of the treatments was evaluated by measuring ADM size as an indicator of regeneration capability.

To determine whether the cytokines affect ADM-formation in 3D cultures, brightfield (BF) microscopic pictures were taken and H&E staining of the embedded collagen gels was done (Figure 20). Overall, ADMs typically displayed an elliptical rather than a fully rounded shape. Cellular structures of ADMs appeared consistent across the treatment groups in the BF images.

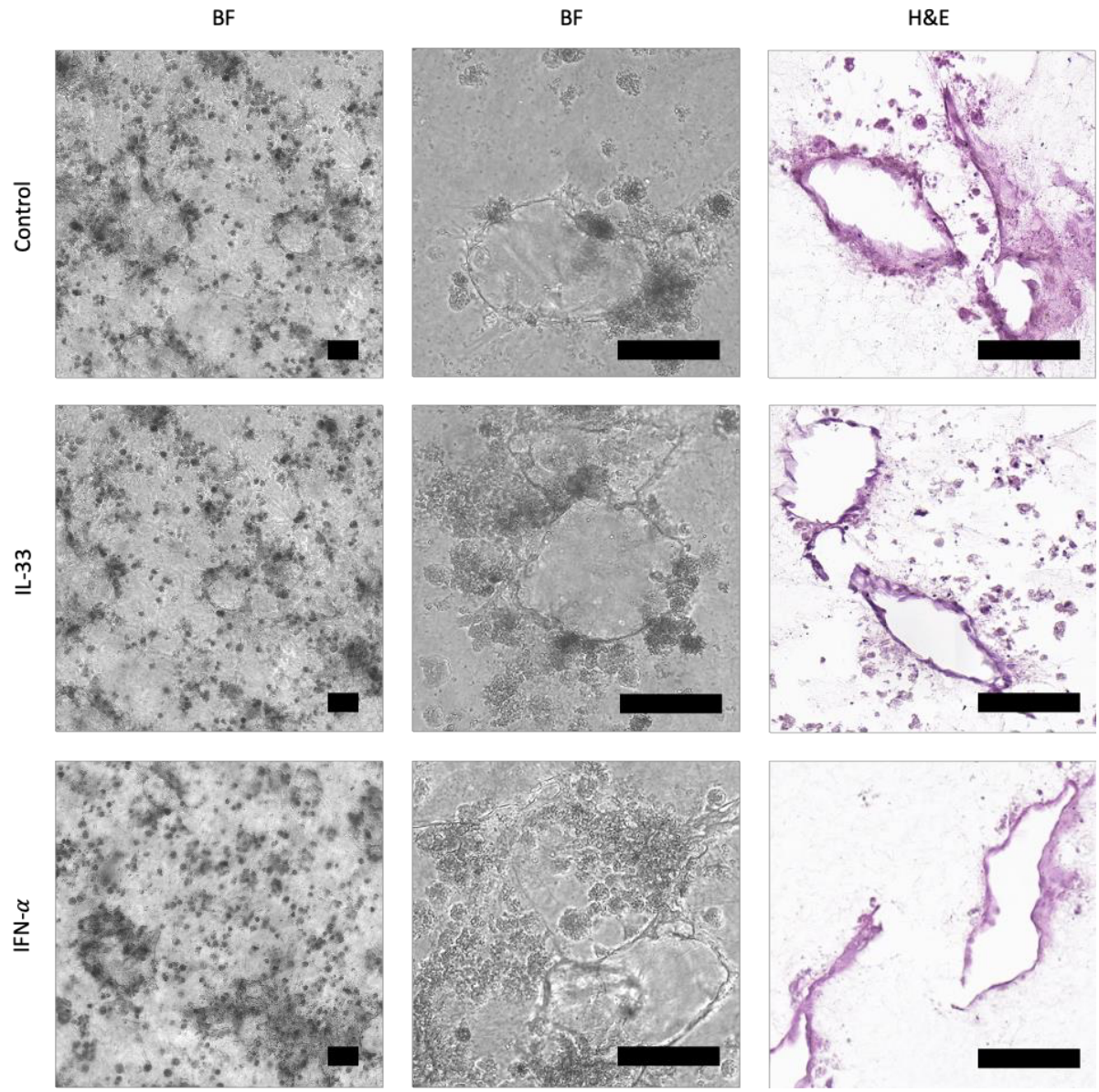

Figure 20. ADMs-formation in acinar 3D cultures. Left and middle figure panel shows representative bright field (BF) images of *in vitro* cultured acinar cells embedded in 3D-collagen cultures on day six. Right figure panel shows representative images of H&E staining of 3D collagen gels, after harvesting on day seven and embedding in paraffin. The upper row shows control 3D cultures, middle one IL-33 treated cultures and lower one IFN-α treated cultures. Scale bars 100 μm.

The number of ADMs was manually counted on representative histology slides. For each treatment group, two different samples were used, of each, one slide was fully counted and a mean was calculated per group (Figure 21A).

Next, of each counted ADM, the major and minor axis of the ellipse were measured. Using Ramanujan's approximation formula, the ellipse circumference was calculated for each ADM. Upon comparison among the treatment groups, significant differences in ADM size were found. ADMs from the control group were largest (mean circumference of 205 μm), followed by ADMs from the IFN-α group (mean circumference of 163 μm) and ADMs from IL-33 group

were smallest (mean circumference of 129 μm). ADM controls were therefore significantly larger than IFN-α ($p = 0.0222$) and IL-33 ($p < 0.0001$), and ADMs from IFN-α were still significantly larger than IL-33 ($p = 0.0296$) (Figure 21B).

These findings demonstrate that pDC-associated cytokines impair ADM formation through both IL-33 and IFN-α, with IL-33 exerting a stronger effect. This suggests that pDCs significantly influence acinar regeneration capabilities, potentially impairing acinar cell regeneration after injury, and could play a partial role in pancreatic atrophy observed in AIP.

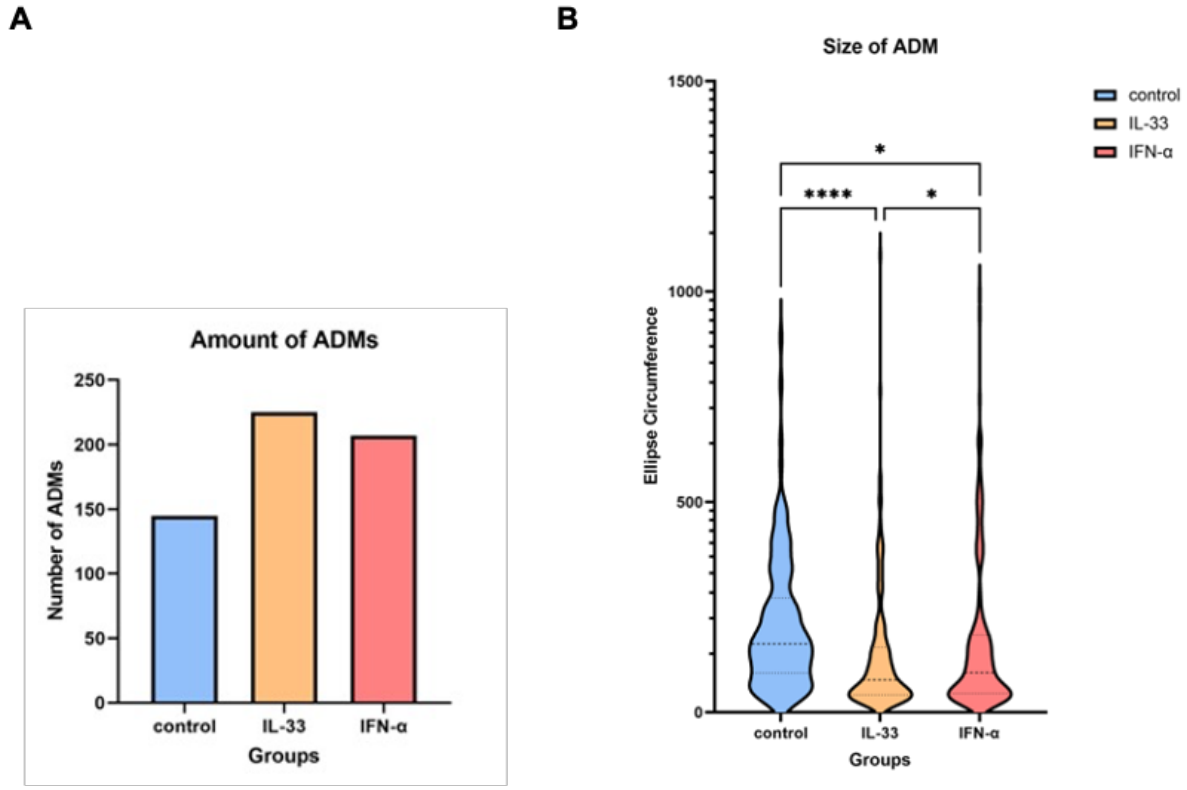

Figure 21. ADM analysis of acinar 3D cultures. For quantification, 3D culture H&E-stained slides were analyzed. **(A)** The average number of ADMs counted of each treatment group. Two samples were counted per treatment group, the mean number of ADMs is shown. **(B)** Of each counted ADM, the major and minor axes of each elliptical formation were measured manually. The elliptical circumference was calculated based on Ramanujan approximation. Data are represented as mean ± SD, (n=145 control ADMs, n=225 IL-33 treated ADMs, n=207 IFN-α treated ADMs). Unpaired T test was used for comparison between groups. A two-tailed p-value was used, p-values < 0.05 were considered significant (* $P < 0.05$; ** $P < 0.01$; *** $P < 0.001$; **** $P < 0.0001$).

5. Discussion

As a rare and complex autoimmune disorder, AIP continues to raise questions about its triggers and the mechanisms driving its recurrent flares. Even though the etiology of AIP is multifactorial, including genetic predispositions, environmental factors and pathologic immune responses, emerging evidence suggests that T cells and pDCs are central to the inflammatory cascade (1, 48, 57). Most likely T cells failing to recognize acinar enzymes or cellular components as self-antigens, trigger an immune-mediated attack on pancreatic cells, resulting in acinar injury (1, 50). This is accompanied by recruitment of further immune cells such as B cells and the production of the disease-typical IgG4 plasma blasts (51). In both human AIP and the MRL/MpJ mouse model of AIP, pDCs accumulate in the pancreatic tissue, which is accompanied by a significant increase of serum IFN-α and IL-33, both pDC-associated cytokines (35, 57, 58, 60). The exact mechanism of activation of pDCs is incompletely understood and recruitment could occur through T and B cells (57, 58). However, damage of acinar cells also results in the release of DAMPs, which may attract and activate pDCs via their TLR7 receptors (22). Another possibility are NETs, which could be produced by neutrophils during acinar damage and lead to pDC activation, in a mechanism similar to Lupus erythematosus (33). Either way, pDC are central to upholding the inflammatory process of AIP, which is emphasized by the fact that depletion of pDC or their cytokines leads to amelioration of disease (57, 58).

During an acute flare of AIP, acinar cells are severely destroyed, which is clinically evident as a reduction in enzyme secretion (61). Unlike AP, however, this acinar cell injury is not accompanied by necrosis, and the clinical presentation is generally milder (1, 10, 11). Despite this less severe course, acinar damage tends to be only partially repaired following a flare, often progressing to fibrotic tissue remodeling and pancreatic atrophy (10, 62). IFN-α and IL-33 may contribute to this process by recruiting additional immune cells (57), potentially initiating a vicious cycle of inflammation that exacerbates acinar cell destruction and inhibiting regenerative processes. Although the terminal destruction of pancreatic tissue has significant clinical implications, including both exocrine and endocrine pancreatic insufficiency, there is a notable lack of studies investigating acinar cell damage and, in particular, the processes of regeneration in AIP. Addressing this gap is crucial for developing strategies to prevent pancreatic atrophy and associated comorbidities. To explore the hypothesis that pDCs and their cytokines, IFN-α and IL-33, induce acinar cell damage and impair regenerative capacities, multiple experiments were conducted in the present study.

First the differences in histological characteristics of murine AIP were compared with murine AP. This revealed significantly more severe acinar cell damage and inflammatory infiltrate in AIP, accompanied by fatty replacement as a sign of pancreatic atrophy. Furthermore, AIP showed abundant ADM formations in H&E and Ck19 staining, which usually allows regeneration of acinar cells but results under persistent ADM conditions in exocrine atrophy. Classification of immune cells via IHC, revealed that the majority of immune cells in AIP are cytotoxic T cells, pDCs and Tregs, whereas macrophages were barely found, although they are the predominant immune cell population in AP. These findings confirm the preexisting literature describing AIP as a T cell- and pDC-driven disease, and making the MRL/MpJ mouse a suitable model for the disorder.

IHC staining of PHH3, a marker of cell proliferation, revealed a significant reduction of acinar cell proliferation in AIP. Additionally, IHC analysis of Irf3 and Irf7, known inducers of type-1 interferons (27), showed significantly higher expression in immune cells in AIP compared to AP. Since Irf3 is typically absent in pDCs and they rely mainly on Irf7 for IFN induction (30), the positive cells likely belong to different immune cell populations. Furthermore, Irf7 was also upregulated in the acinar cells of AIP, suggesting a potential feedback loop within acinar cells in response to IFN. Histological findings from MRL/MpJ mice confirmed the accumulation of pDCs alongside reduced acinar cell proliferation.

To investigate the potential axis of pDCs, IFN-α, acinar cell damage, and impaired regeneration, experiments were performed using acinar cell suspensions treated with the pDC-associated cytokines IL-33 and IFN-α, as well as supernatants from WT or Irf3/7-KO pDCs. The use of Irf3/7-KO pDCs was particularly insightful, as these cells are incapable of producing IFN-α, allowing for the study of IFN-independent effects. Initial analysis of acinar cell stress through LDH measurements proved inconclusive due to pre-existing elevated LDH levels in the Irf3/7-KO pDC supernatants, which introduced bias and limited the utility of this method for evaluating stress in this context.

Subsequent analysis focused on the proinflammatory response, cell death, and proliferation in treated acinar cells using qRT-PCR. A notable finding was the upregulation of *Irf7* in acinar cells treated with IFN-α, a sign of pro-inflammatory signaling which is consistent with the well-documented positive feedback loop in which IFN-α induces *Irf7* expression (27). Interestingly, acinar cells treated with supernatants from Irf3/7-KO pDCs also exhibited significant *Irf7* upregulation, despite the absence of IFN-α production by these pDCs. This suggests that Irf3/7-KO pDCs can induce *Irf7* expression as a sign of stress in acinar cells via an IFN-independent

mechanism. This finding is particularly compelling as it highlights a previously unrecognized pathway of *Irf7* activation that could contribute to the inflammatory environment in AIP. Acinar cells treated with WT pDC supernatant showed a trend towards increased *Irf7* expression, although this did not reach statistical significance. This is likely due to the small sample size in this study, and further experiments with larger cohorts are warranted to expand upon these observations. Overall, these findings indicate that pDCs can contribute to acinar cell stress and inflammation through both IFN-α-dependent and -independent pathways. The discovery of IFN-independent *Irf7* induction by Irf3/7-KO pDCs suggests an alternative mechanism by which pDCs may exacerbate the inflammatory response in AIP, emphasizing the need for further studies to unravel these pathways.

Furthermore, expression of *Tnf-α*, a potent pro-inflammatory cytokine, was significantly upregulated in acinar cells treated with supernatant of Irf3/7-KO pDC. A similar trend was observed in acinar cells treated with supernatant of WT pDC, but did not reach significance. This is quite interesting, since acinar cells are known to produce Tnf-α in a setting of acute pancreatitis (72, 73), indicating that Irf3/7-KO pDC caused acinar cell stress. Additionally, it has been described that acinar cells respond to Tnf-α with cytoskeletal disorganization and increased NF-κB signaling, which can finally increase cell death signaling (74). Interestingly, in an acute pancreatitis model of rats, this effect was confirmed, including increased apoptosis signaling, whilst LDH levels were not affected (72). Considering this in the context of this thesis, it could indicate that even if LDH levels of acinar cells did not differ from those of pDC, cell stress could still be increased and associated with the seen effect of *Tnf-α* upregulation. In addition, a significant upregulation of *Il-6* in acinar cells treated with both supernatant of WT pDC and Irf3/7-KO pDC was found, further supporting that pDCs induce acinar cell stress. Il-6 is an important immunomodulatory cytokine, displaying both inflammatory but also immunoregulatory functions (75). In the context of acute pancreatitis, Il-6 correlates well with the disease course and can serve as a predictor of severity (62,63). Moreover, genetic deletion of *Il-6* in a mouse model of acute pancreatitis alleviated lung failure, a common comorbidity in murine pancreatitis (64). These findings in gene expression of acinar cells, indicates that pDC cause acinar cell stress which results in increased *Il-6* transcription as a response.

Since cell stress and cell death signaling are closely intertwined, expression of the apoptosis inhibitors *Flip* and *Xiap* were analyzed. While no effect was detected in *Xiap* expression, a significant upregulation of *Flip* in acinar cells treated with supernatant of Irf3/7-KO pDC was observed, indicating inhibition of apoptosis. A similar trend was observed in cells treated with

supernatant of WT pDC without reaching significance. This inhibition of apoptosis in Irf3/7-KO pDC treated acinar cells is surprising since the increased levels of *Il-6* and *Tnf-α* expression point towards more cell stress and suggest more cell death signaling. Interestingly however, Tnf-α signaling can lead to different downstream results depending on various environmental and situational factors: even though it is not the primary response, Tnf-α can lead to cell death initiation, but in different contexts can also trigger cell survival and result in *Flip* upregulation (76-78). The latter might be the case in acinar cells treated with supernatant of Irf3/7-KO pDC – as a reaction to *Tnf-α* induction, *Flip* might be upregulated in a process of cell survival mechanisms. Another possibility is, that apoptosis is inhibited because other forms of cell death are ongoing, such as necrosis. In a mouse model of AP, Tlr3 has been shown to regulate cell death signaling in acinar cells, particularly by promoting controlled cell death via apoptosis (65). The depletion of Tlr3 or its downstream effector, Tlr adapter molecule 1, has been linked to an increase in necrosis in AP, which was further associated with elevated expression of *Xiap* (65). A similar mechanism could apply to acinar cells treated with supernatant of Irf3/7-KO pDC, leading to an upregulation of *Flip* associated with increased necrosis.

Putting these results into clinical context, AIP typically presents with a mild course, with necrosis notably absent (1, 10, 11). This suggests that pancreatic atrophy during AIP is likely driven by apoptosis of acinar cells rather than uncontrolled necrosis, as observed in severe AP. Additionally, pDC play a key role in AIP, perpetuating inflammation through the production of IFN-α and IL-33 (57). The above-mentioned findings could support the following interpretation: Ifn-α production by WT pDCs may be essential to induce acinar cell stress while not significantly altering acinar cell death pathways. However, in the absence of a functioning Ifn-α cascade, as seen in Irf3/7-KO pDCs, alternative cellular pathways might be activated in acinar cells. This could lead to heightened stress responses, reflected in upregulation of *Irf7, Tfn*-α, and *Il-6*. Such severe stress might inhibit apoptosis and shift the balance toward other cell death fates, such as necrosis. This hypothesis implies that while the Ifn-α pathway in WT pDCs induces acinar cell stress, it does so in a controlled manner, leading to contained acinar damage and widespread atrophy without triggering uncontrolled inflammation or extensive pancreatic necrosis. Unfortunately, the current data are insufficient to confirm these mechanisms fully. A more detailed analysis of gene expression, through whole transcriptome RNA sequencing, could reveal additional differences and provide deeper insights into the transcriptional pathways involved, particularly those related to cell death signaling.

Taken together, gene expression analysis revealed elevated markers of cell stress signaling (*Irf7, Tnf-α, Il-6*) and potential inhibition of apoptosis in acinar cells treated with supernatant from Irf3/7-KO pDCs. Overall, no significant differences between the treatments with supernatant of WT and Irf3/7-KO pDC were found. This could be due to the small sample size, which is a limiting factor of this study. Further studies with larger sample sizes focusing on the roles of apoptosis and necrosis in acinar cells upon pDC interaction are needed to clarify these questions.

Nevertheless, the results from the gene expression analysis supported the hypothesis that pDCs induce acinar cell stress. To investigate the effects of the pDC-associated cytokines IFN-α and IL-33 on acinar cell regeneration abilities over a longer interval of seven days, acinar 3D cultures were established. ADMs are the primary "growth mode" and can be mimicked by embedding acinar cells in 3D collagen gels. Under these culture conditions, the acinar explants spontaneously develop ADMs within a few days of incubation. Treatment of 3D cultures with IFN-α and IL-33 both resulted in significantly smaller ADM formations compared to untreated cells, with the smallest ADMs in the IL-33 treatment group. This indicates that the pDC-associated cytokines significantly impair ADM formation as a marker for regenerative acinar cells. While the behavior of ADM growth *in vitro* cannot be directly translated to that of normal pancreatic tissue, and the impact on acinar cells within a physiological environment may differ, the use of acinar 3D cultures provides a practical and efficient platform for initial treatment experiments and rapid evaluation of effects. Further investigation of regeneration markers, is necessary to comprehensively assess the influence of IL-33 and IFN-α on re-establishing pancreatic tissue integrity. However, taking these results together, they provide increasing evidence that pDC not only induce acinar cell stress and injury, but also lead to reduced regeneration, and as a consequence pancreatic atrophy, as it is observed both clinically and in the MRL/MpJ model (10, 57, 62).

It is particularly striking that pancreatic atrophy, characterized by fatty replacement of exocrine tissue, is such a prominent feature in the MRL/MpJ mouse model, given this strain's well-documented enhanced wound healing capacity (79-81). In wound healing experiments, MRL/MpJ mice demonstrate faster and more complete healing compared to WT mice, with reduced fibrosis and scarring features that starkly contrast with the pronounced fibrosis observed in the AIP model of these mice (79, 81). Interestingly, MRL/MpJ mice typically exhibit weaker inflammatory responses and earlier activation of tissue repair pathways, as evidenced by their gene expression patterns (79, 81). This also contrasts with the severe immune cell infiltration and limited tissue repair observed in their AIP phenotype (14, 18). While it

remains unclear whether significant differences exist between skin wound healing and pancreatic repair in these mice, their enhanced regenerative ability extends to other tissues, such as the heart (82). This raises the question of why the pancreas fails to recover similarly. One possibility is that the damage to acinar cells is so severe in AIP that even the heightened regenerative capacity of MRL/MpJ mice is insufficient to facilitate recovery. This would mean that the regenerative limitations observed may stem more from the nature and extent of pancreatic injury rather than an inherent failure of their repair mechanisms.

While studies on pancreatic regeneration in AIP are lacking, there is accumulating research on regeneration in acute and chronic pancreatitis. Animal models, like cerulein induced AP, show that acinar cells undergo damage, apoptosis, and necrosis, but undamaged cells are able to regenerate the pancreatic tissue within 1-2 weeks (83, 84). In duct ligation models, which simulate persistent obstructive biliary pancreatitis, AP is extremely severe leading to tissue atrophy, fibrosis and inhibition of regeneration (85). Acinar regeneration in AP typically arises from pre-existing acini, which survived a pancreatitis flare, though some new acinar cells may form through neogenesis (83, 86, 87). If acinar cells are extensively destroyed, regeneration relies on ADM rather than self-renewal (88). However, persistent injury can block redifferentiation of ADMs and result in a sustained loss of acinar identity (89). Notably, acinar cells do not regenerate pancreatic beta or endocrine cells (87).

Other cell types also significantly influence regenerative capacities of acinar cells, including immune cells and pancreatic stellate cells (PSCs) (83). PSC for instance, can serve as resident fibroblasts that are activated during pancreatic injury, leading to an upregulation of myofibroblast markers and production of high amounts of extracellular matrix such as collagen, leading to fibrotic remodeling of the tissue (83, 90). Macrophages on the other hand play an essential role not only during pancreatic inflammation but also regeneration (83). By infiltrating the pancreas during the acute phase of pancreatitis, they exacerbate acinar cell damage and increase their autodigestion (91). In persistent inflammation, they are capable of activating PSCs thereby promoting fibrosis (92). However, depending on the phagocytosis of different apoptotic cells types, phenotypes of macrophages are shaped, inducing variable polarization features (93). Interestingly, specific polarization of macrophages is necessary to induce pancreatic regeneration signaling, revealing that macrophages are central to regeneration regulation (93). The fact that depletion of type 2 macrophages impairs tissue regeneration in elderly mice after pancreatitis, further emphasizes their importance (93). This is consistent with the findings from IHC of MRL/MpJ mice, which showed striking depletion of macrophages accompanied by fatty replacement of exocrine tissue as a sign of pancreatic atrophy in AIP. In

contrast, macrophages were the primary immune cells observed in AP, with no evidence of pancreatic atrophy detected. Another study in cerulein induced AP revealed that Tlr3 signaling in myeloid cells decreases inflammation and the formation of ADMs, thereby supporting regeneration of acinar cells (94). Furthermore, dendritic cells also affect regenerative potential during the later course of murine AP by attenuating inflammation (95). In turn, depletion of dendritic cells leads to significantly worse outcomes of pancreatitis (95). Acinar regeneration in pancreatitis is regulated through a complex network, involving many pro-inflammatory cytokines, pathways usually being expressed in developmental processes, and transcription factors regulating acinar identity (83). Thus, TNF-α and IL-6 both influence acinar regeneration through activating NF-κB and JAK-STAT pathways (96). These findings highlight that the interactions between acinar and immune cells, particularly macrophages and dendritic cells, play a key role in determining both the initial severity of injury and successful regeneration.

To which extent these observations in acute and chronic pancreatitis apply to AIP, is unclear. Unlike the acute, time-point-specific injury to acinar cells in AP, inflammation in AIP is immune-mediated and involves a sustained attack on acinar cells by pDC, T and B cells (1, 57). This continuous damage likely contributes to more extensive pancreatic injury, potentially overwhelming repair mechanisms and preventing effective regeneration. As a result, ADM in AIP may be more indicative of chronic damage rather than a sign of regenerative activity. Similar to chronic pancreatitis, persistent injury in AIP could block the redifferentiation of ADMs, leading to a loss of acinar identity (83). Additionally, PSCs may be activated in AIP, driving increased fibrosis as a consequence of prolonged inflammation. The absence of macrophages in AIP of MRL/MpJ mice is noteworthy, as they play a critical role in mediating acinar cell regeneration in AP (93), potentially contributing to reduced regenerative capacity. Interestingly, dendritic cells, which are essential for attenuating inflammation in AP (95), behave differently in AIP, by actually sustaining the inflammatory cascade through INF-α signaling (57). However, the typically mild clinical course of AIP raises the possibility that pDC might contribute to modulating inflammatory severity while also reactivating other immune cells thereby sustaining disease activity. To better understand these dynamics, future studies should investigate whether regenerative pathways are downregulated in the pancreas of the MRL/MpJ AIP model. Moreover, exploring further how pDCs influence acinar regenerative capacities could provide critical insights into the interplay between immune-mediated inflammation and tissue repair in AIP.

Finally, to explore the hypothesis of acinar cells potentially inducing pDC differentiation in a reciprocal way, bone marrow was incubated with acinar supernatant. Different variations of acinar medium were used ± dexamethasone and ± trypsin inhibitor to exclude for an effect of these substances (dexamethasone having immunosuppressive functions and trypsin inhibitor impairing acinar enzyme activation). Across all experimental groups, acinar supernatant failed to induce pDC differentiation from bone marrow cells. However, these experiments did not assess the impact of acinar cells on already differentiated pDCs, which might still have the capacity to promote pDC activation or recruitment. Moreover, the acinar cell supernatants were generated without specifically inducing cellular stress or damage, apart from the stress caused by isolation methods. Exploring the effects of damaged acinar cells on differentiated pDCs would be particularly valuable, as cellular damage could potentially serve as a stronger trigger for pDC activation. Evidence from studies on pancreatic injury in AP demonstrates that DAMPs released from injured acinar cells recruit immune cells and drive inflammatory responses (64). Additionally, Tlr3 has been implicated as a regulator of acinar cell damage and death signaling in AP (65, 94). A similar mechanism may underlie AIP, where DAMPs from damaged acinar cells could act as Tlr7 ligands, leading to pDC activation. Further *in vivo* studies are needed to investigate and validate this hypothesis.

To conclude, this thesis characterized the AIP immune cell infiltrate in MRL/MpJ mice, showing that CD8+ T cells, pDC and Tregs are the major cell types present. Furthermore, it revealed that severe acinar damage occurs and is accompanied by fatty replacement and significantly reduced proliferation of acinar cells, indicating pancreatic atrophy. This aligns well with the results from acinar 3D cultures, in which the pDC-associated cytokines IL-33 and IFN-α negatively influence ADM size, indicating reduced regeneration abilities of acinar cells. Furthermore, cell culture experiments of acinar cells treated with supernatant of Irf3/7-KO pDC showed altered gene expression in acinar cells; where acinar cells increasingly expressed *Irf7, Tnf-α, Il-6* and the apoptosis inhibitor *Flip*, indicating that pDC might cause cellular stress and decrease apoptosis signaling. Taken together, these findings suggest that pDC affect acinar proliferation via IL-33 and IFN-α and induce inflammatory signaling within the cell. Further studies are needed to completely understand the complex effect of pDC in acinar cell death signaling.

6. References

1. Hart PA, Zen Y, Chari ST. Recent Advances in Autoimmune Pancreatitis. Gastroenterology. 2015;149(1):39-51.
2. Pickartz T, Mayerle J, Lerch MM. Autoimmune pancreatitis. Nat Clin Pract Gastroenterol Hepatol. 2007;4(6):314-23.
3. Kojima M, Sipos B, Klapper W, Frahm O, Knuth HC, Yanagisawa A, et al. Autoimmune pancreatitis: frequency, IgG4 expression, and clonality of T and B cells. Am J Surg Pathol. 2007;31(4):521-8.
4. Uchida K, Masamune A, Shimosegawa T, Okazaki K. Prevalence of IgG4-Related Disease in Japan Based on Nationwide Survey in 2009. International Journal of Rheumatology. 2012;2012:1-5.
5. Akshintala VS, Singh VK. Management of Autoimmune Pancreatitis. Clinical Gastroenterology and Hepatology. 2019;17(10):1937-9.
6. Ghazale A, Chari ST, Smyrk TC, Levy MJ, Topazian MD, Takahashi N, et al. Value of Serum IgG4 in the Diagnosis of Autoimmune Pancreatitis and in Distinguishing It From Pancreatic Cancer. The American Journal of Gastroenterology. 2007;102(8):1646-53.
7. Chari ST, Smyrk TC, Levy MJ, Topazian MD, Takahashi N, Zhang L, et al. Diagnosis of Autoimmune Pancreatitis: The Mayo Clinic Experience. Clinical Gastroenterology and Hepatology. 2006;4(8):1010-6.
8. Shimosegawa T, Chari ST, Frulloni L, Kamisawa T, Kawa S, Mino-Kenudson M, et al. International consensus diagnostic criteria for autoimmune pancreatitis: guidelines of the International Association of Pancreatology. Pancreas. 2011;40(3):352-8.
9. Hart PA, Topazian MD, Witzig TE, Clain JE, Gleeson FC, Klebig RR, et al. Treatment of relapsing autoimmune pancreatitis with immunomodulators and rituximab: the Mayo Clinic experience. Gut. 2013;62(11):1607-15.
10. Hart PA, Kamisawa T, Brugge WR, Chung JB, Culver EL, Czakó L, et al. Long-term outcomes of autoimmune pancreatitis: a multicentre, international analysis. Gut. 2013;62(12):1771-6.
11. Hart PA, Levy MJ, Smyrk TC, Takahashi N, Abu Dayyeh BK, Clain JE, et al. Clinical profiles and outcomes in idiopathic duct-centric chronic pancreatitis (type 2 autoimmune pancreatitis): the Mayo Clinic experience. Gut. 2016;65(10):1702-9.
12. Kamisawa T, Chari ST, Giday SA, Kim MH, Chung JB, Lee KT, et al. Clinical profile of autoimmune pancreatitis and its histological subtypes: an international multicenter survey. Pancreas. 2011;40(6):809-14.
13. Kamata K, Watanabe T, Minaga K, Strober W, Kudo M. Autoimmune Pancreatitis Mouse Model. Curr Protoc Immunol. 2018;120:15 31 1-15 31 8.
14. Kanno H, Nose M, Itoh J, Taniguchi Y, Kyogoku M. Spontaneous development of pancreatitis in the MRL/Mp strain of mice in autoimmune mechanism. Clin Exp Immunol. 1992;89(1):68-73.
15. Choi Y, Simon-Stoos K, Puck JM. Hypo-active variant of IL-2 and associated decreased T cell activation contribute to impaired apoptosis in autoimmune prone MRL mice. Eur J Immunol. 2002;32(3):677-85.
16. Perez CJ, Dumas A, Vallieres L, Guenet JL, Benavides F. Several classical mouse inbred strains, including DBA/2, NOD/Lt, FVB/N, and SJL/J, carry a putative loss-of-function allele of Gpr84. J Hered. 2013;104(4):565-71.
17. Yu H, Mohan S, Masinde GL, Baylink DJ. Mapping the dominant wound healing and soft tissue regeneration QTL in MRL x CAST. Mamm Genome. 2005;16(12):918-24.
18. Qu WM, Miyazaki T, Terada M, Okada K, Mori S, Kanno H, et al. A novel autoimmune pancreatitis model in MRL mice treated with polyinosinic:polycytidylic acid. Clin Exp Immunol. 2002;129(1):27-34.
19. Swiecki M, Colonna M. The multifaceted biology of plasmacytoid dendritic cells. Nature Reviews Immunology. 2015;15(8):471-85.
20. Ziegler-Heitbrock L, Ohteki T, Ginhoux F, Shortman K, Spits H. Reclassifying plasmacytoid dendritic cells as innate lymphocytes. Nature Reviews Immunology. 2022;23(1):1-2.
21. Schmid MA, Kingston D, Boddupalli S, Manz MG. Instructive cytokine signals in dendritic cell lineage commitment. Immunol Rev. 2010;234(1):32-44.

22. Reizis B. Plasmacytoid Dendritic Cells: Development, Regulation, and Function. Immunity. 2019;50(1):37-50.
23. Frenz T, Graalmann L, Detje CN, Doring M, Grabski E, Scheu S, et al. Independent of plasmacytoid dendritic cell (pDC) infection, pDC triggered by virus-infected cells mount enhanced type I IFN responses of different composition as opposed to pDC stimulated with free virus. J Immunol. 2014;193(5):2496-503.
24. Dreux M, Garaigorta U, Boyd B, Decembre E, Chung J, Whitten-Bauer C, et al. Short-range exosomal transfer of viral RNA from infected cells to plasmacytoid dendritic cells triggers innate immunity. Cell Host Microbe. 2012;12(4):558-70.
25. Baglio SR, van Eijndhoven MA, Koppers-Lalic D, Berenguer J, Lougheed SM, Gibbs S, et al. Sensing of latent EBV infection through exosomal transfer of 5'pppRNA. Proc Natl Acad Sci U S A. 2016;113(5):E587-96.
26. O'Neill LAJ, Bowie AG. The family of five: TIR-domain-containing adaptors in Toll-like receptor signalling. Nature Reviews Immunology. 2007;7(5):353-64.
27. Honda K, Taniguchi T. IRFs: master regulators of signalling by Toll-like receptors and cytosolic pattern-recognition receptors. Nature Reviews Immunology. 2006;6(9):644-58.
28. Ju X, Zenke M, Hart DN, Clark GJ. CD300a/c regulate type I interferon and TNF-alpha secretion by human plasmacytoid dendritic cells stimulated with TLR7 and TLR9 ligands. Blood. 2008;112(4):1184-94.
29. Lynch JP, Werder RB, Loh Z, Sikder MAA, Curren B, Zhang V, et al. Plasmacytoid dendritic cells protect from viral bronchiolitis and asthma through semaphorin 4a-mediated T reg expansion. J Exp Med. 2018;215(2):537-57.
30. Colonna M, Trinchieri G, Liu Y-J. Plasmacytoid dendritic cells in immunity. Nature Immunology. 2004;5(12):1219-26.
31. Petro TM. IFN Regulatory Factor 3 in Health and Disease. J Immunol. 2020;205(8):1981-9.
32. Ye Y, Gaugler B, Mohty M, Malard F. Plasmacytoid dendritic cell biology and its role in immune-mediated diseases. Clinical & Translational Immunology. 2020;9(5).
33. Lande R, Ganguly D, Facchinetti V, Frasca L, Conrad C, Gregorio J, et al. Neutrophils Activate Plasmacytoid Dendritic Cells by Releasing Self-DNA–Peptide Complexes in Systemic Lupus Erythematosus. Science Translational Medicine. 2011;3(73).
34. Brinkmann V, Reichard U, Goosmann C, Fauler B, Uhlemann Y, Weiss DS, et al. Neutrophil extracellular traps kill bacteria. Science. 2004;303(5663):1532-5.
35. Minaga K, Watanabe T, Arai Y, Shiokawa M, Hara A, Yoshikawa T, et al. Activation of interferon regulatory factor 7 in plasmacytoid dendritic cells promotes experimental autoimmune pancreatitis. Journal of Gastroenterology. 2020;55(5):565-76.
36. Kawa S, Ota M, Yoshizawa K, Horiuchi A, Hamano H, Ochi Y, et al. HLA DRB1*0405-DQB1*0401 haplotype is associated with autoimmune pancreatitis in the Japanese population. Gastroenterology. 2002;122(5):1264-9.
37. Goni E, Regel I, Mahajan UM, Amodio A, De Marchi G, Beyer G, et al. HLA-DRB1∗16 and -DQB1∗05 alleles are strongly associated with autoimmune pancreatitis in a cohort of hundred patients. Pancreatology. 2022;22(4):466-71.
38. Chang MC, Jan IS, Liang PC, Jeng YM, Yang CY, Tien YW, et al. Human cationic trypsinogen but not serine peptidase inhibitor, Kazal type 1 variants increase the risk of type 1 autoimmune pancreatitis. Journal of Gastroenterology and Hepatology. 2014;29(12):2038-42.
39. Chang MC, Chang YT, Tien YW, Liang PC, Jan IS, Wei SC, et al. T-cell regulatory gene CTLA-4 polymorphism/haplotype association with autoimmune pancreatitis. Clin Chem. 2007;53(9):1700-5.
40. Frulloni L, Lunardi C, Simone R, Dolcino M, Scattolini C, Falconi M, et al. Identification of a novel antibody associated with autoimmune pancreatitis. N Engl J Med. 2009;361(22):2135-42.
41. Okazaki K, Uchida K, Ohana M, Nakase H, Uose S, Inai M, et al. Autoimmune-related pancreatitis is associated with autoantibodies and a Th1/Th2-type cellular immune response. Gastroenterology. 2000;118(3):573-81.
42. Asada M, Nishio A, Uchida K, Kido M, Ueno S, Uza N, et al. Identification of a novel autoantibody against pancreatic secretory trypsin inhibitor in patients with autoimmune pancreatitis. Pancreas. 2006;33(1):20-6.
43. Okazaki K, Uchida K, Fukui T. Recent advances in autoimmune pancreatitis: concept, diagnosis, and pathogenesis. Journal of Gastroenterology. 2008;43(6):409-18.

44. Shiokawa M, Kodama Y, Sekiguchi K, Kuwada T, Tomono T, Kuriyama K, et al. Laminin 511 is a target antigen in autoimmune pancreatitis. Sci Transl Med. 2018;10(453).
45. Takizawa S, Endo T, Wanjia X, Tanaka S, Takahashi M, Kobayashi T. HSP 10 is a new autoantigen in both autoimmune pancreatitis and fulminant type 1 diabetes. Biochem Biophys Res Commun. 2009;386(1):192-6.
46. Guarneri F, Guarneri C, Benvenga S. Helicobacter pylori and autoimmune pancreatitis: role of carbonic anhydrase via molecular mimicry? Journal of Cellular and Molecular Medicine. 2005;9(3):741-4.
47. de Buy Wenniger LJ, Culver EL, Beuers U. Exposure to occupational antigens might predispose to IgG4-related disease. Hepatology. 2014;60(4):1453-4.
48. Schwaiger T, van den Brandt C, Fitzner B, Zaatreh S, Kraatz F, Dummer A, et al. Autoimmune pancreatitis in MRL/Mp mice is a T cell-mediated disease responsive to cyclosporine A and rapamycin treatment. Gut. 2014;63(3):494-505.
49. Kamisawa T, Anjiki H, Egawa N, Kubota N. Allergic manifestations in autoimmune pancreatitis. European Journal of Gastroenterology & Hepatology. 2009;21(10):1136-9.
50. Zen Y, Fujii T, Harada K, Kawano M, Yamada K, Takahira M, et al. Th2 and regulatory immune reactions are increased in immunoglobin G4-related sclerosing pancreatitis and cholangitis. Hepatology. 2007;45(6):1538-46.
51. Maillette de Buy Wenniger LJ, Doorenspleet ME, Klarenbeek PL, Verheij J, Baas F, Elferink RPO, et al. Immunoglobulin G4+ clones identified by next-generation sequencing dominate the B cell receptor repertoire in immunoglobulin G4 associated cholangitis. Hepatology. 2013;57(6):2390-8.
52. Yamanishi H, Kumagi T, Yokota T, Azemoto N, Koizumi M, Kobayashi Y, et al. Clinical significance of B cell-activating factor in autoimmune pancreatitis. Pancreas. 2011;40(6):840-5.
53. Sumimoto K, Uchida K, Kusuda T, Mitsuyama T, Sakaguchi Y, Fukui T, et al. The role of CD19+CD24highCD38high and CD19+CD24highCD27+ regulatory B cells in patients with type 1 autoimmune pancreatitis. Pancreatology. 2014;14(3):193-200.
54. Tabeya T, Yamamoto M, Naishiro Y, Ishigami K, Shimizu Y, Yajima H, et al. The role of cytotoxic T cells in IgG4-related dacryoadenitis and sialadenitis, the so-called Mikulicz's disease. Modern Rheumatology. 2014;24(6):953-60.
55. Shiokawa M, Kodama Y, Kuriyama K, Yoshimura K, Tomono T, Morita T, et al. Pathogenicity of IgG in patients with IgG4-related disease. Gut. 2016;65(8):1322-32.
56. Mayerle J, Lerch MM, Greinacher A. Why is one arm stronger than two arms? IgG4 antibodies in IgG4-related autoimmune pancreatitis. Gut. 2016;65(8):1240-1.
57. Watanabe T, Yamashita K, Arai Y, Minaga K, Kamata K, Nagai T, et al. Chronic Fibro-Inflammatory Responses in Autoimmune Pancreatitis Depend on IFN-α and IL-33 Produced by Plasmacytoid Dendritic Cells. The Journal of Immunology. 2017;198(10):3886-96.
58. Arai Y, Yamashita K, Kuriyama K, Shiokawa M, Kodama Y, Sakurai T, et al. Plasmacytoid Dendritic Cell Activation and IFN-α Production Are Prominent Features of Murine Autoimmune Pancreatitis and Human IgG4-Related Autoimmune Pancreatitis. The Journal of Immunology. 2015;195(7):3033-44.
59. Borufka L, Volmer E, Muller S, Engelmann R, Nizze H, Ibrahim S, et al. In vitro studies implicate an imbalanced activation of dendritic cells in the pathogenesis of murine autoimmune pancreatitis. Oncotarget. 2016;7(28):42963-77.
60. Minaga K, Watanabe T, Hara A, Kamata K, Omoto S, Nakai A, et al. Identification of serum IFN-α and IL-33 as novel biomarkers for type 1 autoimmune pancreatitis and IgG4-related disease. Scientific Reports. 2020;10(1).
61. Ko SBH, Mizuno N, Yatabe Y, Yoshikawa T, Ishiguro H, Yamamoto A, et al. Corticosteroids Correct Aberrant CFTR Localization in the Duct and Regenerate Acinar Cells in Autoimmune Pancreatitis. Gastroenterology. 2010;138(5):1988-96.e3.
62. Kanai K, Maruyama M, Kameko F, Kawasaki K, Asano J, Oguchi T, et al. Autoimmune Pancreatitis Can Transform Into Chronic Features Similar to Advanced Chronic Pancreatitis With Functional Insufficiency Following Severe Calcification. Pancreas. 2016;45(8):1189-95.
63. Lankisch PG, Apte M, Banks PA. Acute pancreatitis. Lancet. 2015;386(9988):85-96.
64. Kearney CJ, Martin SJ. An Inflammatory Perspective on Necroptosis. Mol Cell. 2017;65(6):965-73.

65. Regel I, Raulefs S, Benitz S, Mihaljevic C, Rieder S, Leinenkugel G, et al. Loss of TLR3 and its downstream signaling accelerates acinar cell damage in the acute phase of pancreatitis. Pancreatology. 2019;19(1):149-57.
66. Storz P. Acinar cell plasticity and development of pancreatic ductal adenocarcinoma. Nature Reviews Gastroenterology & Hepatology. 2017;14(5):296-304.
67. Zhang H, Corredor ALG, Messina-Pacheco J, Li Q, Zogopoulos G, Kaddour N, et al. REG3A/REG3B promotes acinar to ductal metaplasia through binding to EXTL3 and activating the RAS-RAF-MEK-ERK signaling pathway. Communications Biology. 2021;4(1).
68. Marstrand-Daucé L, Lorenzo D, Chassac A, Nicole P, Couvelard A, Haumaitre C. Acinar-to-Ductal Metaplasia (ADM): On the Road to Pancreatic Intraepithelial Neoplasia (PanIN) and Pancreatic Cancer. International Journal of Molecular Sciences. 2023;24(12).
69. Zhu L, Shi G, Schmidt CM, Hruban RH, Konieczny SF. Acinar cells contribute to the molecular heterogeneity of pancreatic intraepithelial neoplasia. Am J Pathol. 2007;171(1):263-73.
70. Wu J, Zhang L, Shi J, He R, Yang W, Habtezion A, et al. Macrophage phenotypic switch orchestrates the inflammation and repair/regeneration following acute pancreatitis injury. EBioMedicine. 2020;58:102920.
71. Bouwens L. Cytokeratins and cell differentiation in the pancreas. J Pathol. 1998;184(3):234-9.
72. Gukovskaya AS, Gukovsky I, Zaninovic V, Song M, Sandoval D, Gukovsky S, et al. Pancreatic acinar cells produce, release, and respond to tumor necrosis factor-alpha. Role in regulating cell death and pancreatitis. Journal of Clinical Investigation. 1997;100(7):1853-62.
73. Gu H, Werner J, Bergmann F, Whitcomb DC, Büchler MW, Fortunato F. Necro-inflammatory response of pancreatic acinar cells in the pathogenesis of acute alcoholic pancreatitis. Cell Death & Disease. 2013;4(10):e816-e.
74. Satoh A, Gukovskaya A, Edderkaoui M, Daghighian M, Reevejr J, Shimosegawa T, et al. Tumor Necrosis Factor-α Mediates Pancreatitis Responses in Acinar Cells via Protein Kinase C and Proline-Rich Tyrosine Kinase 2. Gastroenterology. 2005;129(2):639-51.
75. Rose-John S, Jenkins BJ, Garbers C, Moll JM, Scheller J. Targeting IL-6 trans-signalling: past, present and future prospects. Nature Reviews Immunology. 2023;23(10):666-81.
76. van Loo G, Bertrand MJM. Death by TNF: a road to inflammation. Nature Reviews Immunology. 2022;23(5):289-303.
77. Marques-Fernandez F, Planells-Ferrer L, Gozzelino R, Galenkamp KM, Reix S, Llecha-Cano N, et al. TNFα induces survival through the FLIP-L-dependent activation of the MAPK/ERK pathway. Cell Death & Disease. 2013;4(2):e493-e.
78. Micheau O, Lens S, Gaide O, Alevizopoulos K, Tschopp J. NF-κB Signals Induce the Expression of c-FLIP. Molecular and Cellular Biology. 2023;21(16):5299-305.
79. Li X, Mohan S, Gu W, Baylink DJ. Analysis of gene expression in the wound repair/regeneration process. Mamm Genome. 2001;12(1):52-9.
80. Li X, Mohan S, Gu W, Miyakoshi N, Baylink DJ. Differential protein profile in the ear-punched tissue of regeneration and non-regeneration strains of mice: a novel approach to explore the candidate genes for soft-tissue regeneration. Biochim Biophys Acta. 2000;1524(2-3):102-9.
81. Kench JA, Russell DM, Fadok VA, Young SK, Worthen GS, Jones-Carson J, et al. Aberrant wound healing and TGF-beta production in the autoimmune-prone MRL/+ mouse. Clin Immunol. 1999;92(3):300-10.
82. Leferovich JM, Bedelbaeva K, Samulewicz S, Zhang XM, Zwas D, Lankford EB, et al. Heart regeneration in adult MRL mice. Proc Natl Acad Sci U S A. 2001;98(17):9830-5.
83. Murtaugh LC, Keefe MD. Regeneration and repair of the exocrine pancreas. Annu Rev Physiol. 2015;77:229-49.
84. Willemer S, Elsasser HP, Adler G. Hormone-induced pancreatitis. Eur Surg Res. 1992;24 Suppl 1:29-39.
85. Walker NI. Ultrastructure of the rat pancreas after experimental duct ligation. I. The role of apoptosis and intraepithelial macrophages in acinar cell deletion. Am J Pathol. 1987;126(3):439-51.
86. Fitzgerald PJ, Herman L, Carol B, Roque A, Marsh WH, Rosenstock L, et al. Pancreatic acinar cell regeneration. Am J Pathol. 1968;52(5):983-1011.
87. Desai BM, Oliver-Krasinski J, De Leon DD, Farzad C, Hong N, Leach SD, et al. Preexisting pancreatic acinar cells contribute to acinar cell, but not islet beta cell, regeneration. J Clin Invest. 2007;117(4):971-7.

88. Criscimanna A, Speicher JA, Houshmand G, Shiota C, Prasadan K, Ji B, et al. Duct cells contribute to regeneration of endocrine and acinar cells following pancreatic damage in adult mice. Gastroenterology. 2011;141(4):1451-62, 62 e1-6.
89. Strobel O, Dor Y, Alsina J, Stirman A, Lauwers G, Trainor A, et al. In vivo lineage tracing defines the role of acinar-to-ductal transdifferentiation in inflammatory ductal metaplasia. Gastroenterology. 2007;133(6):1999-2009.
90. Apte MV, Haber PS, Applegate TL, Norton ID, McCaughan GW, Korsten MA, et al. Periacinar stellate shaped cells in rat pancreas: identification, isolation, and culture. Gut. 1998;43(1):128-33.
91. Sendler M, Dummer A, Weiss FU, Kruger B, Wartmann T, Scharffetter-Kochanek K, et al. Tumour necrosis factor alpha secretion induces protease activation and acinar cell necrosis in acute experimental pancreatitis in mice. Gut. 2013;62(3):430-9.
92. Treiber M, Neuhofer P, Anetsberger E, Einwachter H, Lesina M, Rickmann M, et al. Myeloid, but not pancreatic, RelA/p65 is required for fibrosis in a mouse model of chronic pancreatitis. Gastroenterology. 2011;141(4):1473-85, 85 e1-7.
93. Criscimanna A, Coudriet GM, Gittes GK, Piganelli JD, Esni F. Activated macrophages create lineage-specific microenvironments for pancreatic acinar- and beta-cell regeneration in mice. Gastroenterology. 2014;147(5):1106-18 e11.
94. Hidalgo-Sastre A, Kuebelsbeck LA, Jochheim LS, Staufer LM, Altmayr F, Johannes W, et al. Toll-like receptor 3 expression in myeloid cells is essential for efficient regeneration after acute pancreatitis in mice. Eur J Immunol. 2021;51(5):1182-94.
95. Bedrosian AS, Nguyen AH, Hackman M, Connolly MK, Malhotra A, Ibrahim J, et al. Dendritic cells promote pancreatic viability in mice with acute pancreatitis. Gastroenterology. 2011;141(5):1915-26 e1-14.
96. Gukovsky I, Gukovskaya A. Nuclear factor-kappaB in pancreatitis: Jack-of-all-trades, but which one is more important? Gastroenterology. 2013;144(1):26-9.

Danksagung

Es erfüllt mich mit großer Freude und Dankbarkeit die Doktorarbeit zum Abschluss gebracht zu haben. An dieser Stelle möchte ich mich bei allen bedanken, die mich während der Erstellung unterstützt haben.

Der größte Dank richtet sich an meine Eltern, die nicht nur mein Studium und meine Auslandsaufenthalte finanziert haben, sondern mir auch stets mit Rat und Tat zur Seite standen. Ohne ihre Unterstützung wäre dieser bedeutende Lebensabschnitt nicht in dem Ausmaß möglich gewesen. Außerdem möchte mich bei meinem Bruder, meiner erweiterten Familie und meinen Freundinnen und Freunden bedanken, die mich immer begleitet und aufgefangen haben. Ganz besonderer Dank geht an meinen Partner Nikolaus, der mit mir alle Höhen und Tiefen durchlebt hat und mir immer zur Seite stand.

Mein Dank gebührt Prof. Dr. med. Julia Mayerle an der Medizinischen Klinik und Poliklinik II, die mir die Arbeit an diesem interessanten Projekt ermöglicht und die notwendigen Rahmenbedingungen zu Verfügung gestellt hat. Besonders bedanken möchte ich mich auch bei PD Dr. rer. biol. hum. Ivonne Regel, die mir bei jeder Projektfrage zur Seite stand und mich tatkräftig von den ersten Versuchen bis zur Auswertung hin unterstützt hat. Ohne ihre Hilfe wären mir einige Stolpersteine in den Weg gefallen. Des Weiteren möchte ich mich bei dem Laborteam bestehend aus Nicole, Lisa, Ahmed, Theresa, Prince, Simon und Maria bedanken, das jederzeit mit Hilfe, Humor und Fachwissen zur Verfügung stand.

Vielen herzlichen Dank für Eure Unterstützung!

Affidativ

LMU LUDWIG-MAXIMILIANS-UNIVERSITÄT MÜNCHEN | Promotionsbüro Medizinische Fakultät | MMRS

Eidesstattliche Versicherung

Orgler-Gasche, Elisabeth

Name, Vorname

Ich erkläre hiermit an Eides statt, dass ich die vorliegende Dissertation mit dem Titel:

Understanding the effects of plasmacytoid dendritic cells on acinar cell damage in Autoimmune Pancreatitis

selbständig verfasst, mich außer der angegebenen keiner weiteren Hilfsmittel bedient und alle Erkenntnisse, die aus dem Schrifttum ganz oder annähernd übernommen sind, als solche kenntlich gemacht und nach ihrer Herkunft unter Bezeichnung der Fundstelle einzeln nachgewiesen habe.

Ich erkläre des Weiteren, dass die hier vorgelegte Dissertation nicht in gleicher oder in ähnlicher Form bei einer anderen Stelle zur Erlangung eines akademischen Grades eingereicht wurde.

Boston, 20.11.2025

Ort, Datum

Elisabeth Orgler-Gasche

Unterschrift Doktorandin bzw. Doktorand

Erklärung zur Übereinstimmung

LMU LUDWIG-MAXIMILIANS-UNIVERSITÄT MÜNCHEN | Promotionsbüro Medizinische Fakultät | MMRS

Erklärung zur Übereinstimmung der gebundenen Ausgabe der Dissertation mit der elektronischen Fassung

Orgler-Gasche, Elisabeth

Name, Vorname

Hiermit erkläre ich, dass die elektronische Version der eingereichten Dissertation mit dem Titel:

Understanding the effects of plasmacytoid dendritic cells on acinar cell damage in Autoimmune Pancreatitis

in Inhalt und Formatierung mit den gedruckten und gebundenen Exemplaren übereinstimmt.

Boston, 20.11.2025	Elisabeth Orgler-Gasche
Ort, Datum	Unterschrift Doktorandin bzw. Doktorand

Publikationsliste

Orgler E*, Baumgartner M*, Duller S, Kumptisch C, Hausmann B, Moser D, Khare V, Lang M, Köcher T, Frick A, Muttenthaler M, Makristathis A, Moissl-Eichinger C, Gasche C. Archaea influence composition of endoscopically visible ileocolonic biofilms. **Gut Microbes**. 2024 Jan-Dec; 16(1):2359500. doi: 10.1080/19490976.2024.2359500. Epub 2024 Jun 2. PMID: 38825783; PMCID: PMC11152093.

Sirtl S, Bretthauer K, Ahmad M, Hohmann E, Schmidt VF, Allawadhi P, Vornhülz M, Klauss S, Goni E, Vielhauer J, **Orgler E**, Saka D, Knoblauch M, Hofmann FO, Schirra J, Schulz C, Beyer G, Mahajan UM, Mayerle J*, Zorniak M*. Severity of gallstone, sludge or microlithiasis induced pancreatitis - all of the same? **Pancreas**. 2024 May 1. doi: 10.1097/MPA.0000000000002349. PMID: 38696426.

Sirtl S, **Orgler E**, Vielhauer J, Beyer G, Mayerle J. Akute Pankreatitis - Diagnose und Management [Acute pancreatitis - diagnosis and management]. **MMW Fortschr Med**. 2023 Nov;165(19):52-57.

Vornhülz M, Sirtl S, **Orgler E**, Weniger M, Schirra J, Beyer G, Mayerle J. Pankreaszysten - Indikationen, Zeitpunkt und Rationale für eine Surveillance [Cystic pancreatic lesions-indications, timing and reasons for surveillance]. **Radiologie (Heidelb).** 2023 Oct. doi: 10.1007/s00117-023-01226-4.

Orgler, E., et al. Autoimmune Gastritis: Update and New Perspectives in Therapeutic Management**. Curr Treat Options Gastro** 21, 64–77 (2023). https://doi.org/10.1007/s11938-023-00406-4

Vornhülz, M., Sirtl, S., **Orgler, E.** et al. Pankreaszysten – Indikationen, Zeitpunkt und Rationale für eine Surveillance. **Wien klin Mag** 26, 38–44 (2023). https://doi.org/10.1007/s00740-022-00475-8

Vornhülz M*, **Orgler E***, Klauss S*, Georg Beyer, Julia Mayerle. Chronische Pankreaserkrankungen. **CME Fortbildung, Springer Medizin Verlag.** 2022; 19 (6): 19–28.

Baumgartner M, Lang M, Holley H, Crepaz D, Hausmann B, Pjevac P, Moser D, Haller F, Hof F, Beer A, **Orgler E**, Frick A, Khare V, Evstatiev R, Strohmaier S, Primas C, Dolak W, Köcher T, Klavins K, Rath T, Neurath MF, Berry D, Makristathis A, Muttenthaler M, Gasche C. Mucosal Biofilms Are an Endoscopic Feature of Irritable Bowel Syndrome and Ulcerative Colitis. **Gastroenterology**. 2021 Oct;161(4):1245-1256.e20. doi: 10.1053/j.gastro.2021.06.024.